Applied Superconductivity:

Josephson Effect and Superconducting Electronics

Manuscript to the Lectures during WS 2003/2004, WS 2005/2006, WS 2006/2007, WS 2007/2008, WS 2008/2009, and WS 2009/2010

Prof. Dr. Rudolf Gross

and

Dr. Achim Marx

Walther-Meißner-Institut

Bayerische Akademie der Wissenschaften

and

Lehrstuhl für Technische Physik (E23)

Technische Universität München

Walther-Meißner-Strasse 8

D-85748 Garching

Rudolf.Gross@wmi.badw.de

Contents

List of Figures

List of Tables

Chapter 3

Physics of Josephson Junctions: The Voltage State

In Chapter 2 we have considered Josephson junctions, for which the current was less than the maximum Josephson current I_s^m. Then, the junction resides in the zero voltage state which is equivalent to the static state. In this chapter we generalize our discussion and treat the situation, where the junction current is larger than the maximum Josephson current and therefore only part of the total current can be carried by the Josephson current. That is, in addition to the Josephson current we have to include other current channels carrying the excess current. In this situation the Josephson junction resides in the finite voltage state, where the phase difference evolves in time. This state corresponds to the dynamic state of the junction. One additional current channel is the ***resistive channel***. At temperatures above zero temperature there is a finite probability for Cooper pairs to be broken up by thermal excitation thereby generating unpaired "normal" electrons. In the presence of a finite voltage across the junction these normal electrons contribute to the current. In contrast to the Josephson current this normal current channel is resistive. The second current channel is the ***capacitive channel*** due to the finite capacitance of the Josephson junction. For example, a tunneling type superconductor/insulator/superconductor junction just represents a parallel plate capacitor. In the present of a time varying junction voltage we have a finite displacement current across this capacitor. Finally, noise is taken into account by adding a fluctuation current.

In this chapter we first describe the additional current channels in the voltage state of a Josephson junction and then in section 3.2 discuss models for the description of the current-voltage characteristics. In particular, we discuss Josephson junctions driven by dc and ac sources and analyze the effect of thermal fluctuations. Initially, we describe the junction dynamics within a classical framework. Then, in section 3.5 we show that this classical treatment is no longer valid for Josephson junctions with small capacitance. We discuss the limits of the classical treatment and the relevance of secondary macroscopic quantum effects. Finally, in section 3.6 we extend our discussion from zero-dimensional Josephson junctions to extended junctions.

3.1 The Basic Equation of the Lumped Josephson Junction

If we want to derive the basic equation describing the Josephson junction in the voltage state, we have to consider the additional current channels relevant in the voltage state. In the following we will consider the resistive and capacitive channel as well as an additional channels due to fluctuations (noise). In our discussion we first consider lumped Josephson junctions that can be characterized by the integral current values. Extended junctions will be discussed later in section 3.6.

3.1.1 The Normal Current: Junction Resistance

At finite temperatures ($T > 0$) there is a finite density of normal electrons due to thermal break-up of Cooper pairs. The presence of the condensate of paired electrons makes the properties of these "normal excitations" somewhat different from those in the normal state. We call them ***quasiparticles***.

In the zero-voltage state of a Josephson junction the quasiparticles do not contribute to the junction current. However, if the gauge-invariant phase difference changes in time resulting in a non-vanishing junction voltage V according to the second Josephson equation, $d\varphi/dt = 2eV/\hbar$, then a quasiparticle component of the total current, the ***normal current*** I_N, is obtained. This current is a resistive current and therefore the ***voltage-state*** of a Josephson junction is also called the ***resistive state***.

We briefly discuss the temperature and voltage dependence of the normal current. First, for temperatures close to the transition temperature ($T \lesssim T_c$) the energy $2\Delta(T)$ (Δ is the energy gap) required to break up a Cooper pairs is much smaller than k_BT. Therefore, almost all Cooper pairs are broken up and the concentration of quasiparticles is close to the electron density in the normal state. In this case we expect that the current-voltage characteristic (IVC) is close to the usual Ohm's law

$$I_N = G_N V \ , \tag{3.1.1}$$

where $G_N = 1/R_N$ is the ***normal conductance*** of the Josephson junction.

Second, if the junction voltage is above the so-called ***gap voltage***

$$V_g = \frac{\Delta_1(T)+\Delta_2(T)}{e} \ , \tag{3.1.2}$$

the external circuit provides sufficient energy eV to break up Cooper pairs. Here, $\Delta_1(T)$ and $\Delta_2(T)$ are the energy gaps in the two junction electrodes. A Cooper pair is broken up in one of the electrodes and the two newly formed quasiparticles pass to the other electrode. This process can set in only above the gap voltage because a minimum energy $\Delta_1(T)+\Delta_2(T)$ is required for this process. Hence, also for $|V| > V_g$ the IVC is expected to be close to an ohmic dependence independent of the temperature.

Third, for $T \ll T_c$ and $|V| < V_g$ there should be a vanishing normal current, since neither the thermal energy k_BT nor the energy eV supplied by the external circuit are sufficient to break up Cooper pairs. That is, the quasiparticle density and hence the normal current is vanishingly small.

The IVC expected from our discussion is shown schematically in Fig. 3.1. For $T > T_c$ and $|V| > V_g$ an ohmic dependence is obtained. For $T \ll T_c$ and $|V| < V_g$ the IVC depends on the sweep direction and on the type of the external source (current or voltage source). Here, for a current source a hysteretic IVC is obtained. The detailed reason for that will be discussed later in section 3.2.1. We note that if the junction is driven by a current source, the total current through the junction, $I = I_s + I_N$ is constant. Since in the voltage state the supercurrent $I_s = I_c \sin\varphi$ is varying in time due to the time evolution of φ, also

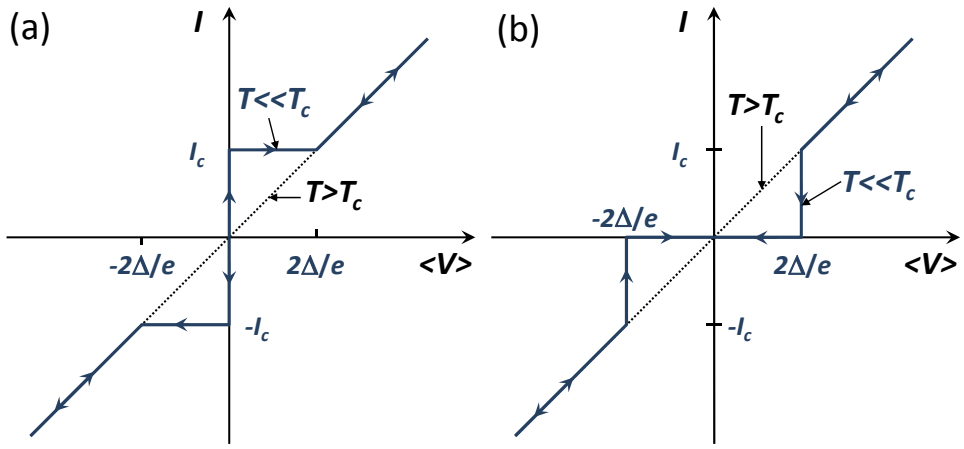

Figure 3.1: Current-voltage characteristics (IVC) of a Josephson junction driven by a constant current source. The voltage $\langle V \rangle$ represents the time-averaged voltage. Curve (a) is for increasing and curve (b) for decreasing driving current.

the normal current has to vary in time to keep the total current constant. Then, also the junction voltage $V = I_N/G_N$ is varying in time. The voltage shown in the IVCs of Fig. 3.1 is the time-averaged voltage $\langle V \rangle$.

Summarizing our discussion we see that in the voltage state of a Josephson junction we have to take into account the quasiparticle current. The quasiparticles are generated either by thermal excitation at finite temperature or due to breaking up of Cooper pairs by the junction voltage even at zero temperature. A circuit model that incorporates both the Josephson current and the normal current channel is shown in Fig. 3.2.

At $T = 0$, the equivalent conductance for the normal channel is given by

$$G_N(V) = \begin{cases} 0 & \text{for } |V| < 2\Delta/e \\ \frac{1}{R_N} & \text{for } |V| \geq 2\Delta/e \end{cases} . \tag{3.1.3}$$

At finite temperatures thermally excited quasiparticles can tunnel already at voltages smaller than the gap voltage resulting in a finite resistance $R_{sg}(T)$ called ***sub-gap resistance***. The magnitude of the sub-gap resistance, or equivalently the sub-gap conductance, is determined by the amount of thermally excited quasiparticles and can be expressed as

$$G_{sg}(T) = \frac{1}{R_{sg}(T)} = \frac{n(T)}{n_{\text{tot}}} G_N . \tag{3.1.4}$$

Here, $n(T)$ is the density of excited quasiparticles at temperature T and n_{tot} is the total density of electrons in the normal state. Hence, at $T > 0$ we expect that the normal conductance channel can be characterized by the voltage and temperature dependent conductance

$$G_N(V,T) = \begin{cases} \frac{1}{R_{sg}(T)} & \text{for } |V| < 2\Delta(T)/e \\ \frac{1}{R_N} & \text{for } |V| \geq 2\Delta(T)/e \end{cases} . \tag{3.1.5}$$

Here, the fact that the energy gap and thereby the gap voltage is temperature dependent has been included. It is evident that the normal channel results in a ***nonlinear conductance*** $G_N(V,T)$ that depends on voltage and temperature.

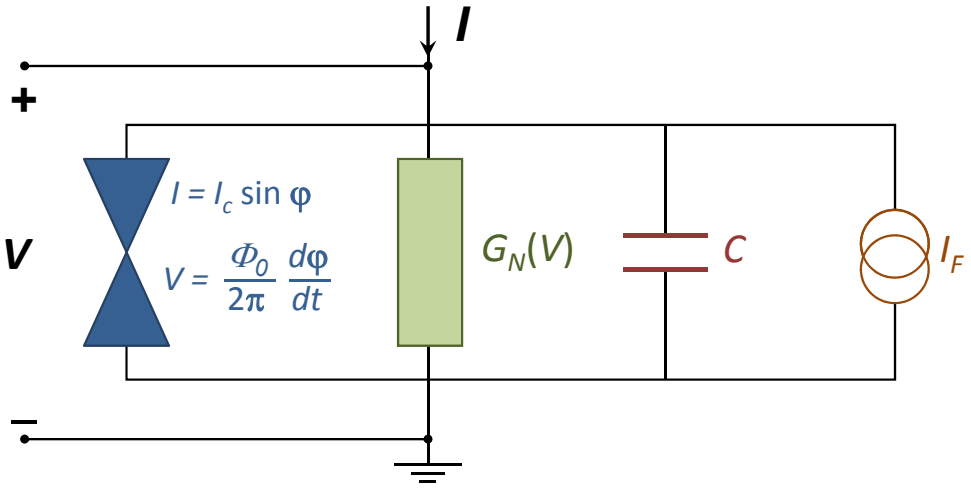

Figure 3.2: Equivalent circuit for a Josephson junction including the Josephson current as well as the normal current and the displacement current channel. Furthermore, noise is taken into account by a noise source providing a fluctuation current.

Our discussion shows that the equivalent circuit of the Josephson junction including the Josephson current and the normal current channel is characterized by a natural current scale I_c and a natural resistance R_N. Therefore, we can define a ***characteristic voltage***

$$V_c \equiv I_c R_N = \frac{I_c}{G_N} , \tag{3.1.6}$$

which usually is called the $I_c R_N$-product of the Josephson junction.

We close this subsection by noting that we did not take into account any frequency dependence of the normal conductance. Of course, at high frequency the normal electrons have to be accelerated resulting in an inductive component of the normal channel and hence in a frequency dependent conductance. However, in most cases the inductance of the superelectron channel dominates over that of the normal channel and therefore we only use a frequency independent conductance for modeling the normal current channel. Finally, we should emphasize that our discussion was focused on Josephson tunnel junctions and did not include other junction types where the Josephson coupling is achieved by a normal metal, a semiconductor, a micro-constriction, etc..

3.1.2 The Displacement Current: Junction Capacitance

In situations where not only V but also its time derivative dV/dt is nonzero, the displacement current I_D plays an important role. For most practical junctions the displacement current can be represented in the usual form

$$I_D = C\frac{dV}{dt} . \tag{3.1.7}$$

Here, C is the junction capacitance, which is the same in the normal and the superconducting state. The capacitance depends on the junction type and its size. For a planar tunnel junction with area A_i and an insulating barrier of thickness d the junction capacitance is just given by

$$C = \frac{\varepsilon\varepsilon_0 A_i}{d} , \tag{3.1.8}$$

where ε is the dielectric constant of the barrier material. The displacement current results in an additional current channel parallel to the Josephson and the normal current channel.

With $V = L_c\dot{I}_s$, $I_N = VG_N$ and $I_D = C\dot{V}$ we can compare the current values in the three different current channels at a given frequency. With $L_s = L_c/\cos\varphi \geq L_c$ and $G_N(V,T) \leq 1/R_N$ we have

$$I_s \leq \frac{V}{\omega L_c} \qquad I_N \leq \frac{V}{R_N} \qquad I_D \simeq \omega C\, V \ . \tag{3.1.9}$$

3.1.3 Characteristic Times and Frequencies

If we characterize the three different current channels in the equivalent circuit shown in Fig. 3.2 by the inductance L_c, the normal resistance R_N and the capacitance C, we immediately can define three characteristic time scales or, equivalently, frequencies. The first one is the ***plasma frequency*** of the junction defined as

$$\omega_p = \frac{1}{\tau_p} \equiv \frac{1}{\sqrt{L_c C}} = \sqrt{\frac{2eI_c}{\hbar C}} \ . \tag{3.1.10}$$

The plasma frequency scales proportional to $\sqrt{J_c/C_A}$, where $C_A = C/A$ is the specific junction capacitance. Evidently, for $\omega < \omega_p$ the displacement current is smaller than the Josephson current.

The second characteristic frequency is related to the L_c/R_N ***time constant*** of the circuit:

$$\omega_c = \frac{1}{\tau_c} \equiv \frac{R_N}{L_c} = \frac{2e}{\hbar} V_c = \frac{2\pi}{\Phi_0} V_c \ . \tag{3.1.11}$$

Here, $L_c = \frac{\hbar}{2eI_c}$ is the Josephson inductance (cf. eq. (2.1.22)) characterizing the superconducting transport channel. We see that ω_c is just the inverse relaxation time in a system consisting of a normal current and a supercurrent. Furthermore, it is seen from (3.1.11) that the characteristic junction frequency ω_c directly follows from the characteristic junction voltage V_c via the second Josephson equation. Therefore, ω_c is usually called the ***characteristic frequency*** of the Josephson junction. Evidently, the normal current is smaller than the critical junction current for $V < V_c$ or equivalently $\omega < \omega_c = R_N/L_c$.

The third characteristic frequency is defined by the $R_N C$ ***time constant*** of the equivalent circuit:

$$\omega_{\mathrm{RC}} = \frac{1}{\tau_{\mathrm{RC}}} \equiv \frac{1}{R_N C} = \frac{\omega_p^2}{\omega_c} \tag{3.1.12}$$

Evidently, the displacement current is smaller than the normal current for $\omega < 1/\tau_{\mathrm{RC}}$.

In order to characterize the capacitance effect at all frequencies up to the frequency ω_c corresponding to the characteristic junction voltage $V_c = I_c R_N$ one can use the dimensionless parameter

$$\beta_C \equiv \frac{\omega_c^2}{\omega_p^2} = \frac{\omega_c}{\omega_{\mathrm{RC}}} = \omega_c \tau_{\mathrm{RC}} = \frac{2e}{\hbar} I_c R_N^2 C \ . \tag{3.1.13}$$

This parameter has been introduced by McCumber[1] and Stewart[2] and therefore is referred to as the ***Stewart-McCumber parameter***. It corresponds to the square of the quality factor

$$Q = \frac{RC}{\sqrt{LC}} = \frac{\omega_p}{\omega_{\mathrm{RC}}} = \frac{\omega_c}{\omega_p} = \sqrt{\beta_C} \tag{3.1.14}$$

of a parallel *LRC* circuit. The quality factor Q compares the decay time constant of the amplitude of an oscillating physical system to its oscillation period. Junctions with $\beta_C \ll 1$ have small capacitance and/or small resistance. These junctions have small R_NC time constants ($\tau_{\mathrm{RC}}\omega_p \ll 1$) and therefore are highly damped. In contrast, junctions with $\beta_C \gg 1$ are those with large capacitance and/or large resistance and hence have a large R_NC time constant ($\tau_{\mathrm{RC}}\omega_p \gg 1$). These junctions are weakly damped.[3]

3.1.4 The Fluctuation Current

In many problems it is important to take into account fluctuations (noise). In most cases, this can be done by using the ***Langevin method***,[4,5] that is, by including a random force in the system equation that describes the fluctuation sources. As we will see below, for Josephson junctions the system equation arises from summing up the different current contributions. Therefore, the random force is just some fluctuation current $I_F(t)$, which is represented by a current noise source in the equivalent circuit shown in Fig. 3.2.

Thermal Noise: There are three different types of fluctuations, namely thermal fluctuations, shot noise and $1/f$ noise. According to the Johnson-Nyquist formula[6,7] for ***thermal noise*** the power spectral density of the current fluctuations are given by

$$S_I(f) = \frac{4k_BT}{R_N} \ . \tag{3.1.15}$$

We note that this expression only holds for an Ohmic resistor at[8]

$$k_BT \gg eV, \hbar\omega \ . \tag{3.1.16}$$

The relative intensity of the thermal noise current can be expressed by the dimensionless parameter given by the ratio of the thermal energy and the coupling energy of the Josephson junction

$$\boxed{\gamma \equiv \frac{k_BT}{E_J} = \frac{2e}{\hbar}\frac{k_BT}{I_c} \ .} \tag{3.1.17}$$

[1] D.E. McCumber, J. Appl. Phys. **39**, 3113 (1968).
[2] W.C. Stewart, Appl. Phys. Lett. **12**, 277 (1968).
[3] Note that for large R_N the conductance of the resistive channel is small and hence results in small damping due to a small normal current.
[4] P. Langevin, *Sur la theorie du mouvement brownien*, Comptes Rendus **146**, 604 (1908).
[5] Sh. Kogan, *Electronic Noise and Fluctuations in Solids*, Cambridge University Press (1996).
[6] H. Nyquist, *Thermal agitation of electric charge in conductors*, Phys. Rev. **32**, 110 (1928).
[7] J.B. Johnson, *Thermal agitation of electricity in conductors*, Phys. Rev. **32**, 97 97 (1928).
[8] The case $\hbar\omega \gg k_BT, eV$ is discussed in section 3.5.5. In this limit quantum fluctuations are dominant.

This equation can be rewritten into the form

$$\gamma \equiv \frac{I_T}{I_C} \qquad \text{with} \qquad I_T = \frac{2e}{\hbar} k_B T \ . \tag{3.1.18}$$

Here, I_T is the equivalent ***thermal noise current***. Inserting numbers we see that $I_T \simeq 0.15\,\mu$A at liquid helium temperature ($T = 4.2$ K).

Shot Noise: If the voltage across the junction is large so that $eV \gg k_B T$ ($V > 0.5$ mV at 4.2 K), then ***shot noise*** is of major importance and we have to use the Schottky formula[9,10] to express the power spectral density of the current fluctuations:

$$S_I(f) = 2eI_N \qquad \text{at} \qquad eV \gg k_B T,\, \hbar\omega \ . \tag{3.1.19}$$

Shot noise consists of random fluctuations of the electric current in an electrical conductor, which are caused by the fact that the current is carried by discrete charges (electrons). Shot noise is to be distinguished from current fluctuations in equilibrium, which happen without any applied voltage and without any average current flowing. These equilibrium current fluctuations are known as Johnson-Nyquist noise discussed above.

Shot noise is a Poisson process and the charge carriers which make up the current will follow a Poissonian distribution. The strength of the current fluctuations can be expressed by the variance

$$\Delta I^2 \equiv \langle (I - \langle I \rangle)^2 \rangle \tag{3.1.20}$$

of the current I, where $\langle I \rangle$ is the average current. However, the value measured in this way depends on the frequency range of fluctuations (bandwidth of the measurement): The measured variance of the current grows linearly with bandwidth. Therefore, a more appropriate quantity is the noise power, which is essentially obtained by dividing through the bandwidth (and, therefore, has the SI units A^2/Hz). It can be defined as the zero-frequency Fourier transform of the current-current correlation function:

$$S(f) = \int_{-\infty}^{+\infty} (\langle I(t)I(0)\rangle - \langle I(0)\rangle^2)\, dt \ . \tag{3.1.21}$$

We note that this expression is the total noise power, which includes the equilibrium fluctuations (Johnson-Nyquist noise).

$1/f$ **Noise:** At low frequencies $1/f$ ***noise*** often is the dominant noise source. In contrast to thermal or shot noise the physical nature of $1/f$ noise is often not clear.[11,12,13] Typically, for Josephson junctions $1/f$ noise becomes dominant only below about 1 kHz. Therefore, in the following we will not consider the effect of $1/f$ noise, since its effect in most cases is negligible compared to the other noise sources.

[9] W. Schottky, *Über spontane Stromschwankungen in verschiedenen elektrischen Leitern*, Ann. Physik **57**, 541 (1918).
[10] W. Schottky, *Small-shot effect and flicker effect*, Phys. Rev. **28**, 74 (1926).
[11] Sh. Kogan, *Electronic Noise and Fluctuations in Solids*, Cambridge University Press (1996).
[12] P. Dutta, P.M. Horn, Rev. Mod. Phys. **53**, 497 (1981)
[13] F.N. Hooge, T.G.M. Kleinpenning, L.K.J. Vandamme, Rep. Prog. Phys. **44**, 532 (1981).

3.1.5 The Basic Junction Equation

According to the discussion of the last subsections there are four essential components in the net current I flowing through the Josephson junction. Kirchhoff's law then requires that

$$I = I_s + I_N + I_D + I_F \ . \tag{3.1.22}$$

This equation together with the voltage-phase relation

$$\frac{d\varphi}{dt} = \frac{2e}{\hbar} V \tag{3.1.23}$$

forms the basic equation for the Josephson junction. From (3.1.22) and (3.1.23) we can calculate $I(t)$ provided that $V(t)$ is known and vice versa. In principle, after writing down this equation with concrete expressions for the different current contributions the solid-state physics part of the problem has been solved.

With the expressions derived above for the normal, the displacement and the fluctuation current we can express (3.1.22) as

$$I = I_c \sin\varphi + G_N(V)V + C\frac{dV}{dt} + I_F \ . \tag{3.1.24}$$

Using (3.1.23) we obtain

$$\boxed{I = I_c \sin\varphi + G_N(V)\,\frac{\Phi_0}{2\pi}\frac{d\varphi}{dt} + C\,\frac{\Phi_0}{2\pi}\frac{d^2\varphi}{dt^2} + I_F \ .} \tag{3.1.25}$$

This equation is nonlinear with nonlinear coefficients. Due to these nonlinearities concepts such as superposition fail. Furthermore, a nonintuitive behavior is obtained. For example, a dc driving current results in a time-dependent voltage. In general, the behavior of the Josephson junction in the voltage state is governed by a complex differential equation, which in most cases has to be solved numerically. In the following we will make some simplifying assumptions to arrive at simple solutions of (3.1.25).

3.2 The Resistively and Capacitively Shunted Junction Model

To gain some insight into the dynamics of the Josephson junction we simplify the model by taking the normal conductance to be constant. That is, we assume

$$G_N(V) \quad = \quad G = \frac{1}{R} = const \ . \tag{3.2.1}$$

We then arrive at the ***Resistively and Capacitively Shunted Junction*** (RCSJ) model. The equivalent circuit of this model is shown in Fig. 3.3. The Josephson junction is characterized by the Josephson inductance $L_s = L_c/\cos\varphi$ with $L_c = \hbar/2eI_c$ and the resistance R is usually taken to be the normal resistance of the junction. However, more generally we can interpret R to be given by (3.1.5), so that the resistance is given by R_{sg}, if the average junction voltage is below the gap voltage, and is R_N, when the average voltage is above the gap voltage. Of course this description can only be approximate, since the junction voltage is time dependent. Nevertheless, the RCSJ-model will result in a still nonlinear but tractable differential equation. Rewriting (3.1.25) we obtain

$$\left(\frac{\hbar}{2e}\right) C \frac{d^2\varphi}{dt^2} + \left(\frac{\hbar}{2e}\right) \frac{1}{R}\frac{d\varphi}{dt} + I_c \left[\sin\varphi - \frac{I}{I_c} + \frac{I_F(t)}{I_c}\right] \quad = \quad 0 \ . \tag{3.2.2}$$

Multiply by $\frac{\hbar}{2e}$ and using the Josephson coupling energy $E_{J0} = \hbar I_c/2e$ and the normalized currents

$$i \quad = \quad \frac{I}{I_c} \qquad\qquad i_F(t) \ = \ \frac{I_F(t)}{I_c} \tag{3.2.3}$$

we obtain

$$\left(\frac{\hbar}{2e}\right)^2 C \frac{d^2\varphi}{dt^2} + \left(\frac{\hbar}{2e}\right)^2 \frac{1}{R}\frac{d\varphi}{dt} + \frac{d}{d\varphi}\left\{E_{J0}\left[1 - \cos\varphi - i\varphi + i_F(t)\varphi\right]\right\} \quad = \quad 0 \ . \tag{3.2.4}$$

In order to interpret this equation of motion we compare it to the equation of motion of a particle with mass M and damping η in the potential U:

$$M\frac{d^2x}{dt^2} + \eta\frac{dx}{dt} + \nabla U \quad = \quad 0 \ . \tag{3.2.5}$$

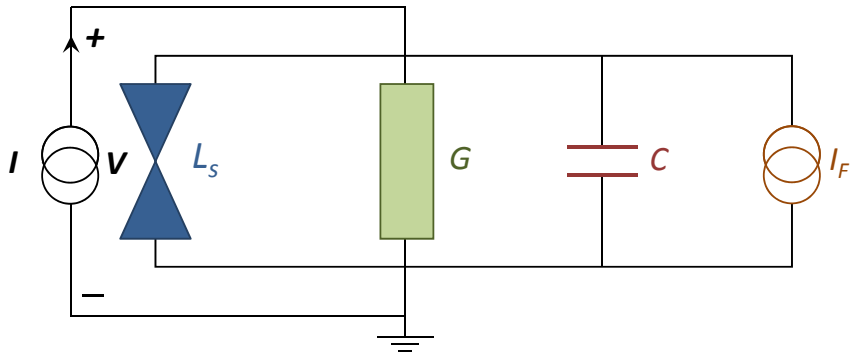

Figure 3.3: Equivalent circuit for the Resistively and Capacitively Shunted Junction (RCSJ) Model. The Josephson junction can be characterized by the inductance $L_s = L_c/\cos\varphi$ with $L_c = \hbar/2eI_c$, the resistive channel is approximated by a voltage independent conductance G.

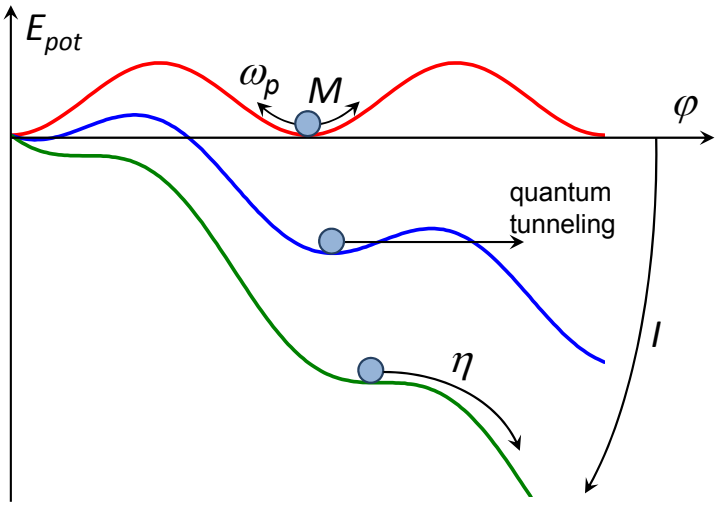

Figure 3.4: Analogy between the motion of the gauge-invariant phase difference of a Josephson junction and the damped motion of a particle of mass M in the tilt washboard potential. Note that the applied currents result in a tilt of the potential.

We immediately see that the equation of motion of the gauge-invariant phase difference of a Josephson junction is equivalent to the motion of a particle of mass M and damping η in a potential U with

$$M = \left(\frac{\hbar}{2e}\right)^2 C \tag{3.2.6}$$

$$\eta = \left(\frac{\hbar}{2e}\right)^2 \frac{1}{R} \tag{3.2.7}$$

$$U = E_{J0}\left[1-\cos\varphi - i\varphi + i_F(t)\varphi\right] \ . \tag{3.2.8}$$

This situation is visualized in Fig. 3.4. We see that the mass of the particle is proportional to the capacitance and the damping proportional to $1/R$. Furthermore, the potential U is nothing else than the ***tilt washboard potential*** (cf. eq. (2.1.14)).

Equation (3.2.4) is often written in reduced units. By using the normalized time

$$\tau \equiv \frac{t}{\tau_c} = \frac{t}{2eI_cR/\hbar} \tag{3.2.9}$$

as well as the Stewart-McCumber parameter β_C (cf. (3.1.13)) we can write the basic equation (3.2.4) describing the Josephson junction within the RCSJ approximation as

$$\boxed{\beta_C \frac{d^2\varphi}{d\tau^2} + \frac{d\varphi}{d\tau} + \sin\varphi - i - i_F(\tau) = 0 \ .} \tag{3.2.10}$$

We can use the analogy between the motion of the phase and that of a particle to discuss the meaning of the plasma frequency.[14] If we neglect damping and consider the case of zero driving current (horizontal potential in Fig. 3.4) and small amplitudes ($\sin\varphi \simeq \varphi$), we can write (3.2.10) as

$$\beta_C \frac{d^2\varphi}{d\tau^2} + \varphi = 0 \ . \tag{3.2.11}$$

[14]The expression plasma oscillation is used, since the oscillations show the same dispersion as plasma oscillations.

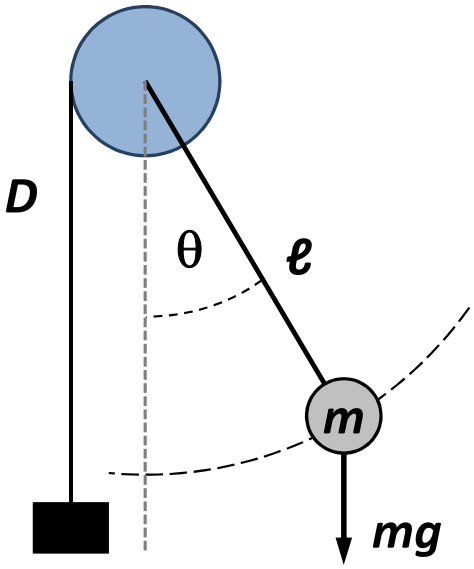

Figure 3.5: The pendulum analogue of a Josephson junction. The torque D deflecting the pendulum is represented by an unwinding mass.

The solution of this equation is

$$\varphi \;=\; c\cdot\exp\left(\imath\frac{\tau}{\sqrt{\beta_C}}\right) \;=\; c\cdot\exp\left(\imath\frac{t}{\sqrt{\beta_C}\tau_c}\right) \;=\; c\cdot\exp\left(\imath\omega_p t\right)\;. \tag{3.2.12}$$

That is, the plasma frequency represents the oscillation frequency of the particle around the potential minimum at small amplitudes.

We also note that there is a finite probability of the particle to tunnel through the potential well. This process is known as the macroscopic quantum tunneling of the gauge-invariant phase difference and has been observed experimentally. Furthermore, the phase particle can escape from the potential well by thermal activation. These processes will be discussed in sections 3.5.6 and 3.4, respectively.

The pendulum analogue

Besides the motion of a particle of mass M in the tilt washboard potential another mechanical analogue whose dynamics is described by an equation of the form (3.2.10) is the physical pendulum (see Fig. 3.5). We consider a pendulum of mass m and length ℓ that is deflected by an angle θ with respect to the normal by a torque D directed parallel to the rotation axis. The restoring torque is given by the length ℓ of the pendulum times the gravitational force $mg\sin\theta$. With these expressions we obtain the following equation of motion:

$$D \;=\; \Theta\,\ddot{\theta}+\Gamma\,\dot{\theta}+mg\ell\,\sin\theta\;. \tag{3.2.13}$$

Here, $\Theta = m\ell^2$ is the moment of inertia of the pendulum. The term $\Gamma\dot{\theta}$ describes the damping of the pendulum with the damping constant Γ.

If we compare (3.2.13) to (3.1.25) we immediately see that both equations are equivalent with the assignments $I \leftrightarrow D$, $I_c \leftrightarrow mg\ell$, $\Phi_0/2\pi R \leftrightarrow \Gamma$, and $C\Phi_0/2\pi \leftrightarrow \Theta$. The angle θ corresponds to the

gauge invariant phase difference φ. Hence, in order to analyze the dynamics of the Josephson junction we just can consider the dynamics of an oscillating or rotating pendulum. For example, for $D = 0$ we can consider the oscillations of the pendulum around is equilibrium position. The oscillation frequency is $\omega = \sqrt{mg\ell/\Theta} = \sqrt{g/\ell}$. This frequency of course corresponds to the plasma frequency $\omega_p = \sqrt{2\pi I_c/\Phi_0 C}$ of the Josephson junction what can be easily shown with the above assignments. A finite torque acting on the pendulum corresponds to a finite current applied to the Josephson junction. It results in a finite deflection angle θ_0 of the pendulum or, equivalently, a finite value φ_0 of the phase difference across the Josephson junction. If the torque is large enough to deflect the pendulum by 90° (corresponding to $J_s = J_c \sin\varphi = J_c$), any further increase of the torque results in a rotation of the pendulum. In this case the average angular velocity $\dot{\theta}$ is larger than zero. Equivalently, $\dot{\varphi} > 0$ corresponds to the finite voltage state of the Josephson junction.

3.2.1 Underdamped and Overdamped Josephson Junctions

The analogy between the motion of a "phase" particle in the tilt washboard potential and the motion of the gauge-invariant phase difference of a Josephson junction can be used to discuss the difference between underdamped and overdamped Josephson junctions. For underdamped Josephson junctions ($\beta_C = 2eI_cR^2C/\hbar \gg 1$) the junction capacitance and/or the resistance are large. This means that the mass $M \propto C$ of the particle is large and/or the damping $\eta \propto 1/R$ is small. In contrast, for overdamped junctions ($\beta_C = 2eI_cR^2C/\hbar \ll 1$) the junction capacitance and/or the resistance are small, that is, the mass M of the particle is small and/or the damping η is large.

Discussing the motion of the phase particle for this two limiting cases we start at an applied current larger than the critical current, that is, at a strong tilt of the potential so that the particle can move freely down the potential. Reducing the current we are reducing the tilt of the potential until at $I < I_c$ local minima are obtained. In the case of strong damping the particle will immediately stop its motion and will be trapped in one of the local minima. This is due to the small mass or equivalently small kinetic energy of the particle and the large damping. For the Josephson junction this means that the phase does no longer evolve in time and the junction switches into the zero voltage state as soon as the applied current is reduced below I_c (see Fig. 3.6a). The situation is completely different in the case of small damping. In this case the massive particle has sufficient kinetic energy and due to the small damping can easily move down the potential well even if there are local minima. In order to stop the particle, we have to bring the potential almost to the horizontal position. For the Josephson junction this means that we have to reduce the current almost to zero to achieve the zero voltage state of the junction (see Fig. 3.6b).

Starting from the zero voltage state at zero applied current and then increasing the current, both the under- and overdamped junction stay in the zero voltage state until the critical current is reached. In both cases the kinetic energy of the particle is zero and there is no reason why it should move down the potential well (we are neglecting thermally activated processes or quantum tunneling of the phase). However, above the critical current the behavior is different again. Whereas in the strongly damped case the particle is moving slowly (corresponding to small voltage) at currents slightly above I_c due to the strong damping, in the underdamped case the particle is immediately accelerating to an average velocity corresponding to the average slope of the potential and the amount of damping.

This different behavior results in different current-voltage characteristics of under- and overdamped Josephson junctions. Whereas for overdamped junctions the same IVC is obtained for increasing and decreasing current, for the underdamped junction the average voltage depends on whether one is decreasing or increasing the current. Decreasing the current the underdamped junction stays in the voltage state also below I_c due to the large kinetic energy and the small damping of the moving phase. Increasing the current from zero current the underdamped junction stays in the zero voltage state until the critical current, because now the particle has no kinetic energy and will therefore stay in the potential minimum

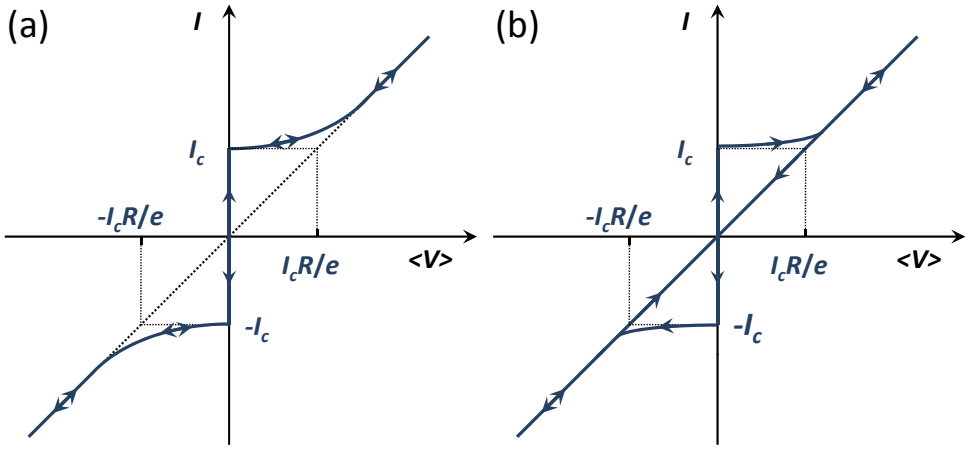

Figure 3.6: Current-voltage characteristics of an overdamped (a) and underdamped (b) Josephson junction. The arrows indicate the direction of the current variation.

even at small damping. In summary, this results in a hysteretic IVC of the underdamped Josephson junction as shown schematically in Fig. 3.6b. In contrast, for overdamped junctions the mass of the phase particle and, hence, its kinetic energy is small and/or the damping is large. Therefore, the motion of the phase particle is the same for increasing and decreasing the applied current. That is, overdamped junctions do not have hysteretic IVCs.

3.3 Response to Driving Sources

In the following subsections we will use the RCSJ-model to discuss the response of a Josephson junction to external driving sources quantitatively.

3.3.1 Response to a dc Current Source

We first discuss the response of a Josephson junction to a dc current source. Doing so we start to consider the time-averaged voltage of the junction in the presence of an applied dc current. We recall that in the voltage state we have an oscillating Josephson current. With the oscillation period T we can write

$$\langle V \rangle \;=\; \frac{1}{T}\int_0^T V(t)\,dt \;=\; \frac{1}{T}\int_0^T \frac{\hbar}{2e}\,\frac{d\varphi}{dt}\,dt \;=\; \frac{1}{T}\,\frac{\hbar}{2e}[\varphi(T)-\varphi(0)] \;=\; \frac{\Phi_0}{T}\;. \tag{3.3.1}$$

Here, we have used the fact that during one oscillation period the phase difference changes by 2π, that is, $\varphi(T)-\varphi(0)=2\pi$. We see that the time-averaged voltage of the junction is determined by the flux quantum divided by the oscillation period.

We also have to recall that for a driving dc current source the total current of the junction has to be constant and equal to the driving current. That is, neglecting the fluctuation current we have to satisfy the condition

$$I \;=\; I_s(t)+I_N(t)+I_D(t) \;=\; I_c\sin\varphi(t)+\frac{V(t)}{R}+C\frac{dV(t)}{dt} \;=\; const\;, \tag{3.3.2}$$

where

$$\varphi(t) \;=\; \int_0^t \frac{2e}{\hbar}\,V(t')\,dt'\;. \tag{3.3.3}$$

We see, that for $I > I_c$ part of the current has to flow as normal or displacement current. This is only possible of course at a finite junction voltage. The finite junction voltage, in turn, results in a time varying Josephson current and, since the total current is fixed, in a temporal variation of the sum of the normal and displacement current. This results in a time varying voltage $V(t)$ and an even more complicated non-sinusoidal oscillation of the Josephson current. The oscillating voltage has to be calculated self-consistently. We immediately see that the oscillation period is $T=\Phi_0/\langle V\rangle$. The oscillation frequency is then $f=\langle V\rangle/\Phi_0$, which is just the Josephson frequency for a junction with an applied voltage equal to the average junction voltage. Of course the normal current has the same periodicity, since the sum of the currents is fixed by the applied current.

Fig. 3.7 shows the oscillating junction voltage for an applied current slightly above the critical current and for $I \gg I_c$. For $I \gtrsim I_c$, we have a highly non-sinusoidal oscillation with a long oscillation period. The time averaged voltage, which is proportional to $1/T$ is very low. In the case $I \gg I_c$, most of the current has to flow as a normal current resulting in a more constant junction voltage. That is, the relative oscillation of the junction voltage is small. Then, the oscillation of the Josephson current and, in turn, the normal current is almost sinusoidal resulting in an about sinusoidal variation of the junction voltage. Note that for a sinusoidal oscillation of the Josephson current the time-average of the Josephson current is zero. This results in a linear dependence of the time averaged voltage on the current, that is, in an ohmic IVC.

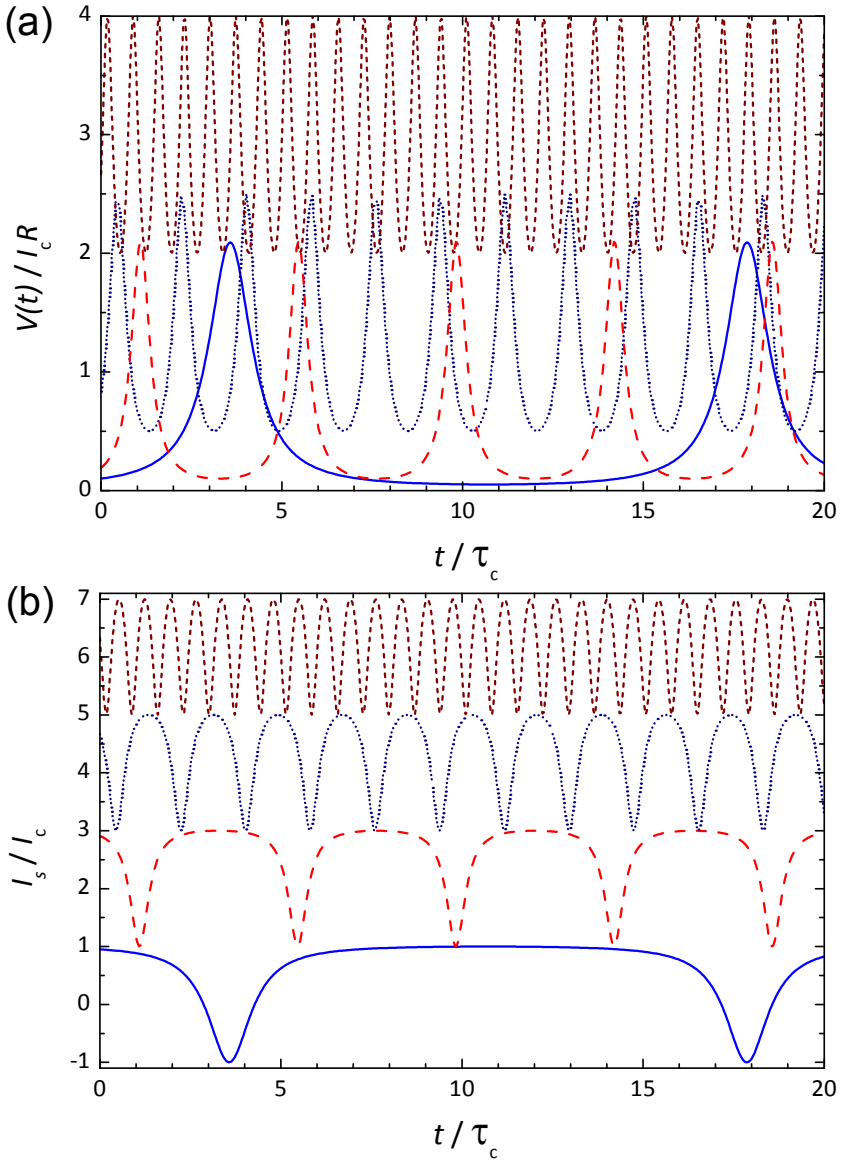

Figure 3.7: The variation of the junction voltage (a) and the Josephson current (b) with time for a current biased Josephson junction at different values of the applied current: $I/I_c = 1.05$, 1.1, 1.5, and 3.0. The time is normalized to $\tau_c = \hbar/2eI_cR$. In (b) the curves for $I_s/I_c = 1.1$, 1.5, and 3.0 are displaced vertically by 2, 4, and 6, respectively.

Current-Voltage Characteristics

Strong Damping: For strong damping, $\beta_C \ll 1$, and neglecting the noise current we can rewrite (3.2.10) as

$$\frac{d\varphi}{d\tau} + \sin\varphi - i = 0 \ . \tag{3.3.4}$$

If $I \leq I_c$ (i.e. $i \leq 1$), we expect that all current is flowing as supercurrent. Indeed we see that

$$\varphi = \sin^{-1} i \qquad \text{for} \quad i \leq 1 \tag{3.3.5}$$

is a solution, since φ does not depend on time. The voltage-phase relation then implies that the junction is in the zero voltage state.

When $i > 1$, the current can no longer flow as a pure supercurrent. Some of the current has to flow through the resistive channel creating a finite junction voltage that will cause a temporal evolution of the phase. Then, the full time dependence of (3.3.4) is required. Equation (3.3.4) can be solved by rewriting it as

$$d\tau = \frac{d\varphi}{i - \sin\varphi} \ . \tag{3.3.6}$$

Integration results in a periodic function $\varphi(t)$ with period[15]

$$T = \frac{2\pi\tau_c}{\sqrt{i^2-1}} \ . \tag{3.3.7}$$

With $\langle V(t)\rangle = \frac{1}{T}\int_0^T V(t)\,dt = \frac{\Phi_0}{T}$ (cf. (3.3.1)) and using $\tau_c = \frac{\Phi_0}{2\pi}\frac{1}{I_c R}$, we obtain

$$\langle V(t)\rangle = I_c R\sqrt{\left(\frac{I}{I_c}\right)^2 - 1} \qquad \text{for} \quad \frac{I}{I_c} > 1 \ . \tag{3.3.8}$$

This current versus time-averaged voltage curve is shown in Fig. 3.8. For $I \leq I_c$, the gauge-invariant phase difference increases according to (3.3.5), but the voltage remains zero. As the applied current exceeds the critical current I_c, part of the current must flow as a normal current through the resistive channel thereby creating a nonvanishing voltage across the junction. This results in an oscillation of the Josephson current and, in turn, of the normal current, since the total current is fixed by the external circuit. In total this results in a complex oscillation of the junction voltage as shown in Fig. 3.7. The time-averaged junction voltage is just given by the flux quantum divided by the oscillation period T.

[15] From the table of integrals we know that for $a^2 > 1$ we have

$$\int \frac{dx}{a - \sin x} = \frac{2}{\sqrt{a^2-1}} \tan^{-1}\left(\frac{-1 + a\,\tan(x/2)}{\sqrt{a^2-1}}\right) \ .$$

Integration of (3.3.6) then yields

$$\tau - \tau_0 = \frac{2}{\sqrt{i^2-1}} \tan^{-1}\left(\frac{-1 + i\,\tan(\varphi/2)}{\sqrt{i^2-1}}\right) \qquad \text{for } i > 1 \ .$$

Here, τ_0 is an integration constant. Recalling that $\tau = t/\tau_c$ and setting the integration constant equal to zero, we can solve this equation for the gauge-invariant phase difference:

$$\varphi(t) = 2\tan^{-1}\left\{\sqrt{1 - \frac{1}{i^2}}\,\tan\left(\frac{t\sqrt{i^2-1}}{2\tau_c}\right) + \frac{1}{i}\right\} \ .$$

Although this equation is quite complex we see that $\varphi(t)$ is periodic with a period

$$T = \frac{2\pi\tau_c}{\sqrt{i^2-1}} \ .$$

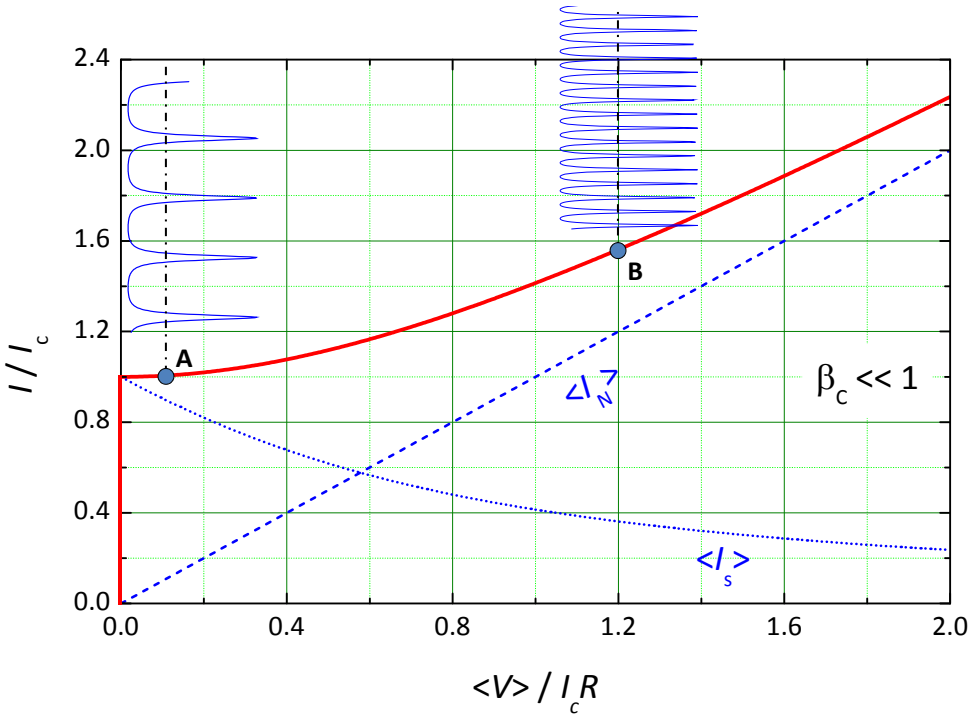

Figure 3.8: Current versus time-averaged voltage for an overdamped Josephson junction ($\beta_C \ll 1$). Also shown are the time-averaged components of the normal and the supercurrent as well as the time evolution of the junction voltage $V(t)$ for two bias points A and B on the IVC.

Weak Damping: In the underdamped case, $\beta_C \gg 1$, the characteristic frequency $\omega_{\rm RC} = 1/R_N C$ is very small. Therefore, at almost all frequencies the large junction capacitance is effectively shunting the oscillating part of the junction voltage so that the junction voltage is almost constant: $V(t) \simeq \overline{V}$. Accordingly, the time evolution of the phase is almost linear

$$\varphi(t) \;=\; \frac{2e}{\hbar}\,\overline{V}\,t + const \;. \tag{3.3.9}$$

The almost linear time dependence of the gauge-invariant phase difference in turn results in an about sinusoidal oscillation of the Josephson current with a vanishing mean value

$$\overline{I_s(t)} \;=\; \overline{I_c \sin\left(\frac{2e}{\hbar}\overline{V}t + const\right)} \;\simeq\; 0 \;. \tag{3.3.10}$$

Thus, the total current has to be carried almost completely by the resistive channel and the IVC is given by an ohmic dependence

$$\overline{I} \;=\; I_N(\overline{V}) \;=\; \frac{\overline{V}}{R} \tag{3.3.11}$$

down to low voltages $\overline{V} \simeq \hbar\omega_{\rm RC}/e \ll V_c = I_c R_N$. Since the related current is $\overline{I} \ll I_c$, this results in a hysteretic IVC as already discussed qualitatively above. Recall that for a real junction we have a voltage dependent normal resistance $R = R(V)$. Then, the IVC is determined by the voltage dependence of the normal resistance.

Additional Topic

Intermediate Damping: For $\beta_C \sim 1$, the calculation of the IVC cannot be carried out analytically even for the simplest model. Examples for numerical calculations can be found in literature.[16] These calculations show that with increasing McCumber parameter the IVCs become more hysteretic (see Fig. 3.9a). The so-called ***return-current*** I_R, at which the junction switches back to the zero-voltage state is decreasing with increasing β_C. With finite damping, the return current is determined by the tilt of the washboard at which the energy dissipated in advancing the phase from one minimum to the adjacent exactly equals the work done by the drive current during this same motion. Using this criterion, we can calculate the normalized return current $i_R = I_R/I_c$ analytically for $\beta_C \gg 1$.

If the applied current I is close to I_R and thus for $\beta_C \gg 1$ much smaller than I_c, we can neglect both the normal current and the damping in zeroth order approximation. The junction equation than reads as $I = I_c \sin\varphi + C\frac{\phi_0}{2\pi}\frac{d^2\varphi}{dt^2}$. In this case the energy is conserved and is equal to the work $\int F dx$ (compare section 2.1.3) done by the drive current. Here, the generalized force is given by the current and the generalized coordinate x by $\frac{\phi_0}{2\pi}\varphi$. That is, the energy is given by the first integral of the junction equation:

$$\begin{aligned} E &= \frac{\phi_0}{2\pi}\int_0^{\varphi} I\, d\varphi' = \frac{\phi_0}{2\pi}\int_0^{\varphi}\left(I_c\sin\varphi' + C\frac{\phi_0}{2\pi}\frac{d^2\varphi'}{dt^2}\right) d\varphi' \\ &= \frac{\Phi_0 I_c}{2\pi}\left[(1-\cos\varphi) + \frac{1}{\omega_p^2}\int_0^{t}\frac{d^2\varphi}{dt'^2}\frac{d\varphi}{dt'}\, dt'\right] \\ &= E_{J0}\left\{\frac{1}{2}\frac{1}{\omega_p^2}\left(\frac{d\varphi}{dt}\right)^2 + (1-\cos\varphi)\right\} . \end{aligned} \tag{3.3.12}$$

Here, we have used $E_{J0} = \frac{\Phi_0 I_c}{2\pi}$ and $\omega_p^2 = \frac{2\pi I_c}{\Phi_0 C}$. Using this equation the energy dissipation can be expressed explicitly. Within the RCSJ model we obtain

$$\begin{aligned} W_{\rm diss} &= \int_0^T I_N V dt = \int_0^T I_N \frac{\hbar}{2e}\frac{d\varphi}{dt}\, dt = \int_0^{2\pi}\frac{V}{R}\frac{\hbar}{2e}\, d\varphi = \int_0^{2\pi}\left(\frac{d\varphi}{dt}\right)\left(\frac{\hbar}{2e}\right)^2\frac{1}{R}\, d\varphi \\ &= \frac{\Phi_0 V_p}{2\pi R}\int_o^{2\pi}\left\{2\left(\frac{E}{E_{J0}} - 1 + \cos\varphi\right)\right\}^{1/2} d\varphi . \end{aligned} \tag{3.3.13}$$

Here, we have used $d\varphi/dt$) from (3.3.12) and the plasma voltage

$$V_p = \omega_p\frac{\Phi_0}{2\pi} = \omega_p\frac{\hbar}{2e} = \frac{V_c}{\sqrt{\beta_C}} . \tag{3.3.14}$$

The resistive state is only possible, if the minimum value of the junction kinetic energy is positive, that is, if $E \geq 2E_{J0}$. Thus, the limit $I = I_R$ corresponds to $E = 2E_{J0}$. In this limit the right hand side of (3.3.13) can be calculated resulting in

$$W_{\rm diss} = 4\frac{\Phi_0 I_c}{\pi}\frac{1}{\sqrt{\beta_C}} \tag{3.3.15}$$

[16] K. K. Likharev, *Dynamics of Josephson Junctions and Circuits*, Gordon and Breach Science Publishers, New York (1986).

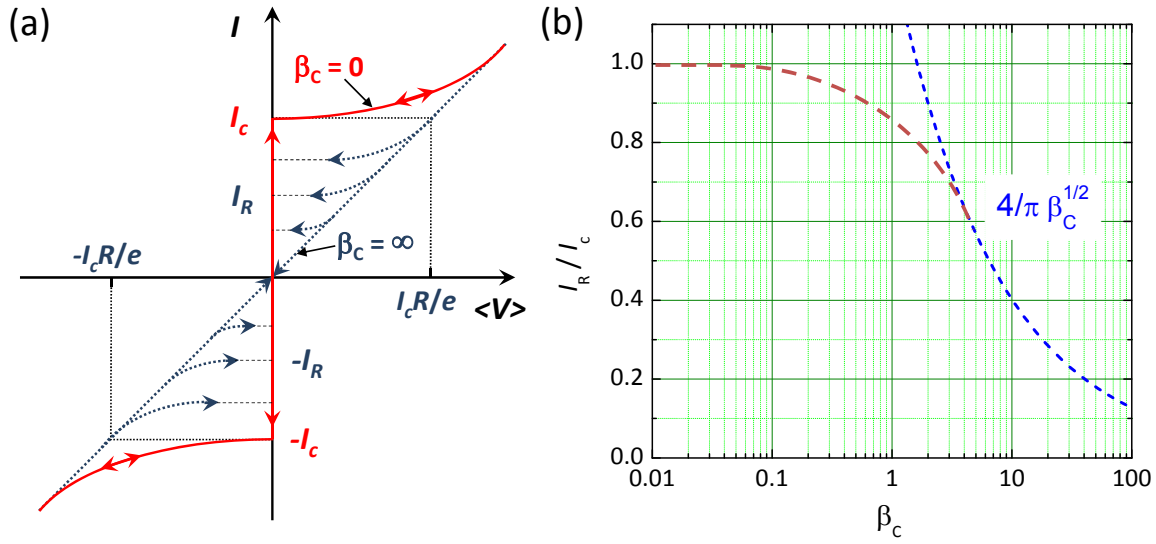

Figure 3.9: (a) RCSJ model IVCs at intermediate damping. The arrows mark the return current values I_R at which the junction jumps back to the zero-voltage state. (b) The normalized return current I_R/I_c plotted versus the Stewart-McCumber parameter β_C. The dashed line shows the large β_C approximation according to equation (3.3.16). The dotted line qualitatively shows the behavior at large damping (low β_C).

and hence in

$$\frac{I_R}{I_c} = \frac{4}{\pi}\frac{1}{\sqrt{\beta_C}} . \tag{3.3.16}$$

This result is plotted in Fig. 3.9b. Note that it is valid only for $\beta_C \gg 1$.

3.3.2 Response to a dc Voltage Source

If we drive the junction by a dc voltage source, the phase difference will evolve linearly in time as $\varphi(t) = \frac{2e}{\hbar}V_{dc}t + const$ and, in turn, the Josephson current $I_s(t) = I_c \sin\varphi(t)$ will oscillate sinusoidally. Then, the time average of the Josephson current is zero. Furthermore, since $dV/dt = 0$, also the displacement current is zero. Accordingly, the total current has to be carried by the normal current resulting in the IVC

$$I = \frac{V_{dc}}{R_N} . \tag{3.3.17}$$

That is, within the RCSJ model we obtain a simple ohmic dependence. In the more general case we have a voltage dependent resistance $R_N(V)$ and hence a nonlinear IVC.

3.3.3 Response to ac Driving Sources

In the previous section we have considered the response of a Josephson junction driven by a dc source. We now use the RCSJ model to analyze the dynamics of a Josephson junction driven both by an ac and dc source. We will see that the response of the supercurrent gives rise to constant-voltage ***Shapiro steps***[17] in the IVCs, whereas the ***photon-assisted tunneling*** response of the quasiparticles gives rise to shifted images of the energy gap structure in the IVCs.

[17] S. Shapiro, Phys. Rev. Lett. **11**, 80 (1963).

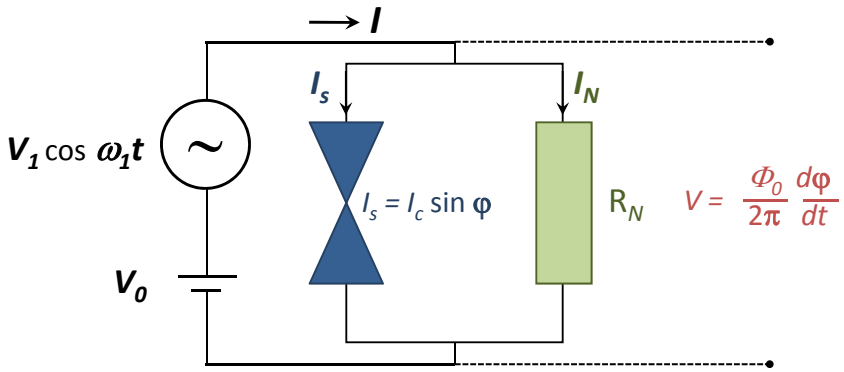

Figure 3.10: A dc and ac voltage source attached to an overdamped Josephson junction. The capacitance of the junction is assumed to be negligibly small (large damping, $\beta_C \ll 1$).

Response to an ac Voltage Source, Strong Damping

We first consider the most simple case of strong damping, $\beta_C \ll 1$, and an applied voltage

$$V(t) = V_{\rm dc} + V_1 \cos \omega_1 t \ . \tag{3.3.18}$$

The equivalent circuit for this situation is shown in Fig. 3.10. From the integration of the voltage-phase relation we obtain

$$\varphi(t) = \varphi_0 + \frac{2\pi}{\Phi_0} V_{\rm dc} t + \frac{2\pi}{\Phi_0} \frac{V_1}{\omega_1} \sin \omega_1 t \ , \tag{3.3.19}$$

where φ_0 is an integration constant. Inserting this into the current-phase relation we obtain

$$I_s(t) = I_c \sin \left\{ \varphi_0 + \frac{2\pi}{\Phi_0} V_{\rm dc} t + \frac{2\pi}{\Phi_0} \frac{V_1}{\omega_1} \sin \omega_1 t \right\} \ . \tag{3.3.20}$$

We see that the frequency of the Josephson current is a superposition of the constant frequency $\omega_{\rm dc} = \frac{2\pi}{\Phi_0} V_{\rm dc}$ and a sinusoidally varying phase. Therefore, the frequency of the current is not the same as that of the driving ac voltage source. The reason for this is the fact that the nonlinear current-phase relation can couple different frequencies with the driving frequency.

In order to analyze the time dependence of the Josephson current we rewrite (3.3.20) as a Fourier series. In order to do so we use the Fourier-Bessel series identity

$$e^{\imath b \sin x} = \sum_{n=-\infty}^{+\infty} \mathcal{J}_n(b)\, e^{\imath n x} \ . \tag{3.3.21}$$

Here, $\mathcal{J}_n$ is the n^{th} order Bessel function of first kind. It is evident from (3.3.20) that the argument of the sine function is of the form $(a + b \sin x)$. Hence, in order to use the identity (3.3.21) we write

$$\sin(a + b \sin x) = \Im \left\{ e^{\imath (a + b \sin x)} \right\} \ . \tag{3.3.22}$$

The Fourier-Bessel series together with the fact that $\mathcal{J}_{-n}(b) = (-1)^n \mathcal{J}_n(b)$ allows us to write

$$e^{\imath (a + b \sin x)} = \sum_{n=-\infty}^{+\infty} \mathcal{J}_n(b)\, e^{\imath (a + n x)} = \sum_{n=-\infty}^{+\infty} (-1)^n \mathcal{J}_n(b)\, e^{\imath (a - n x)} \ . \tag{3.3.23}$$

Finally, the imaginary part of (3.3.22) then gives

$$\sin(a+b\sin x) \;=\; \sum_{n=-\infty}^{+\infty}(-1)^n\,\mathscr{J}_n(b)\,\sin(a-nx)\;. \tag{3.3.24}$$

With $x=\omega_1 t$, $b=\frac{2\pi V_1}{\Phi_0\omega_1}$ and $a=\varphi_0+\omega_{\rm dc}t=\varphi_0+\frac{2\pi}{\Phi_0}V_{\rm dc}t$, we can rewrite the current equation (3.3.20) as

$$\boxed{I_s(t) \;=\; I_c\sum_{n=-\infty}^{+\infty}(-1)^n\,\mathscr{J}_n\left(\frac{2\pi V_1}{\Phi_0\omega_1}\right)\sin\left[(\omega_{\rm dc}-n\omega_1)t+\varphi_0\right]\;.} \tag{3.3.25}$$

We see that due to the nonlinear current-phase relation we obtain a current response, in which the frequency $\omega_{\rm dc}$ couples to multiples of the driving frequency ω_1.

The most interesting aspect of (3.3.25) is the fact that the ac voltage source driving the junction can result in a dc current (denoted as Shapiro steps), if the argument of the sine function becomes zero. That is, we obtain a dc current response for

$$\boxed{\omega_{\rm dc} \;=\; n\omega_1 \qquad\text{or}\qquad V_{\rm dc} \;=\; V_n \;=\; n\,\frac{\Phi_0}{2\pi}\,\omega_1\;.} \tag{3.3.26}$$

For a specific n the amplitude of the average dc current is

$$\boxed{|\langle I_s\rangle_n| \;=\; I_c\left|\mathscr{J}_n\left(\frac{2\pi V_1}{\Phi_0\omega_1}\right)\right|} \tag{3.3.27}$$

with the detailed value depending on the initial value φ_0 (see inset of Fig. 3.11).

For all other voltages $V_{\rm dc}\neq V_n$ we have a series of sinusoidally time dependent terms with a vanishing dc component. Thus, for $V_{\rm dc}\neq V_n$ we have

$$\langle I\rangle \;=\; \frac{V_{\rm dc}}{R_N}+\langle\frac{V_1}{R_N}\cos\omega_1 t\rangle \;=\; \frac{V_{\rm dc}}{R_N}\;. \tag{3.3.28}$$

We see that all the current has to be carried by the normal current resulting in an ohmic behavior. Only for $V_{\rm dc}=V_n$ an average dc Josephson current appears. With respect to the IVCs this means that we have an ohmic dependence with sharp current spikes at $V_{\rm dc}=V_n$ (see Fig. 3.11). The amplitude of the current spikes is given by (3.3.27) and depends on the amplitude V_1 of the ac source. The appearance of current steps at fixed voltages V_n that already has been predicted by **B. Josephson** is due to the formation of higher harmonics of the signal frequency due to the nonlinearity of the Josephson junction. The n^{th} step corresponds to the phase locking of the junction oscillation by this n^{th} harmonic.

When we are applying for example an ac driving voltage source with $\omega_1/2\pi=10\,$GHz for various values of the applied dc voltage $V_{\rm dc}$, a constant dc current will appear at $V_{\rm dc}=0$ and $V_n=n\,\frac{\Phi_0}{2\pi}\,\omega_1\simeq n\cdot 20\,\mu$V. That is, we obtain current steps in the IVCs, which have constant spacing $\delta V=\frac{\Phi_0}{2\pi}\,\omega_1\simeq 20\,\mu$V. Note that the spacing only depends on the frequency of the ac voltage source and on fundamental constants.

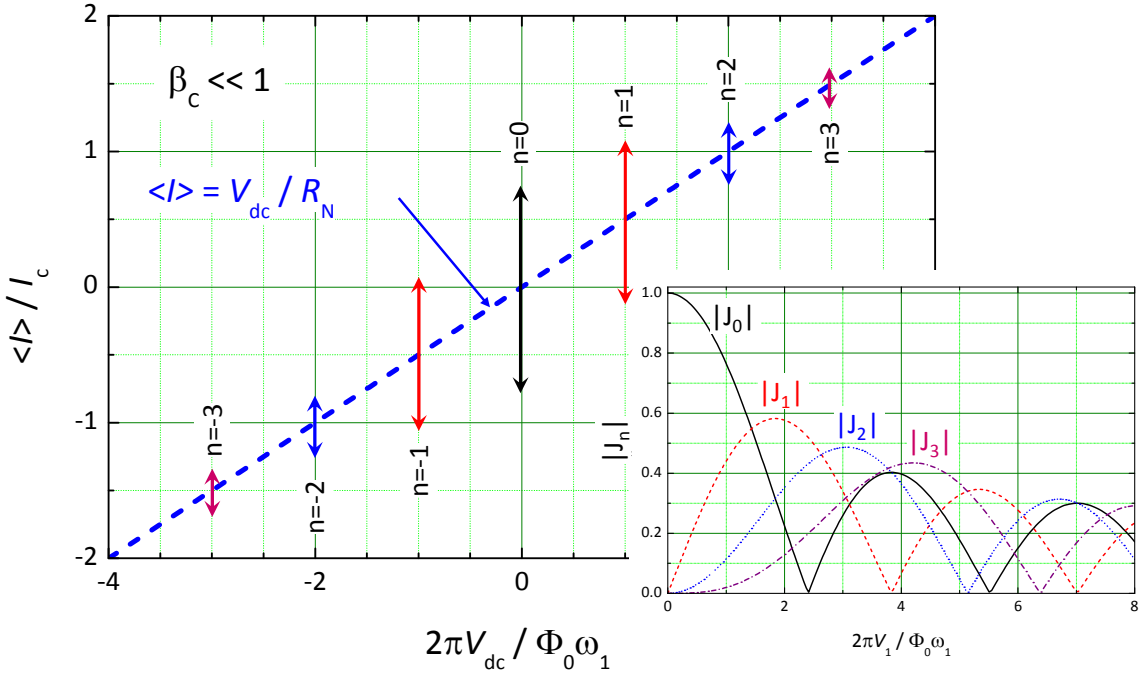

Figure 3.11: The dc component of the current plotted versus the applied dc voltage for a RCSJ model junction driven by a voltage source $V(t) = V_{\rm dc} + V_1 \cos \omega_1 t$. At the voltages $V_n = n \frac{\Phi_0}{2\pi} \omega_1$ current steps, the so-called Shapiro steps appear. Their height has a Bessel function dependence on the amplitude V_1 of the ac voltage as shown in the inset.

Response to an ac Current Source, Strong Damping

In most experimental arrangements the external source has a larger impedance than the Josephson junction and therefore represents a current source. In this case Kirchhoff's law allows us to write

$$I_c \sin\varphi + \frac{1}{R_N} \frac{\phi_0}{2\pi} \frac{d\varphi}{dt} \quad = \quad I_{\rm dc} + I_1 \sin \omega_1 t \ . \tag{3.3.29}$$

Here, we again have neglected the displacement current what is possible only in the limit of strong damping ($\beta_C \ll 1$) and we also did not take into account fluctuations.

The nonlinear differential equation (3.3.29) is difficult to solve. In order to understand what is going on we use the tilt washboard potential to perform a qualitative discussion (in the same way a qualitative discussion can be performed based on the pendulum analogue). We recall that the current tilts the washboard potential. Therefore, the dc current can be considered to result in a constant tilt angle, whereas the ac current results in oscillations around this tilt angle with the amplitude given by the amplitude I_1 of the ac current. If we increase $I_{\rm dc}$ from zero at a constant ac amplitude I_1 we expect that the junction stays in the zero voltage state as long as $I_{\rm dc} + I_1 \leq I_c$ at all times. In this case the tilt angle is always small enough so that there is a local minimum in the tilted washboard potential.

As soon as $I_{\rm dc} + I_1 > I_c$, the phase particle can leave the local minimum and move down the washboard potential. However, due to the ac current the total current varies between $I_{\rm dc} + I_1 > I_c$ and $I_{\rm dc} - I_1 < I_c$. Therefore, for some part of the ac cycle the phase particle can move, whereas for the rest of the cycle it is trapped again in a local minimum. In total the motion of the particle is complicated and therefore it is difficult to calculate the resulting time-averaged voltage. An interesting situation appears when the average junction voltage reaches the values $V_n = n \frac{\Phi_0}{2\pi} \omega_1$ (compare (3.3.26)). For these values the motion of the phase particle in the tilt washboard potential is synchronized by the ac driving current.

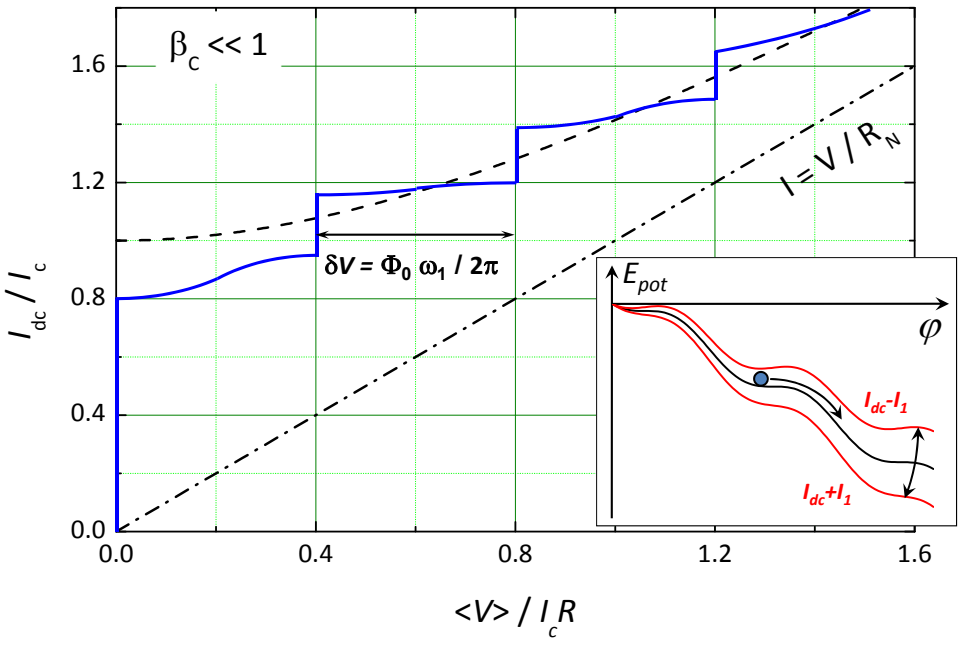

Figure 3.12: The time-averaged junction voltage plotted versus the applied dc current for an overdamped RCSJ model junction driven by a current source $I(t) = I_{\rm dc} + I_1 \sin \omega_1 t$ (full line, $I_1/I_c \simeq 0.2$). The dashed line shows the RCSJ model IVC without ac driving current. Also shown is the ohmic line (dash dot). The inset shows the tilt washboard potential. Due to the finite ac amplitude the tilt angle varies during one rf cycle.

For example, if the phase particle moves from one local minimum to the adjacent one during each cycle $T = 2\pi/\omega_1$ of the ac source, there is a phase change $\dot{\varphi}/T = 2\pi/T = \omega_1$. This corresponds to an average voltage $\langle V \rangle = \frac{\Phi_0}{2\pi}\dot{\varphi} = \frac{\Phi_0}{2\pi}\omega_1$. We see that this exactly corresponds to the voltage V_n of (3.3.26) for $n = 1$. We can generalize our discussion and assume that during each cycle of the ac source the phase particle is moving down n local minima. Then, the phase change is

$$\dot{\varphi} \;=\; n\,\frac{2\pi}{T} \;=\; n\,\omega_1 \;. \tag{3.3.30}$$

This results in an average dc voltage of

$$\langle V \rangle \;=\; n\,\frac{\Phi_0}{2\pi}\,\omega_1 \;=\; V_n \;. \tag{3.3.31}$$

We see that for the voltages V_n given by (3.3.26) the phase particle is moving down the potential well by a fixed number of minima during each cycle. That is we have a synchronization of the phase change with the external ac source. This synchronization is not only possible for a particular value of the dc current but for a complete interval of the dc current. The width of the dc current interval is proportional to the amplitude of the current spike according to (3.3.27).

The resulting IVC is shown schematically in Fig. 3.12 for an overdamped junction. Note that the appearance of the current steps occurs at precisely the values V_n given by (3.3.26). Experimental IVCs for an underdamped and overdamped Josephson junction are shown in Fig. 3.13.

Response to ac Driving Sources: Intermediate Damping

So far we have discussed only the effect of strong damping by neglecting the junction capacitance. The most visible effect of the junction capacitance on the IVCs is between the current steps rather than upon

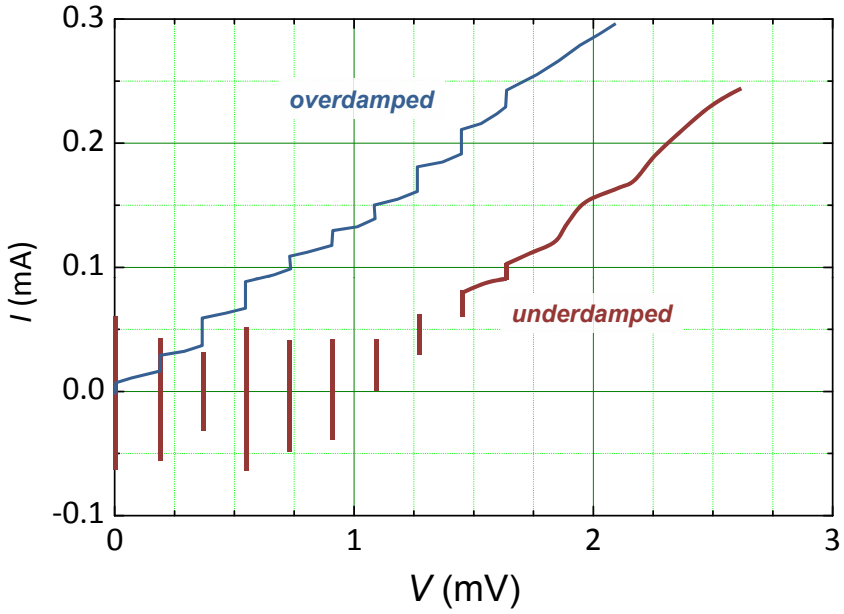

Figure 3.13: Experimental IVCs obtained for an underdamped and overdamped Nb Josephson junction under microwave radiation. The IVCs clearly show the constant voltage steps at $V_n = n\frac{\Phi_0}{2\pi}\omega_1$ (data from C.A. Hamilton, Rev. Sci. Instr. **71**, 3611 (2000)).

the steps themselves. With the increase of β_C the supercurrent contribution to the IVCs at $\langle V\rangle \neq V_n$ decreases, so that the IVCs become hysteretic in the vicinity of each step.[18]

3.3.4 Photon-Assisted Tunneling

In the discussion of the Shapiro steps we have approximated the normal resistance by an ohmic resistance R_N. However, in a superconducting tunnel junction the normal resistance $R(V)$ is highly nonlinear with a sharp step at the gap voltage $V_g = 2\Delta/e$ manifesting itself as a strong increase of the quasiparticle current at V_g. Therefore, instead of using the simple approximation $I = V/R_N$ it is more appropriate to use the quasiparticle tunneling current $I_{\rm qp}(V)$. However, in the $I_{\rm qp}(V)$ curve we have to take into account the effect of the ac source on the quasiparticle tunneling. This can be done by the method introduced by **P.K. Tien** and **J.P. Gordon**.[19] They assumed that the effect of the rf driving voltage has no effect on the internal energy levels of the two electrodes but shifts these levels up or down in one electrode with respect to those in the other electrode as shown in Fig. 3.14. That means, that the energy of a quasiparticle becomes $E_{\rm qp} + eV_1\cos\omega_1 t$ so that the quantum mechanical phase factor $\exp(-\imath Et/\hbar)$ becomes frequency modulated. It can be written as

$$\exp\left(-\frac{\imath}{\hbar}\int(E_{\rm qp}+eV_1\cos\omega_1)dt\right) \;=\; \exp\left(-\frac{\imath}{\hbar}E_{\rm qp}t\right)\cdot\exp\left(-\imath\frac{eV_1}{\hbar\omega_1}\sin\omega_1 t\right)\;. \qquad (3.3.32)$$

Using the Bessel function identity as discussed above we can write the factor containing V_1 as a sum of terms of the form $\mathscr{J}_n(eV_1/\hbar\omega_1)\mathrm{e}^{-in\omega_1 t}$. This result can be interpreted as a splitting up of the quasiparticle levels into many levels at $E_{\rm qp} \pm n\hbar\omega_1$ with probabilities given by the amplitude coefficient $\mathscr{J}_n(eV_1/\hbar\omega_1)$.

[18] see e.g. K. K. Likharev, *Dynamics of Josephson Junctions and Circuits*, Gordon and Breach Science Publishers, New York (1986).

[19] P.K. Tien, J.P. Gordon, Phys. Rev. **129**, 647 (1963).

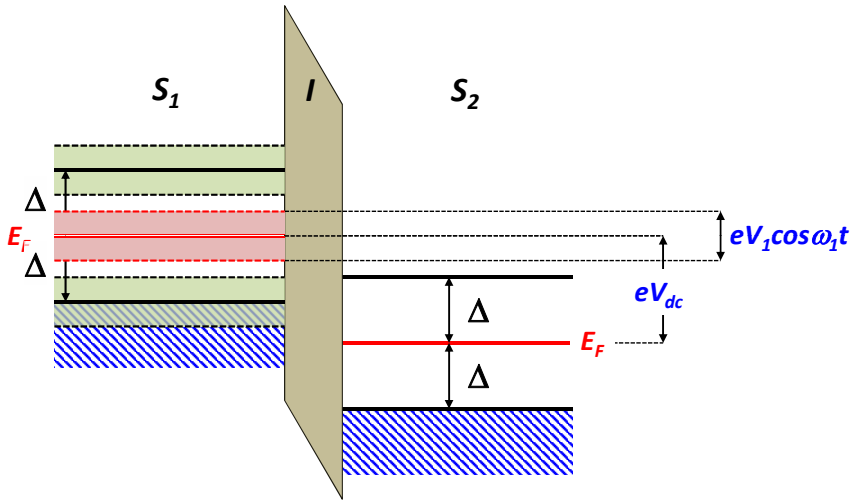

Figure 3.14: Illustration of the periodic shift of the quasiparticle levels of a superconducting tunnel junction due to an applied ac voltage of amplitude V_1.

With this modified density of states the quasiparticle tunneling current is obtained to

$$I_{\rm qp}(V) \;=\; \sum_{n=-\infty}^{+\infty} \mathscr{J}_n^2\left(\frac{eV_1}{\hbar\omega_1}\right) I^0_{\rm qp}(V+n\hbar\omega_1/e)\;. \tag{3.3.33}$$

We see that the sharp increase of the quasiparticle tunneling current at the gap voltage is broken up into many steps of smaller current amplitude at the voltages $V_g \pm n\hbar\omega_1/e$. An experimental example is shown in Fig. 3.15.

Note that the steps in the quasiparticle tunneling curve resemble the Shapiro steps that occur at voltages

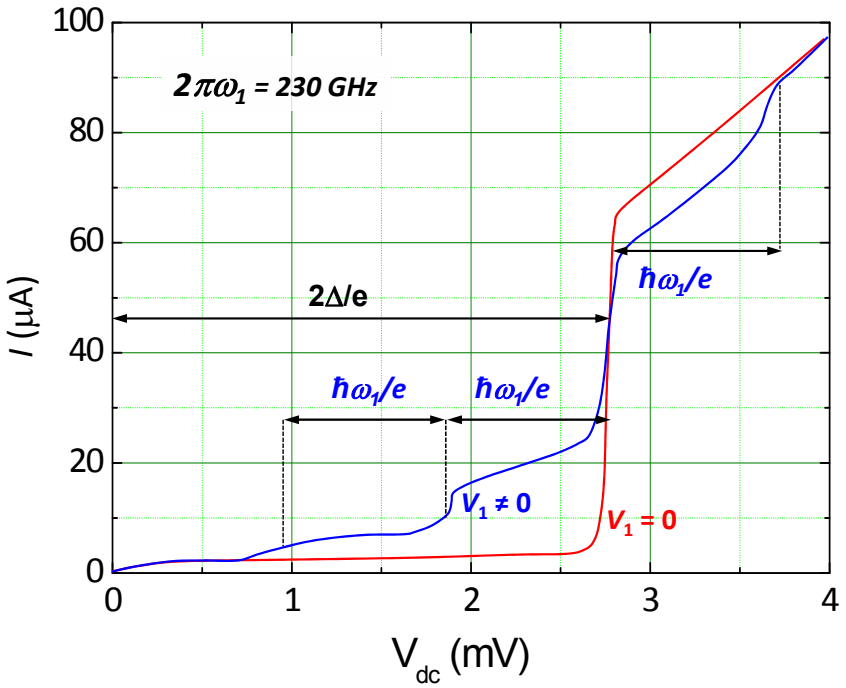

Figure 3.15: Quasiparticle current-voltage characteristics of a niobium SIS Josephson junction without and with microwave irradiation of frequency $2\pi\omega_1 = 230\,\text{GHz}$ corresponding to $\hbar\omega_1/e \simeq 950\,\mu\text{V}$.

$V_n = n\hbar\omega_1/2e$. However, there are profound differences. First, the voltage separation of the quasiparticle steps is just twice of that of the Shapiro steps because e and not $2e$ appears in the denominator. Second, the steps have no constant voltage. The sharpness of the voltage is determined by the sharpness of the increase of the quasiparticle tunneling curve at the gap voltage. Third, their amplitude varies as the square of the Bessel function of the half argument.

3.4 Additional Topic: Effect of Thermal Fluctuations

In the previous subsections we have discussed the response of a RCSJ model Josephson junction to external voltage or current sources. However, in our discussion we did not take into account fluctuations. Therefore, in this section we analyze the effect of additional fluctuations. We will restrict our discussion to thermal fluctuations, which have a correlation function[20]

$$\langle I_F(t) I_F(t+\tau)\rangle \;=\; \frac{2k_BT}{R_N}\delta(\tau)\ . \tag{3.4.1}$$

If the fluctuations are small, their effect are small phase fluctuations around the equilibrium value. Here, small means that the mean square of the phase fluctuations $\langle\overline{\varphi}^2\rangle$ is much less than the width

$$\Delta\varphi \;=\; \widetilde{\varphi}_n - \varphi_n \;=\; \pi - 2\arcsin(i) \tag{3.4.2}$$

of the potential well surrounding the point φ_n (compare (2.1.10) and Fig. 2.3 in section 2.1.3).

If the fluctuations become larger and $\langle\overline{\varphi}^2\rangle$ becomes comparable to $(\Delta\varphi)^2$, there is a finite probability for the phase to escape from the local minimum of the potential well to one of the adjacent states $\varphi_{n\pm1}$. This probability can be characterized by the rates $\Gamma_{n\pm1}$ or the corresponding lifetimes $\tau_{n\pm1} = \hbar/\Gamma_{n\pm1}$. This is shown in Fig. 3.16. The escape of the phase to one of the adjacent minima results in a $\pm 2\pi$ change of the phase. Whereas for zero applied external current we have $\Gamma_{n+1} = \Gamma_{n-1}$ and therefore the time-averaged change of the phase difference, $\langle\dot{\varphi}\rangle$, is equal to zero, there is a net time-averaged change $\langle\dot{\varphi}\rangle \neq 0$ for $I \neq 0$, since now $\Gamma_{n+1} \neq \Gamma_{n-1}$. Once the phase has escaped from the potential minimum the further evolution of the phase difference strongly depends on the damping of the junction.

In order to quantify the effect of thermal fluctuations we have to calculate the rates $\Gamma_{n\pm1}$ as a function of the applied bias current and the intensity of the fluctuations. The simplest result can be again obtained in the framework of the RCSJ model, when the Langevin equation has the form

$$I \;=\; I_c\sin\varphi + \frac{1}{R_N}\,\frac{\Phi_0}{2\pi}\,\frac{d\varphi}{dt} + C\,\frac{\Phi_0}{2\pi}\,\frac{d^2\varphi}{dt^2} + I_F\ . \tag{3.4.3}$$

As the general theory of Brownian motion[21,22] shows, this equation is equivalent to the following ***Fokker-Planck equation***:[23,24,25,26,27]

$$\frac{1}{\omega_c}\frac{\partial\sigma}{\partial t} + \frac{\partial}{\partial\varphi}(\sigma v) + \frac{1}{\beta_C}\frac{\partial}{\partial v}\left(\sigma\left[f(\varphi) - v\right]\right) \;=\; \frac{\gamma}{\beta_C^2}\frac{\partial^2\sigma}{\partial v^2}\ . \tag{3.4.4}$$

[20] Note that according to the Wiener-Khintchine theorem the spectral density $S(f)$ of the fluctuations is twice the Fourier transform of the correlation function. That is, equation (3.4.1) is equivalent to $S(f) = 4k_BT/R_N$.

[21] H.A. Kramers, Physica **7**, 284 (1940).

[22] S. Chandrasekhar, Rev. Mod. Phys. **15**, 1 (1943).

[23] A.D. Fokker, *Die mittlere Energie rotierender elektrischer Dipole*, Ann. Phys. **43**, 810 (1914).

[24] M. Planck, *Über einen Satz der statistischen Dynamik und seine Erweiterung in der Quantentheorie*, Preuss. Akad. Wiss. (1917), p.324

[25] Yu.M. Ivanchenko, L.A. Zilberman, Sov. Phys. JETP **55**, 2395 (1968).

[26] V. Ambegaokar, B.I. Halperin, Phys. Rev. Lett. **22**, 1364 (1969).

[27] The Fokker-Planck equation has the form of a continuity equation in which the role of the flow in space is played by a quantity $J(\mathbf{r},t)$ consisting of a drift and a diffusion flow. Depending on the meaning of the variable $\mathbf{r}$, it may be not only the diffusion in the configuration space but also diffusion in the space of velocities, diffusion of energy, diffusion of the phase of oscillation etc.

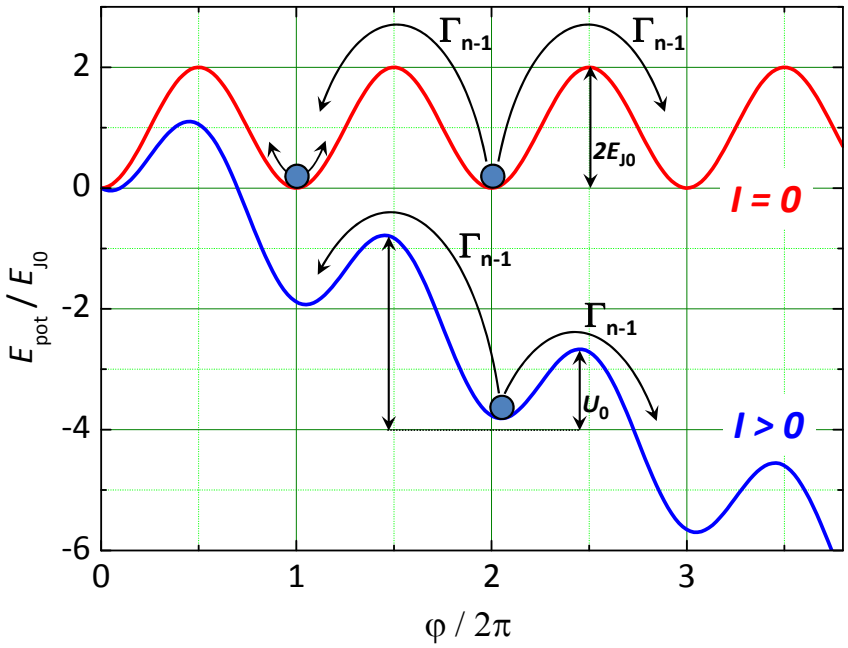

Figure 3.16: The thermally activated motion of the phase in the presence of thermal fluctuations for zero applied current and a finite applied current $I < I_c$. Small fluctuations result in fluctuations of the phase particle around the potential minimum. Large fluctuations result in a finite probability to escape into one of the adjacent phase states.

Here[28,29]

$$f(\varphi) = -\frac{1}{E_{J0}}\frac{\partial U(\varphi)}{\partial \varphi} = \frac{I}{I_c} - \sin\varphi \tag{3.4.5}$$

is the effective normalized force,

$$v = \frac{d\varphi/dt}{\omega_c} = \frac{V}{I_c R_N} \tag{3.4.6}$$

the effective normalized momentum, and $\sigma(v,\varphi,t)$ is the probability density of finding the system at a specific point (φ, v) in phase space at the time t. After σ is found from (3.4.4), the statistical average of every variable $X(\varphi,v,t)$ can be calculated as

$$\langle X\rangle(t) = \int_{-\infty}^{+\infty}\!\!\int \sigma(\varphi,v,t)X(\varphi,v,t)\; d\varphi dv \;. \tag{3.4.7}$$

For small fluctuations (3.4.4) has the simple static ($d\sigma/dt = 0$) solution

$$\sigma(v,t) = \mathscr{F}^{-1}\exp\left(-\frac{G(\varphi,\sigma)}{k_B T}\right) \qquad \text{with} \tag{3.4.8}$$

$$\mathscr{F} = \int_{-\infty}^{+\infty}\!\!\int \exp\left(-\frac{G(\varphi,\sigma)}{k_B T}\right)\; d\varphi dv \;, \tag{3.4.9}$$

[28] Yu. M. Ivanchenko, L.A. Zilberman, Sov. Phys. JETP **55**, 2359 (1968).
[29] V. Ambegaokar, B.I. Halperin, Phys. Rev. Lett. **22**, 1364 (1969).

which is essentially the ***Boltzmann distribution***. Here, $G = E - F \cdot x$ is the total energy with E the free energy. We see that we have a constant probability

$$p = \int_{-\infty}^{+\infty} dv \int_{\varphi \approx \varphi_n} \sigma(\varphi, v)\, d\varphi \tag{3.4.10}$$

to find the system in the n^{th} metastable state.

If the fluctuations are larger, the transition rate $\Gamma_{n\pm1}$ to the adjacent phase states becomes significant and p can change in time. The corresponding law describing the amount of phase slippage is simply

$$\frac{dp}{dt} = (\Gamma_{n+1} - \Gamma_{n-1})\, p \ , \tag{3.4.11}$$

if $\omega_A/\Gamma_{n\pm1} \gg 1$. Here, ω_A is the so-called ***attempt frequency***. In most cases $\Gamma_{n+1} \gg \Gamma_{n-1}$. Then, in the limit $\omega_A/\Gamma_{n+1} \gg 1$ an universal expression can be derived for Γ_{n+1} and ω_A:[30,31]

$$\Gamma_{n+1} = \frac{\omega_A}{2\pi} \exp\left(-\frac{U_0}{k_B T}\right) \tag{3.4.12}$$

with[32,33]

$$\omega_A = \begin{cases} \omega_0 = \omega_p (1-i^2)^{1/4} & \text{for } \omega_c \tau \gg 1, \\ \tau^{-1} = \omega_c (1-i^2)^{1/2} & \text{for } \omega_c \tau \ll 1 \end{cases} . \tag{3.4.13}$$

Here, U_0 is given by (2.1.15) and ω_0 and ω_c are the plasma frequency and the characteristic frequency in the washboard potential tilt by the applied current $i = I/I_c$, respectively. Note that at $I = 0$ the attempt frequency ω_A is given by the plasma frequency ω_p, since this frequency represents the characteristic frequency at which the phase oscillates back and forth in the potential well. In the presence of a finite current, the potential is tilt and hence the characteristic frequency is not exactly the plasma frequency but the frequency of small oscillations at around the minimum of the tilted washboard potential. It is evident that unless I is close to I_c we have $\omega_A \simeq \omega_p$ in good approximation. Note that in the limit of strong damping ($\beta_C = \omega_c \tau_{RC} \ll 1$) one has to replace the undamped plasma frequency by the characteristic frequency of an overdamped oscillator, namely $\omega_A = \omega_p \sqrt{\beta_C} = \omega_p \sqrt{\omega_c R_N C} = \omega_c$ (compare (3.1.13) in section 3.1.2).

3.4.1 Underdamped Junctions: Reduction of I_c by Premature Switching

For $E_{J0} \gg k_B T$, the thermally activated escape from the potential minimum over the barrier height U_0 to the next minimum has a small probability $\propto \exp(-U_0(I)/k_B T)$ at each attempt. The dependence of the barrier height on the applied current, $U_0(I)$, can be approximated well by

$$U_0(I) \simeq 2E_{J0} \left(1 - \frac{I}{I_c}\right)^{3/2} . \tag{3.4.14}$$

[30] H.A. Kramers, Physica **7**, 284 (1940).

[31] S. Chandrasekhar, Rev. Mod. Phys. **15**, 1 (1943).

[32] Using the notation $i = I/I_c$, the minimum of the resulting potential occurs at $\varphi = \arcsin(i)$ (compare section 2.1.3). Here, the curvature of the potential is $d^2U/d\varphi^2 = (\hbar I_c/2e)\cos\varphi = (\hbar I_c/2e)\sqrt{1-i^2}$ using the relation $\arcsin x = \arccos\sqrt{1-x^2}$. The classical frequency of small oscillations about the minimum is $\omega_A = \omega_p (1-i^2)^{1/4}$.

[33] If the McCumber parameter β_C is smaller than the critical value $\sqrt{(1-i^2)}$ the oscillation process in the potential well is aperiodic and the relaxation takes the time $\tau = 1/\omega_c\sqrt{1-i^2}$ (for a detailed discussion see K.K. Likharev, *Dynamics of Josephson Junctions and Circuits*, Gordon and Breach Science Publishers, New York (1986), section 3.2.)

We see that $U_0 = 2E_{J0}$ for $I = 0$ and $U_0 \to 0$ for $I \to I_c$.

Since the barrier height goes to zero on approaching the critical current, the escape probability increases exponentially from a very small value $\sim \frac{\omega_A}{2\pi} \exp(-2E_{J0}/k_BT)$ at $I \ll I_c$ up to a large value $\sim \omega_A/2\pi$ at $I \simeq I_c$. Note that for an underdamped junction the phase will accelerate down the tilt washboard potential until it reaches its average velocity determined by the damping $\sim 1/R_N$ of the junction. That is, after the phase has escaped from the potential well at the current I, the junction voltage switches to the value IR_N.

Since the escape is a stochastic process, the exact escape current I_M detected in an experiment will be different every time ramping up the current. That is, we will measure a distribution of current values I_M characterized by a width δI and a mean reduction $\langle \Delta I_c \rangle = I_c - \langle I_M \rangle$ below the critical current I_c obtained in the absence of any fluctuations. The determination of these values requires numerical calculations.[34] However, with the approximation (3.4.14) and the escape rate $\sim \frac{\omega_A}{2\pi} \exp(-U_0(I)/k_BT)$ the mean depression of I_c can be approximated by[35]

$$\langle \Delta I_c \rangle \;=\; I_c - \langle I_M \rangle \;\;\simeq\;\; I_c \left[\frac{k_BT}{2E_{J0}} \ln\left(\frac{\omega_p \Delta t}{2\pi} \right) \right]^{2/3} . \tag{3.4.15}$$

Here, Δt is the time spent sweeping the applied current through the dense part of the distribution of observed critical current values. Since in experiments Δt is of the order of seconds and $\omega_p \sim 10^{10}\mathrm{s}^{-1}$, the logarithm typically is of the order of $\ln 10^{10} \simeq 23 \gg 1$. Since the logarithm is so large, it only weakly depends on the actual sweep rate of the applied current. Then, fluctuation effects cause a major reduction in I_c as soon as k_BT is larger than about 5% of E_{J0}. One can further show that the width δI of the distribution is approximately given by the mean depression of I_c divided by the same logarithmic factor.

3.4.2 Overdamped Junctions: The Ambegaokar-Halperin Theory

When a thermal noise current is included into the driving term, **Ambegaokar** and **Halperin** showed[36] that the simple IVC for overdamped Josephson junctions, $V = R_N\sqrt{I^2 - I_c^2}$ for $I > I_c$ is fundamentally modified. In particular, they found that the finite amount of phase slippage results in a nonvanishing junction voltage even in the limit $I \to 0$. The corresponding resistance is the so-called phase slip resistance

$$R_p \;=\; \lim_{I\to 0} \frac{\langle V \rangle}{I} . \tag{3.4.16}$$

This resistance has been calculated by **Ambegaokar** and **Halperin** for strong damping ($\beta_C \ll 1$). They obtained

$$R_p(T) \;=\; R_N \left\{ \mathscr{I}_0 \left[\frac{\gamma_0(T)}{2} \right] \right\}^{-2} \tag{3.4.17}$$

with

$$\gamma_0(T) \;=\; \frac{2E_{J0}(T)}{k_BT} \;=\; \frac{\Phi_0 I_c(T)}{\pi k_BT} . \tag{3.4.18}$$

[34] T. Fulton, L.N. Dunkelberger, Phys. Rev. **B9**, 4760 (1974).

[35] For a detailed discussion see K. K. Likharev, *Dynamics of Josephson Junctions and Circuits*, Gordon and Breach Science Publishers, New York (1986), section 3.4.

[36] V. Ambegaokar, B.I. Halperin, Phys. Rev. Lett. **22**, 1364 (1969).

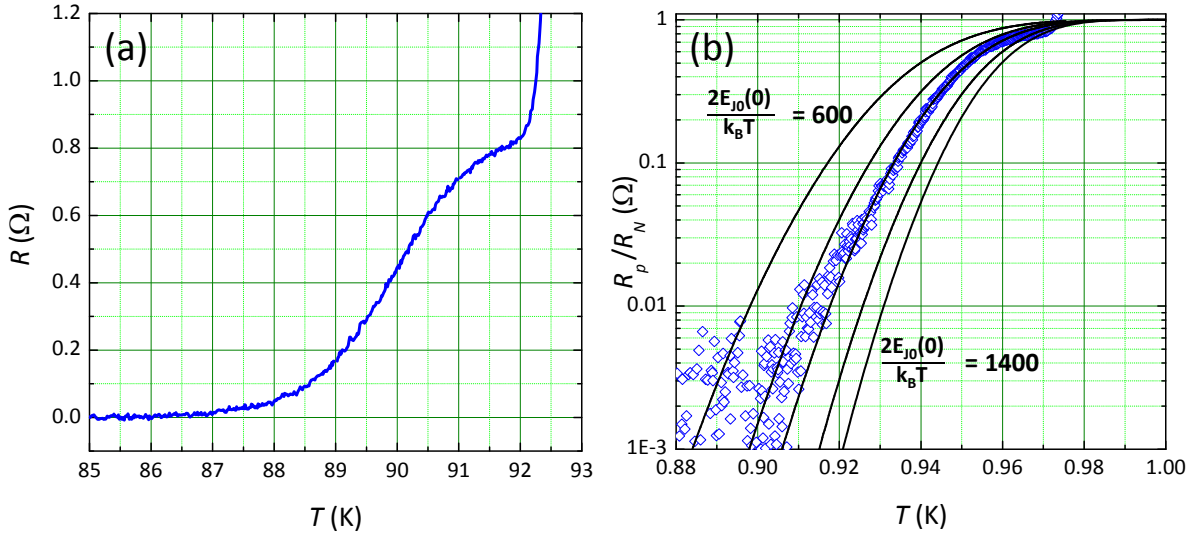

Figure 3.17: (a) Resistance versus temperature curve of a $YBa_2Cu_3O_7$ grain boundary Josephson junction showing the foot structure due to the thermally activated phase slippage. (b) Experimental $R_p(T)/R_N$ dependence (diamonds) as well as theoretical curves according to (3.4.17) and (3.4.18) for $\gamma_0(T) = \frac{\Phi_0 I_c(T)}{\pi k_B T} = \frac{2E_{J0}(0)}{k_B T}(1-T/T_c)^2$ with $\frac{2E_{J0}(0)}{k_B T}$ ranging between 600 and 1400 (adapted from R. Gross *et al.*, Phys. Rev. Lett. **64**, 228 (1990)).

Here $\mathscr{I}_0(x) = \mathscr{J}_0(\imath x)$ is the modified Bessel function and we have used $U_0 = 2E_{J0}$ what is justified for $I \to 0$. For $E_{J0}/k_BT \gg 1$ the Bessel function dependence can be approximated by the exponential dependence $\mathscr{I}_0(x) = \mathrm{e}^x/2\pi\sqrt{x}$ resulting in

$$\frac{R_p(T)}{R_N} \propto E_{J0} \exp\left(-\frac{2E_{J0}}{k_BT}\right) \qquad \text{or} \tag{3.4.19}$$

$$\langle\dot{\varphi}\rangle \propto \frac{2eI_cR_N}{\hbar} \exp\left(-\frac{2E_{J0}}{k_BT}\right) = \omega_c \exp\left(-\frac{2E_{J0}}{k_BT}\right) . \tag{3.4.20}$$

We see that the attempt frequency is given by the characteristic junction frequency ω_c and not by the plasma frequency. As already discussed above, this is caused by the strong damping ($\beta_C = \omega_c\tau_{RC} \ll 1$). In this case one has to replace the undamped plasma frequency by the characteristic frequency of an overdamped oscillator, namely $\omega_A = \omega_p\sqrt{\beta_C} = \omega_p\sqrt{\omega_c R_N C} = \omega_c$.

In terms of the tilt washboard potential model the phase particle in an overdamped Josephson junction diffuses over the barriers in a continuous process rather than making a single escape as in the underdamped limit. This difference occurs, since the strong damping brings the phase particle back into equilibrium in the next local minimum before it can diffuse to the next barrier. Therefore, it has no chance to run away as it was the case for the underdamped junction. The phase diffusion results in an activated nonlinear resistance.

Fig. 3.17 shows the temperature dependence of the normalized junction resistance, R_p/R_N, due to thermally activated phase slippage. The data are obtained for an overdamped $YBa_2Cu_3O_7$ grain boundary Josephson junction.[37] The thermally activated phase slippage manifests itself as a foot structure in the $R(T)$ dependence of the Josephson junction. After the junction electrodes become superconducting below the transition temperature T_c of the electrode material there is still a measurable resistance due to the thermally activated phase slippage of the junction. This resistance becomes vanishingly small only at a

[37] R. Gross, P. Chaudhari, D. Dimos, A. Gupta, G. Koren, *Thermally Activated Phase Slippage in High-T_c Grain Boundary Josephson Junctions*, Phys. Rev. Lett. **64**, 228 (1990).

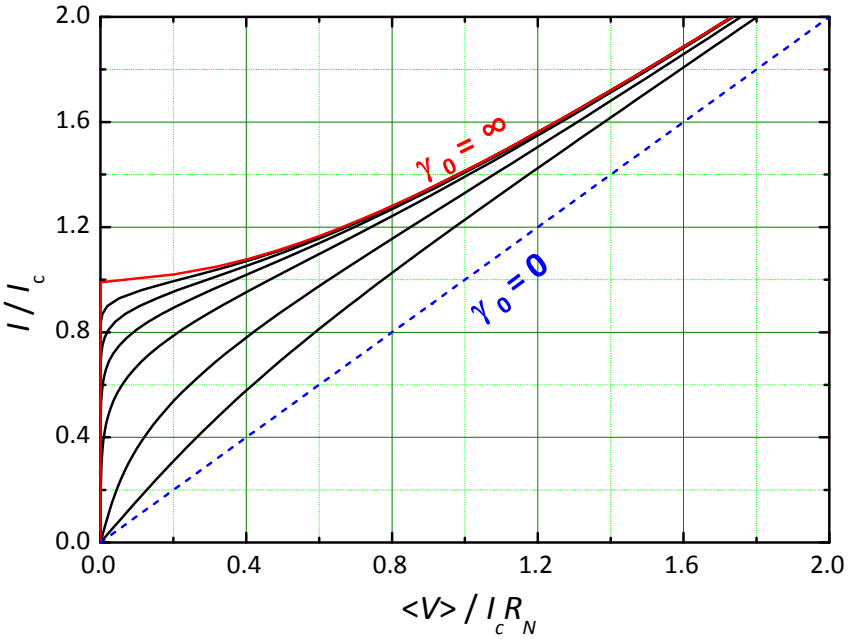

Figure 3.18: Current-voltage characteristics calculated according to (3.4.21) for a strongly overdamped Josephson junction ($\beta_C \ll 1$). The normalized barrier height was $\gamma_0 = 0$, 1, 2, 5, 10, 20, 50, and ∞.

much lower temperature, at which the coupling energy $E_{J0}(T)$ has become sufficiently large to suppress the phase slippage. Also shown is a fit of the experimental data to equation (3.4.17). The fit can be used to determine the temperature dependence of the junction critical current $I_c(T)$ close to T_c as shown in Fig. 3.17 for a $YBa_2Cu_3O_7$ grain boundary Josephson junction. A direct measurement of $I_c(T)$ close to the critical temperature is difficult because of the finite slope of the IVCs due to thermally activated phase slippage (see Fig. 3.18). Hence, it is impossible to define I_c as the current flowing without measurable resistance.

Thermally activated phase slippage causes a rounding of the IVCs of Josephson junctions at $I \sim I_c$. This is evident, because already at current values $I < I_c$ the phase can move down the tilt washboard potential due to thermal activation resulting in a finite voltage. The IVCs in the presence of thermally activated phase slippage are shown in Fig. 3.18. Of course the rounding strongly decreases with increasing γ_0, that is, with increasing barrier height. Note that the small linear resistance at low currents is the single junction analog of the so-called ***thermally activated flux-flow*** resistance in bulk superconductors, in which the activation energy is thought to be the energy to move a fluxon rather than the energy for a phase slip in a single junction.

According to Ambegaokar and Halperin, for strong damping ($\beta_C \ll 1$) the IVC can be calculated analytically giving

$$\langle V \rangle = \frac{2I_cR_N}{\gamma_0}\frac{e^{\pi\gamma_0 i}-1}{e^{\pi\gamma_0 i}}\left\{\int_0^{2\pi} d\varphi\, e^{-\gamma_0 i\varphi/2} I_0\left(\gamma_0 \sin\frac{\varphi}{2}\right)\right\}^{-1}, \tag{3.4.21}$$

where $i = \frac{I}{I_c}$.

We note that for small Josephson junctions ($L < \lambda_J$) the measurement of the resistance $R_p(T)$ also can be used to determine the magnetic field dependence of the critical current close to T_c. At constant

temperature the magnetic field dependence of $R_p(T)$ is obtained to[38,39]

$$R_p(B) = R_N \left\{ I_0 \left[\frac{\gamma_0(B)}{2} \right] \right\}^{-2} \tag{3.4.22}$$

with

$$\gamma_0(B) = \frac{2E_{J0}(B)}{k_B T} = \frac{\Phi_0 I_c(B)}{\pi k_B T} \ . \tag{3.4.23}$$

[38] Stephan Schuster, Diploma Thesis, University of Tübingen (1993).

[39] B. Mayer, R. Gross, S. Schuster, A. Beck, L. Alff, Appl. Phys. Lett. **62**, 783 (1993).

3.5 Secondary Quantum Macroscopic Effects

3.5.1 Quantum Consequences of the Small Junction Capacitance

In our discussion so far we have treated the Josephson junction as a classical system. Both the gauge-invariant phase difference φ and its time derivative $\dot{\varphi}$, which is proportional to the charge $Q = CV = \frac{\hbar}{2e}C\dot{\varphi}$, have been treated as purely classical variables that in principle can be measured simultaneously with arbitrary precision. Within our classical description the dynamics of a Josephson junction was completely analogous to that of a classical particle of mass $M = (\hbar/2e)^2C$ moving in the tilt washboard potential or the motion of a pendulum (compare section 3.2).

In order to discuss the limits of this classical description let us consider a strongly underdamped junction. If the phase φ changes in time ($\dot{\varphi} \propto V \neq 0$), then the energy of the electric field is given by

$$K = \frac{1}{2}CV^2 = \frac{Q^2}{2C} = \frac{1}{2}C\left(\frac{\hbar}{2e}\right)^2\dot{\varphi}^2 = \frac{1}{2}E_{J0}\frac{\dot{\varphi}^2}{\omega_p^2} \tag{3.5.1}$$

with $Q \equiv CV = \int I dt$. We see that this energy is just the energy related to the extra charge Q on one junction electrode relative to the other due to the finite voltage V. With the energy contribution K of the electric field and the potential energy $U = E_{J0}(1-\cos\varphi)$ (cf. eq. (2.1.8)) of the junction we can express the total energy of the junction as

$$E = K+U = E_{J0}\left(1-\cos\varphi+\frac{1}{2}\frac{\dot{\varphi}^2}{\omega_p^2}\right) . \tag{3.5.2}$$

We see that it is very convenient to use φ as a principle variable (coordinate) of the system. In this case $U(\varphi)$ should be interpreted as the potential energy and $K \propto \dot{\varphi}^2$ as the kinetic energy. Note that for an overdamped junction equation (3.5.1) does not make sense, since such a junction is closely coupled to the environment through its normal current I_N and the energy is not conserved even over a short time scale.

Returning to the current-phase and voltage-phase relation describing the Josephson junction there is no doubt in their quantum nature. On the other hand, the structure of these equations contradicts basic quantum mechanical principles. We are assuming that all variables (observables) characterizing the state of the junction such as I, Q, V, φ, etc. can be measured simultaneously with arbitrary precision. Quantum mechanics, however, does not allow this and, in general, only the probability distribution of the variables can be calculated. From this we can conclude that the description of the Josephson junction by the current-phase and voltage-phase relation is at best an approximate description of a more precise quantum theory.

Following the recipes of quantum mechanics, we can just consider equation (3.5.2), $E = Q^2/2C + U(\varphi)$, as the Hamiltonian of the junction. We can rewrite the kinetic energy as

$$K = \frac{Q^2}{2C} = \frac{1}{2}\frac{1}{(\hbar/2e)^2C}\left(\frac{\hbar}{2e}Q\right)^2 . \tag{3.5.3}$$

This equation corresponds to the mechanical analogue $K = p^2/2M$. Hence, with the mass analogue $M = (\hbar/2e)^2C$ (cf. eq. (3.2.6)) the quantity $\frac{\hbar}{2e}Q$ corresponds to the momentum p. Therefore, we can make the operator replacement

$$\frac{\hbar}{2e}Q \rightarrow -\imath\hbar\frac{\partial}{\partial\varphi} , \tag{3.5.4}$$

that is, with the number $N = Q/2e$ of Cooper pairs we can write

$$Q = -\imath\, 2e\, \frac{\partial}{\partial\varphi} \qquad N = -\imath\, \frac{\partial}{\partial\varphi}\ . \tag{3.5.5}$$

Then, the form of the Hamiltonian is

$$\begin{aligned} \mathscr{H} &= \frac{Q^2}{2C} + E_{J0}(1-\cos\varphi) = -\frac{(2e)^2}{2C}\,\frac{\partial^2}{\partial\varphi^2} + E_{J0}(1-\cos\varphi) \\ &= -4E_C\,\frac{\partial^2}{\partial\varphi^2} + E_{J0}(1-\cos\varphi)\ . \end{aligned} \tag{3.5.6}$$

Here, $E_C = e^2/2C$ is the charging energy of the junction for a single electron charge.[40] Note that this Hamiltonian describes only the Cooper pairs neglecting the quasiparticle degrees of freedom, which however are unimportant as soon as we consider the case $T = 0$.

The commutation rule for the operators is obtained to

$$[\varphi, Q] = \imath 2e \quad ; \quad [\varphi, N] = \imath \quad \text{or} \quad [\varphi, \frac{\hbar}{2e}Q] = \imath\hbar\ . \tag{3.5.7}$$

Here $N \equiv Q/2e$ is the deviation of the number of Cooper pairs in the junction electrodes from the equilibrium value. Equation (3.5.7) simply represents the uncertainty relation for the number of Cooper pairs and the phase difference:

$$\Delta N \cdot \Delta\varphi \geq 1\ . \tag{3.5.8}$$

Note that this relation is completely analogous to the uncertainty relation between the number of photons and the phase of coherent light.

In many situations it is convenient to use the variable $\phi = \frac{\hbar}{2e}\varphi = \frac{\Phi_0}{2\pi}\varphi$ corresponding to a magnetic flux. In this case we have $\partial/\partial\varphi = \frac{\hbar}{2e}\partial/\partial\phi$ and obtain the Hamiltonian

$$\begin{aligned} \mathscr{H} &= \frac{Q^2}{2C} + E_{J0}\left(1-\cos 2\pi\frac{\phi}{\Phi_0}\right) = -\frac{(2e)^2}{2C}\,\frac{\hbar^2}{(2e)^2}\,\frac{\partial^2}{\partial\phi^2} + E_{J0}\left(1-\cos 2\pi\frac{\phi}{\Phi_0}\right) \\ &= -\frac{\hbar^2}{2C}\,\frac{\partial^2}{\partial\phi^2} + E_{J0}\left(1-\cos 2\pi\frac{\phi}{\Phi_0}\right) \end{aligned} \tag{3.5.9}$$

and the commutator

$$[\phi, Q] = \imath\hbar\ . \tag{3.5.10}$$

That is, Q and ϕ are canonically conjugate variables just like coordinate x and momentum p.

[40] Note that in some cases $E_C = (2e)^2/2C$, that is, the charging energy of a Cooper pair is used.

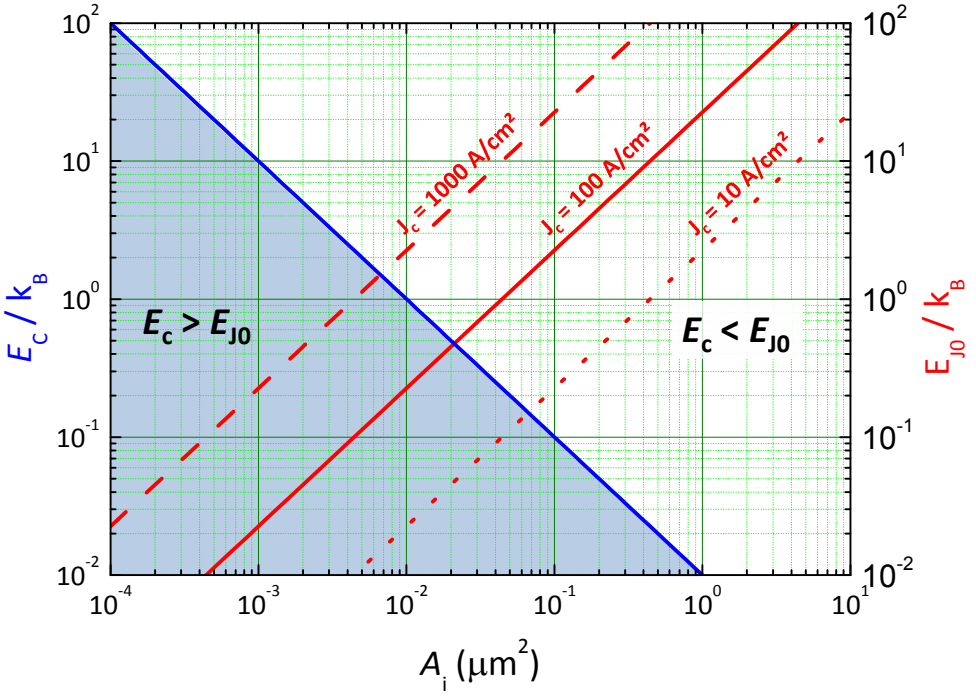

Figure 3.19: The Josephson coupling energy E_{J0} and the charging energy E_C plotted versus the junction area A_i for three different critical current densities J_c. Note that $E_{J0} \propto J_c \propto \exp(-2\kappa d)$ decreases exponentially with increasing thickness d of the tunneling barrier at constant junction area, whereas the charging energy $E_C \propto 1/C \propto d$ increases only linearly with increasing barrier thickness. We therefore have taken the charging energy the same for all three J_c values.

Equations (3.5.6) and (3.5.7) allow us to calculate the deviations of the junction properties from those predicted by the "classical" description. These deviations are called ***secondary macroscopic effects*** to be distinguished from the ordinary or primary effects like the Josephson effect itself.[41,42]

The degree of deviation from the classical description can be estimated by considering again an isolated Josephson junction ($I = 0$) in the low damping limit. The potential energy is given by a cosine potential $E_{J0}(1 - \cos\varphi)$ with a depth determined by the characteristic energy E_{J0}. Approximating this potential close to a minimum by a parabolic potential, the Hamiltonian (3.5.6) reduces to that of a harmonic oscillator with frequency ω_p and level spacing $\hbar\omega_p$. It is obvious that the classical description holds as long as the level spacing is much smaller than the depth of the potential well, i.e. E_{J0}. That is, the degree of deviation from the classical description depends on the ratio of the two energies

$$\frac{\hbar\omega_p}{E_{J0}} = \sqrt{\frac{8E_C}{E_{J0}}} \,. \tag{3.5.11}$$

In order to get a feeling, in which cases the condition $\hbar\omega_p \ll E_{J0}$ or $E_C \ll E_{J0}$ holds for real Josephson junctions, we have to recall that $E_C \propto 1/C \propto 1/A$, whereas $E_{J0} \propto I_c \propto A$. We hence immediately see that we will enter the quantum regime ($E_C \gg E_{J0}$) on decreasing the junction area. In order to make an estimate we consider a planar tunnel junction of typical area $A_i = 10\,\mu\text{m}^2$ with a tunneling barrier of thickness $d = 1$ nm and dielectric constant $\varepsilon = 10$. The critical current density is $J_c \simeq 100$ A/cm^2 giving a coupling energy $E_{J0} \simeq 3 \times 10^{-21}$J. With $\varepsilon_0 = 8.8 \times 10^{-12}$ F/m we obtain the junction capacitance $C = \varepsilon\varepsilon_0 A_i/d \simeq 9 \times 10^{-13}$F and, hence, $E_C \simeq 1.6 \times 10^{-26}$J. We see, that for this typical junction area and

[41] A.I. Larkin, K.K. Likharev, Yu.N. Ovchinnikov, Physica **B 126**, 414 (1985).
[42] A. Leggett, Suppl. Theor Phys. **69**, 80 (1982).

current density the charging energy E_C is by about 5 orders of magnitude smaller than the Josephson coupling energy E_{J0} and also much smaller than k_BT down to temperatures in the mK-regime. This is justifying our classical treatment of Josephson junctions in the previous sections. However, we see that the classical treatment is no longer possible for very small junctions or junctions with very small critical current density J_c. This is shown in Fig 3.19, where we have plotted the Josephson coupling energy and the charging energy as a function of the junction area for different values of the critical Josephson current density. For the typical current density $J_c = 100\,\mathrm{A/cm^2}$ the charging energy becomes comparable to the coupling energy at a junction area of about $0.02\,\mu\mathrm{m}^2$ corresponding to a capacitance of about 1 fF. We also see that in order to observe the quantum phenomena we have to go to temperatures below about 100 mK in order to have $k_BT \ll E_C$.

3.5.2 Limiting Cases: The Phase and Charge Regime

In the following we discuss the two limiting cases $\hbar\omega_p \ll E_{J0}$ and $\hbar\omega_p \gg E_{J0}$ corresponding to $E_C \ll E_{J0}$ and $E_C \gg E_{J0}$, respectively. We will see that for the former the phase is a well defined quantity, whereas for the latter it is the charge. Hence, we denote the two limiting cases as the ***phase regime*** and the ***charge regime***.

The Phase Regime: $\hbar\omega_p \ll E_{J0}$**,** $E_C \ll E_{J0}$

In this limit, the lowest energy levels of the system are localized near the bottom of the potential wells, that is, near the points $\varphi_n = 2\pi n$. For this case we can expand the $\cos\varphi$ in the potential energy U into a Taylor series with respect to small deviations $\delta\varphi = \varphi - \varphi_n$ and neglect all terms except $(\delta\varphi)^2/2 + const$. Then, as already discussed above the Hamiltonian is reduced to that of a harmonic oscillator with frequency ω_p and the energy eigenvalues

$$E_n = \hbar\omega_p \left(1 + \frac{1}{2}\right) . \tag{3.5.12}$$

Our discussion shows that for $\hbar\omega_p/E_{J0} \ll 1$ or, equivalently, $E_C/E_{J0} \ll 1$ the ground state of the system should be a narrowly peaked wave function centered at $\varphi = \varphi_n$ in order to minimize the dominating term $E_{J0}\cos\varphi$. That is, the fluctuations in the phase are very small and according to $\Delta Q \cdot \Delta\varphi \geq 2e$ those of the charge Q on the electrodes large. The physical reason for this is simple. The large fluctuations of the charge are possible due to the very small energy E_C required to add an extra Cooper pair to a junction electrode. That is, charge pairs can easily fluctuate back and forth resulting in a large uncertainty in the extra charge Q on the junction electrodes and, hence, due to $\Delta Q \cdot \Delta\varphi \geq 2e$ in a negligible uncertainty of φ. Then, the dynamics of the phase can be treated classically. Since the phase is well defined we denote the limit $\hbar\omega_p \ll E_{J0}$ as the phase regime.

In order to find the energy levels of the system we can use the Hamiltonian (3.5.6)

$$\mathscr{H} = -4E_C \frac{\partial^2}{\partial\varphi^2} + E_{J0}(1 - \cos\varphi) . \tag{3.5.13}$$

With the parameters $a = (E - E_{J0})/E_C$, $b = E_{J0}/2E_C$ and $z = \varphi/2$ we can rewrite this Hamiltonian to obtain the usual Mathieu equation

$$\frac{\partial^2\Psi}{\partial z^2} + (a + 2b\cos 2z)\ \Psi = 0 . \tag{3.5.14}$$

This differential equation is well known from the periodic potential problem in solid-state physics, leading to energy bands in crystals. The general solution is the superposition

$$\Psi(\varphi) \;=\; \sum_q c_q \psi_q \tag{3.5.15}$$

of the Bloch waves

$$\psi_q(\varphi) \;=\; u_q(\varphi)\,\exp(\imath q\varphi) \qquad \text{with} \qquad u_q(\varphi) \;=\; u_q(\varphi+2\pi)\;. \tag{3.5.16}$$

Here, q is a "charge" or "pair number" variable and $u_q(\varphi)$ is a periodic function with period 2π. If only integer numbers of pairs are physically relevant, q is taking only integer values and Ψ would be 2π-periodic. However, q is a continuous variable, since it does not represent the total charge on an isolated piece of metal, but rather on the capacitor formed by the two junction electrodes. This charge can be varied continuously for example by a third gate electrode, which can change the charge in the junction region, although the tunnel current is restricted to the transfer of a discrete number of charges (e or $2e$ depending on whether one considers unpaired or paired electrons).

Since the problem under consideration is one-dimensional, it can be solved easily by numerical means. To get more insight into the physics we apply a variational approach to find an approximation for the ground state by using a trial function. For $E_C/E_{J0} \ll 1$, we use a Gaussian trial function

$$\Psi(\varphi) \;\propto\; \exp\left(-\frac{\varphi^2}{4\sigma^2}\right)\;, \tag{3.5.17}$$

where the rms spread σ in φ is chosen to minimize the expectation value of (3.5.6). For $E_C/E_{J0} \ll 1$, the minimum energy is

$$E_{\min} \;=\; E_{J0}\left(1-\left[1-\sqrt{\frac{2E_C}{E_{J0}}}\right]^2\right) \;=\; E_{J0}\left(1-\left[1-\frac{\hbar\omega_p}{2E_{J0}}\right]^2\right)\;. \tag{3.5.18}$$

That is, $E_{\min} \simeq 0$ for $\frac{\hbar\omega_p}{E_{J0}} \ll 1$. Fig. 3.20 shows the energy diagram of the Josephson junction for two different values of E_C/E_{J0}. In Fig. 3.20a we have sketched the situation for the phase regime for $E_C/E_{J0} = 0.1$ resulting in $E_{\min} \simeq 0.1E_{J0}$. We note that we have a periodic potential $E_{J0}(1-\cos\varphi)$ and therefore always a finite tunneling coupling between the phase states in adjacent minima. However, the tunneling probability is proportional to $\exp[-(2E_{J0}-E)/\hbar\omega_p]$ (compare section 3.5.6) and therefore is very small in the phase regime ($\hbar\omega_p \ll E_{J0}$) and the lowest energy states ($(2E_{J0}-E) \sim 2E_{J0}$). Therefore, the tunneling splitting of the low lying phase states is exponentially small and becomes significant only for higher states with $(2E_{J0}-E) \ll 2E_{J0}$ as indicated by the broadening of the states in Fig. 3.20a.

The Charge Regime: $\hbar\omega_p \gg E_{J0}$, $E_C \gg E_{J0}$

In contrast, for the phase limit $E_C/E_{J0} \ll 1$ discussed above, now the term $E_C(\partial^2/\partial\varphi^2)$ is dominant. To minimize it in the ground state the wave function $\Psi(\varphi)$ should approach a constant. However, in this case all values of the phase are equally probable. That is, phase fluctuations are very large and in turn charge fluctuations small. The former are enabled by the small energy scale E_{J0} required for phase fluctuations by 2π and the latter are prevented by the large energy scale $4E_C$ for charge fluctuations by $2e$.

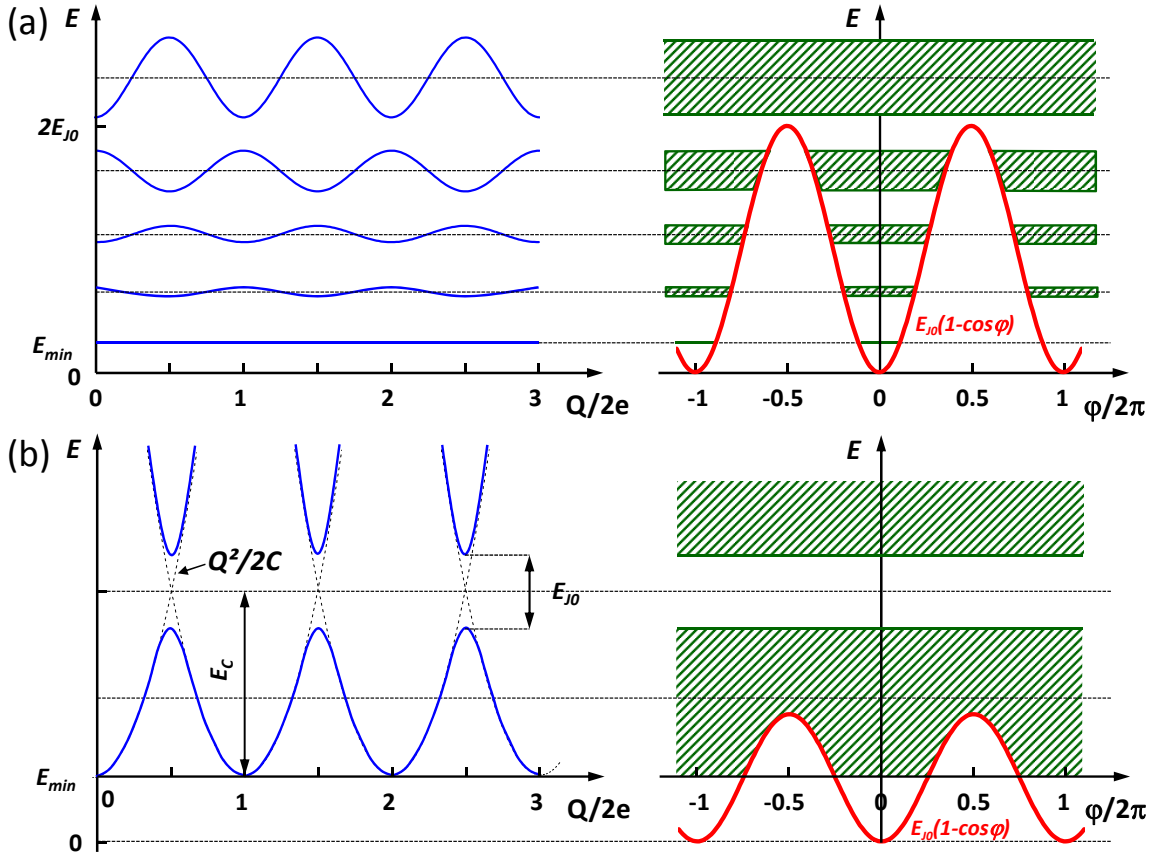

Figure 3.20: Sketch of the energy diagrams of an isolated Josephson junction ($I = 0$) in the case of low damping for (a) $E_C/E_{J0} = 0.1$ and (b) $E_C/E_{J0} = 2.5$.

In the charge limit, an appropriate trial function, which is periodic and satisfies the boundary conditions of zero slope at the edges of the cell, is

$$\Psi(\varphi) \quad \propto \quad (1 - \alpha \cos\varphi) \quad , \tag{3.5.19}$$

which yields the approximate ground-state energy

$$E_{\min} \quad \simeq \quad E_{J0}\left(1 - \frac{E_{J0}}{8E_C}\right) \quad . \tag{3.5.20}$$

We see that in the charge limit $\hbar\omega_p \gg E_{J0}$ or, equivalently, $E_C \gg E_{J0}$ the binding energy is of second order in E_{J0}, whereas it is of first order in the semi-classical limit of equation (3.5.18). In Fig. 3.20b we have sketched the situation for the charge regime for $E_C/E_{J0} = 2.5$ resulting in $E_{\min} \simeq 0.95E_{J0}$.

In the charge regime the periodic potential $E_{J0}(1 - \cos\varphi)$ is weak resulting in a strong coupling between neighboring phase states and, in turn, in broad bands. This is evident by considering equation (3.5.14): In the phase limit the factor $b = E_{J0}/2E_C$ is large, whereas it is small for the charge limit. This means that we have a strong periodic potential in the phase limit and only a weak one in the charge regime. We easily can compare this to the situation known for electrons moving in the periodic potential of a crystal. A strong periodic potential results in a localization of the charge carriers (well defined position, undefined momentum). This is equivalent to the phase regime, where we have a strong periodic potential resulting in exponentially narrow bands located at the points $E_n \simeq (n + \frac{1}{2})\hbar\omega_p$. In this case we have a

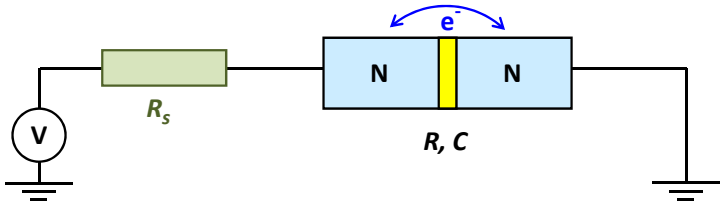

Figure 3.21: Coulomb blockade for a small normal metal tunnel junction with capacitance C und tunneling resistance R. The series resistor R_s must be sufficiently large to avoid the suppression of the Coulomb blockade effect by quantum fluctuations.

well defined phase but an undefined charge state. In contrast, a weak periodic potential results in broad energy bands and delocalized charge carriers with well defined momentum and undefined position. This situation is equivalent to the charge regime, where we have a weak periodic potential resulting in broad bands. In this case we have a well defined charge state but an undefined phase state.

3.5.3 Coulomb and Flux Blockade

Coulomb Blockade in Normal Metal Tunnel Junctions

In the charge regime the large energy E_C results in the phenomenon called ***Coulomb blockade***. To discuss this phenomenon we consider a normal conducting tunnel junction with junction capacitance C (see Fig. 3.21). Suppose the voltage across the junction is V and the related charge and energy $Q = CV$ and $E = Q^2/2C$, respectively. Naively we could assume that there will be a finite tunneling current as soon as there is a finite voltage across the junction. However, if a single electron tunnels from one electrode to the other, the charge on the one electrode changes to $Q - e$. The electrostatic energy after the tunneling process is then $\widetilde{E} = (Q-e)^2/2C$. Since the tunneling process is energetically allowed only if $\widetilde{E} \leq E$, the tunneling current sets in only for $|Q| \geq e/2$ or, equivalently,

$$|V| \quad \geq \quad V_{\rm CB} = \frac{e}{2C} \ . \tag{3.5.21}$$

We see that the tunneling process is only allowed above a certain threshold voltage. This effect is called Coulomb blockade.[43,44] Of course the Coulomb blockade can be experimentally observed only if $E_C > k_B T$, i.e., if thermal fluctuations are small enough. This results in the condition $C < e^2/2k_BT$ for the capacitance ($C \lesssim 1$ fF at 1 K). For a tunnel junction with barrier thickness $d = 1$ nm and dielectric constant $\varepsilon = 5$, the junction area has to be smaller than about $0.02\,\mu\text{m}^2$ to observe the effect at a temperature of about 1 K.

We further have to consider quantum fluctuations. The effect of quantum fluctuations can be estimated using the uncertainty relation $\Delta E \cdot \Delta t \geq \hbar$. Since the tunnel junction has a finite tunneling resistance, charge fluctuations will decay with the characteristic time constant $\tau_{\rm RC} = RC$. If we use $\Delta t = 2\pi RC$ and $\Delta E = e^2/2C$ we obtain $e^2 R \gtrsim h$ or $R \geq h/e^2 = R_K$. We see that the tunneling resistance must be larger than the quantum resistance $R_K = 24.6\,\text{k}\Omega$. For a junction area $A = 0.02\,\mu\text{m}^2$ this results in a resistance times area product of above about $1\,\mu\Omega\text{cm}^2$. This can be easily satisfied.

[43] D.V. Averin, K.K. Likharev, J. Low Temp. Phys. **62**, 345 (1986).
[44] T.A. Fulton, G.J. Dolan, Phys. Rev. Lett. **59**, 109 (1987).

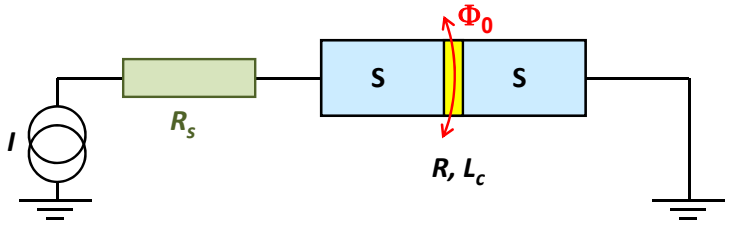

Figure 3.22: Phase blockade for a Josephson junction with Josephson inductance L_c und tunneling resistance R. The series resistor R_s must be sufficiently small to avoid the suppression of the phase blockade effect by quantum fluctuations.

Coulomb Blockade in Superconducting Tunnel Junctions

In the last paragraph we only have considered a normal conducting tunnel junction. We now switch to a superconducting tunnel junction. For simplicity we neglect the role of the unpaired quasiparticles and their interaction with the condensate in the following.[45] In our classical treatment of Josephson junctions we have seen that there is a finite supercurrent flowing between the electrodes at zero voltage. The magnitude of the supercurrent was determined by the phase difference of the macroscopic wave functions describing the two electrodes. Charging effects have been completely neglected in this treatment. However, we immediately see that for $Q^2/2C > k_BT, eV$ the flow of the Cooper pairs with charge $Q = 2e$ is prevented by the Coulomb blockade and charging effects play a dominant role.[46,47] In analogy to the normal metal case we obtain the threshold voltage

$$|V| \geq V_{\mathrm{CB}} = \frac{2e}{2C} = \frac{e}{C} \ . \tag{3.5.22}$$

The blockade of the pair transport means that the charge on both electrodes is fixed. Due to the uncertainty relation $\Delta Q \cdot \Delta\varphi \geq 2e$ this means that the phase is completely smeared out. As already discussed above, a well defined charge state results in a undefined phase and a loss of the Josephson effect. On the other hand, a well defined phase state results in an undefined charge state and the loss of the Coulomb blockade effect.

Phase or Flux Blockade in a Josephson Junction

In analogy to the Coulomb blockade in the charge regime we have a phase or flux blockade in the phase regime (see Fig. 3.22). Due to the large Josephson coupling energy $E_{J0} = \Phi_0 I_c/2\pi$ the phase φ cannot be changed by applying a current across the junction, since it is trapped in one of the minima of the tilt washboard potential. Only if we exceed the critical current I_c, phase changes are possible. That is, in analogy to the Coulomb blockade in the charge regime we can speak about a ***phase blockade*** in the phase regime with the critical current I_c playing the role of the blockade voltage V_{CB}. Since a phase change of 2π is equivalent to moving a single flux quantum across a Josephson junction, we alternatively can denote the phenomenon as ***flux blockade***. Note that the flux quanta are crossing the junction perpendicular to the current direction, whereas the charge carriers are tunneling in current direction.

[45] For a discussion of this point see M. Tinkham, *Introduction to Superconductivity*, McGraw-Hill Book Company, New York (1996).

[46] M.T. Touminen. J.M. Hergenrother, T.S. Tighe, M. Tinkham, Phys. Rev. Lett. **69**, 1997 (1992); Phys. Rev. **B 47**, 11599 (1993).

[47] P. Joyez, P. Lafarge, A. Filipe, D. Esteve, M.H. Devoret, Phys. Rev. Lett. **72**, 2458 (1994).

With the Josephson inductance $L_c = \hbar/2eI_c$ we can write the Josephson coupling energy $E_{J0} = \hbar I_c/2e = \Phi_0^2/4\pi^2 L_c$ and we obtain the current value for the flux blockade to

$$I_{\rm FB} \;\geq\; I_c \;=\; \frac{\Phi_0/2\pi}{L_c} \;=\; \frac{\overline{\Phi}_0}{L_c} \;. \tag{3.5.23}$$

Here, we have used $\overline{\Phi}_0 = \Phi_0/2\pi$. We immediately see the analogy to equation (3.5.22) by making the replacements $I \leftrightarrow V$, $e \leftrightarrow \overline{\Phi}_0$ and $C \leftrightarrow L$.

Of course the phase blockade effect can be observed only if $E_{J0} \gg k_B T$, what can be easily satisfied by using a sufficiently large junction area. The effect of quantum fluctuations can be estimated again using the uncertainty relation $\Delta E \cdot \Delta t \geq \hbar$. Since the tunnel junction has a finite tunneling resistance, phase or equivalently voltage fluctuations will decay with the characteristic time constant $\tau_{\rm LR} = L_c/R$. If we use $\Delta t = 2\pi L_c/R$ and $\Delta E = 2E_{J0} = \hbar I_c/e$ we obtain $R \lesssim h/e^2 = R_K$. We see that in the phase regime the tunneling resistance must be smaller than the quantum resistance $R_K = 24.6\,\mathrm{k\Omega}$.

3.5.4 Coherent Charge and Phase States

Coherent Charge States

In order to discuss the effect of finite Josephson coupling on the charge states in the charge regime, we consider the Cooper pair box sketched in the inset of Fig. 3.23. A Cooper pair box is a small superconducting island, which is coupled to a reservoir via a superconducting tunnel junction. The charge state of the island can be changed continuously by a gate electrode. Suppose the island is in the charge state $|0\rangle$ at $V_g = 0$. If we change the charge by $n \cdot 2e$, we switch the island into the charge state $|n\rangle$. If the different charge states would be completely independent, the energy of each state would correspond to a parabola $(Q - n \cdot 2e)^2/2C_\Sigma$ with $C_\Sigma = C + C_g$ (see Fig. 3.23). These parabola are shown in Fig. 3.20b as dashed lines. However, the charge states are only independent of each other for $E_{J0} = 0$. For a small but finite Josephson coupling there will be an interaction of the charge state $|n\rangle$ and $|n+1\rangle$ at the crossing points of the corresponding parabola at $Q = (n + \frac{1}{2}) \cdot 2e$. The resulting coherent superposition states are represented by the wave functions

$$\Psi_\pm \;=\; a|n\rangle \pm b|n+1\rangle \;, \tag{3.5.24}$$

where a and b are complex numbers. As a consequence, we obtain a splitting of the charge energy at the crossing points, which is called ***level anti-crossing***. The magnitude of the splitting is given by the Josephson coupling energy. A detailed discussion of the level anti-crossing for interacting quantum two-level systems is given in Appendix F.

Fig. 3.23 shows the expected average charge $\langle Q \rangle = 2e\langle N \rangle$ on the superconducting island as a function of the applied gate voltage V_g. Without interaction of neighboring charge states $|n\rangle$ and $|n+1\rangle$ a step-like behavior is expected with a step height of $2e$. However, in reality at the transition regions between the different charge states (crossing points of the parabola shown in Fig. 3.20b) the steps are rounded due to the finite interaction resulting in a superposition of the adjacent charge states. In experiments the charge state of the superconducting island usually is measured using a single electron electrometer. The expected dependence shown in Fig. 3.23 has been confirmed in experiments.[48]

The presence of a coherent quantum mechanical superposition of charge states has been measured recently by **Nakamura**, **Pashkin** and **Tsai**.[49] In their experiment they switched a Cooper pair box for a

[48] V. Bouchiat, D. Vion, P. Joyez, D. Esteve, M.H. Devoret, Physica Scripta **T 76**, 165 (1998).

[49] Y. Nakamura, Yu.A. Pashkin, J.S. Tsai, Nature **398**, 786 (1999).; Physica **B 280**, 405 (2000); Phys. Rev. Lett. **87**, 246601 (2001); Physica **C 367**, 191 (2002).

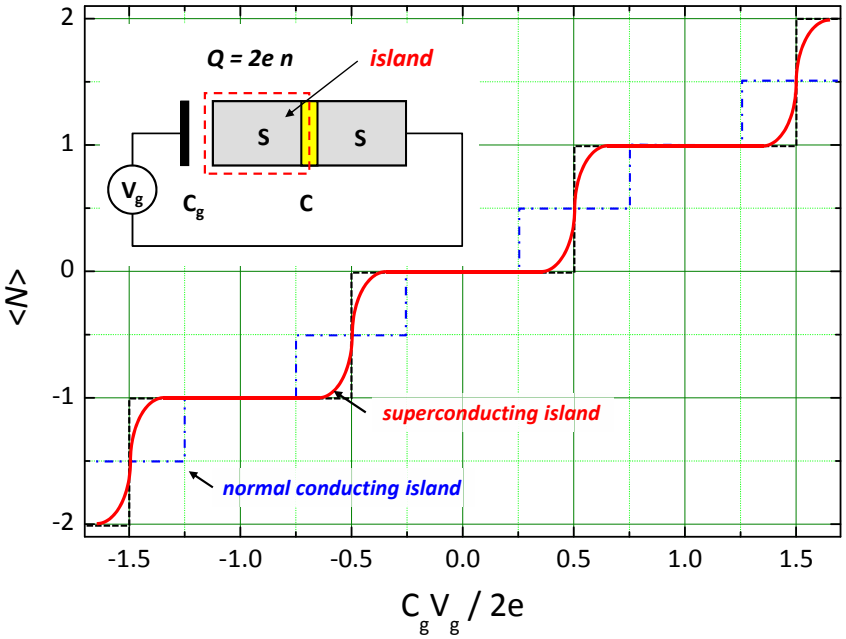

Figure 3.23: Average charge number $\langle N\rangle = \langle Q\rangle/2e$ on a Cooper pair box as a function of the applied gate voltage. The Cooper pair box consists of a superconducting island coupled via a tunnel junction of capacitance C to a reservoir (see inset). The charge state of the island can be varied via a gate capacitor of capacitance C_g. For a superconducting island without any interaction of the different charge states a step-like dependence (dashed curve) is obtained. Due to the finite interaction between neighboring states $|n\rangle$ and $|n+1\rangle$ the steps are rounded (solid line). For comparison, also the dependence expected for a normal conducting island without interaction is shown (dash-dotted line).

short period Δt from $n = 0$ to $n = \frac{1}{2}$ by a pulsed gate. According to quantum mechanics, at $n = \frac{1}{2}$ the system is in a superposition state and coherently oscillates between the states $|0\rangle$ and $|1\rangle$ at a frequency $f = E_{J0}/h$. The probability of finding the system in the charge state $|0\rangle$ after switching off the gate pulse at the time Δt, ranges between 0 and 1. It depends on the length Δt of the gate pulse. Varying the length of the gate pulse, a continuous oscillation of the probability between 0 and 1 is found. These oscillations are called ***Rabi oscillations*** (see Appendix F). A more detailed discussion of the quantum dynamics of coherent charge as well as phase states is given in Chapter 9.

Coherent Phase States

In the same way as we can generate coherent superposition states by the interaction of two adjacent charge states, we can obtain coherent phase states by the interaction of two adjacent phase states. This can be achieved for example by incorporating a single Josephson junction into a superconducting loop of inductance L (rf-SQUID, see section 4.2). To the potential energy of the Josephson junction we then have to add a term $(\Phi - \Phi_{\text{ext}})^2/2L = \frac{1}{2}LI_{\text{cir}}^2$ due to the magnetic energy of the flux in the ring generated by a circulating screening current I_{cir} (compare section 4). The total potential is then given by (compare (3.5.9))

$$U(\phi) \quad = \quad \frac{(\phi - \phi_{\text{ext}})^2}{2L} + E_{J0}\left(1 - \cos 2\pi\frac{\phi}{\Phi_0}\right) \quad . \tag{3.5.25}$$

Here, $\phi = \frac{\hbar}{2e}\varphi = \frac{\Phi_0}{2\pi}\varphi$ and the flux Φ in the loop is related to the phase difference across the junction by $\varphi = 2\pi\frac{\Phi}{\Phi_0}$, i.e. $\Phi = \phi$. The potential (3.5.25) is shown in Fig. 3.24 for $\Phi_{\text{ext}} = \Phi_0/2$. We obtain

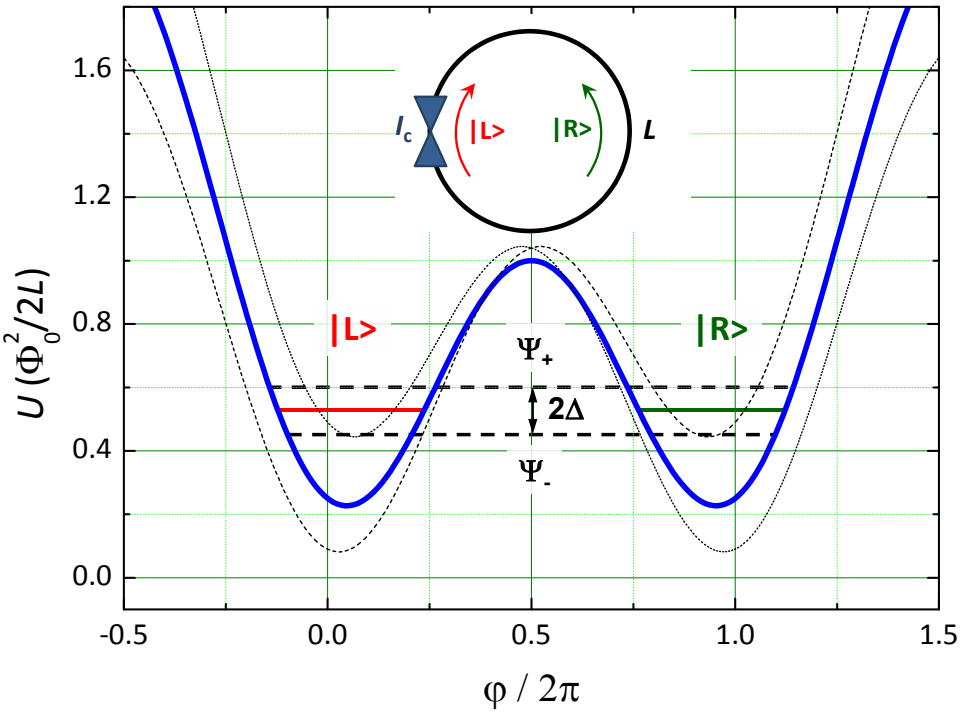

Figure 3.24: Double well potential for the generation of phase superposition states calculated according to (3.5.25) for $\Phi_{\rm ext} = \Phi_0/2$ and $\beta_L = 2LI_C/\Phi_0 = 3$. Shown are the states $|L\rangle$ and $|R\rangle$ corresponding to clockwise and anticlockwise circulating currents (solid lines) and the superposition states Ψ_+ and Ψ_- (dashed line) split by 2Δ. The thin dashed and dotted lines show the potential for $\Phi_{\rm ext} = 0.3\Phi_0$ and $0.7\Phi_0$, respectively.

a double well potential with two degenerate phase states $|L\rangle$ and $|R\rangle$ corresponding to a clockwise and anticlockwise circulating current, respectively. The two phase states are tunnel coupled resulting in the superposition states

$$\Psi_\pm \quad = \quad a|L\rangle \pm b|R\rangle \tag{3.5.26}$$

with energies $E_\pm = \varepsilon_0 \pm \Delta$ with ε_0 the energy of the degenerate phase states and Δ the tunnel splitting. If we move away with the external flux from the value $\Phi_0/2$, the double well potential is tilted to the left or the right lowering the $|L\rangle$ and $|R\rangle$ state, respectively.

Experimental evidence (e.g. Rabi oscillations) for the quantum coherent superposition states corresponding to macroscopic quantum states has been found recently.[50,51,52] Meanwhile several experimental geometries appropriate for the realization of a double well potential similar to that shown in Fig. 3.24 have been studied.[53,54] A detailed discussion of the quantum dynamics of the superposition state will follow in Chapter 9.

3.5.5 Quantum Fluctuations

Quantum mechanics shows that the classical theory of the harmonic oscillator coincides with the quantum one in all details but one: There is a finite motion of the quantum oscillator (quantum fluctuation) at the

[50] J.E. Mooji, T.P. Orlando, L. Levitov, L. Tian, C.H. van der Wal, S. Lloyd, Science **285**, 1036 (1999).
[51] C.H. van der Wal, A.C.J. ter Haar, F.K. Wilhelm, R.N. Schouten, C.P.J.M. Harmans, T.P. Orlando, S. Lloyd, J.E. Mooij, Science **290**, 773 (2000).
[52] J.R. Friedman, V. Patel, W. Chen, S.K. Tolpygo, J.E. Lukens, Nature **406**, 43 (2000).
[53] I. Chiorescu, Y. Nakamura, C.J.P.M. Harmans, J.E. Mooij, Science **299**, 1869 (2003).
[54] Y. Yu, S. Han, X. Chu, S.-I. Chu, Z. Wang, Science **296**, 889 (2002).

lowest energy level $n = 0$. In general, a quantum fluctuation is the temporary change in the amount of energy in a point in space, arising from Heisenberg's uncertainty principle $\Delta E \cdot \Delta t \geq \hbar$. That means that conservation of energy can appear to be violated, but only for small times. This allows the creation of virtual excitations.[55]

The quantum fluctuations can be described in a convenient way by including a Langevin force I_F to the classical basic junction equation, which has the adequate statistical properties.[56,57,58] If we assume that the junction environment is in thermal equilibrium, we can use the Callen-Welton fluctuation-dissipation theorem and write the spectral density of I_F as

$$S_I(f) \;=\; 2\pi\, S_I(\omega) \;=\; 4\,\frac{E(\omega,T)}{R_N}\;. \tag{3.5.27}$$

Here, $E(\omega,T)$ is the average energy of the quantum oscillator with frequency ω at temperature T:

$$\begin{aligned} E(\omega,T) &= \frac{\hbar\omega}{2} + \hbar\omega\,\frac{1}{\exp\left(\frac{\hbar\omega}{k_BT}\right)-1} \\ &= \frac{\hbar\omega}{2}\,\coth\left(\frac{\hbar\omega}{2k_BT}\right)\;. \end{aligned} \tag{3.5.28}$$

This expression describes the smooth transition from the ***Johnson-Nyquist formula*** (classical limit, compare (3.1.15)) at low frequencies ($\hbar\omega, eV \ll k_BT$) to a purely quantum noise at high frequencies ($\hbar\omega \gg k_BT, eV$).

In the classical limit ($\hbar\omega, eV \ll k_BT$) the argument of the coth-function is small and we can use the approximation $\coth x \simeq 1/x$ resulting in the classical Johnson-Nyquist formula

$$S_I(\omega) \;=\; \frac{1}{2\pi}\,\frac{4k_BT}{R_N} \tag{3.5.29}$$

In the quantum limit ($\hbar\omega \gg k_BT, eV$) the argument of the coth-function is large and we can use the approximation $\coth x \simeq 1$ resulting in

$$S_I(\omega) \;=\; \frac{1}{2\pi}\,\frac{2\hbar\omega}{R_N}\;. \tag{3.5.30}$$

3.5.6 Macroscopic Quantum Tunneling

One of the most convincing demonstrations of the quantum aspects of the Josephson effect is probably the observation of ***macroscopic quantum tunneling*** in an underdamped Josephson junction. The process of macroscopic quantum tunneling refers to the escape process of the "phase particle" from a minimum of the tilted washboard potential by tunneling through the barrier (see Fig. 3.25) rather than by thermal activation over the barrier as discussed in section 3.4. The process is called ***macroscopic*** because the tunneling quantity is not a single electron but the phase variable, which describes the collective state of a large, macroscopic number of electrons.

[55] In the modern view, energy is always conserved, but the eigenstates of the Hamiltonian (energy observable) are not the same as (do not commute with) those of the particle number operators.

[56] H.B. Callen, T.E. Welton, Phys. Rev. **83**, 34 (1951).

[57] I.R. Senitzky, Phys. Rev. **124**, 642 (1961).

[58] M. Lax, Phys. Rev. **145**, 110 (1966).

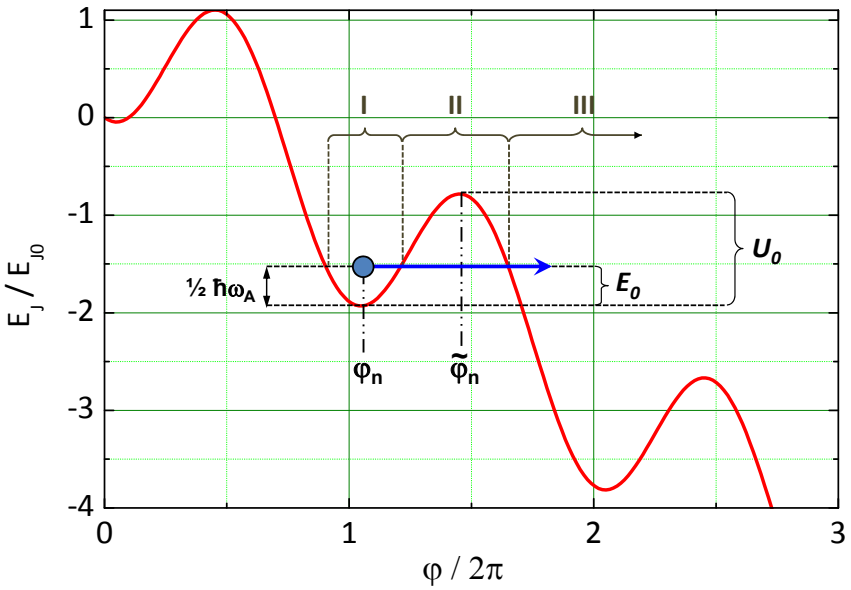

Figure 3.25: Macroscopic quantum tunneling of the gauge-invariant phase difference. U_0 is the barrier height and E_0 the energy of the "phase particle" with respect to the local minimum.

Quantum effects usually are difficult to be observed on a macroscopic scale, since they involve microscopic objects. Since in macroscopic quantum tunneling the system switches from the zero voltage state with the phase variable trapped in a minimum of the tilted washboard potential to the voltage state, where the phase variable is running down the potential, the study of macroscopic quantum tunneling is a particularly sensitive technique to reveal quantum effects. The two states are easily distinguishable. The only competing classical process is thermal activation over the barrier. However, this process can be frozen out by going to low enough temperatures. Another process preventing the observation of quantum effects is the presence of damping. It is reflected in the quantum Hamiltonian by coupling the phase degree of freedom to an environmental Hamiltonian with many degrees of freedom. In our discussion for simplicity we first neglect this coupling to the environment.

In the presence of a dc bias current, the Hamiltonian (3.5.6) is modified by the additional term $-\hbar I\varphi/2e$. As already discussed before, the minimum of the resulting potential occurs at $\varphi = \arcsin i$ with $i = I/I_c$ (compare (2.1.9)). The curvature of the potential at the minimum is[59]

$$\frac{\partial^2 U}{\partial \varphi^2} \quad = \quad E_{J0}\sqrt{1-i^2} \tag{3.5.31}$$

and the classical frequency of small oscillations about the minimum is (compare (3.4.13))

$$\omega_A \quad = \quad \omega_p (1-i^2)^{1/4} \ . \tag{3.5.32}$$

When solved quantum mechanically, the ground state wave function of a harmonic oscillator in such a potential minimum is approximately Gaussian, i.e. $\Psi \propto \exp(-c\cdot(\delta\varphi)^2)$, where $\delta\varphi$ is the deviation of the phase from the minimum value.[60] However, there is one important difference between the harmonic oscillator solution and that for the tilted washboard potential: In contrast to the harmonic oscillator

[59] We use the relation $\arcsin x = \arccos\sqrt{1-x^2}$.

[60] The wave function of the ground state of a harmonic oscillator is

$$\Psi_0 \quad = \quad C_0 \left(\frac{\mu\omega_0}{\pi\hbar}\right)^{1/4} \exp\left\{-\frac{\mu\omega_0}{2\hbar}(\delta\varphi)^2\right\} \mathrm{e}^{-\imath\omega_0 t/2} \ .$$

potential, for the tilted washboard potential the barrier is of finite width. Therefore, there is an exponentially small but finite tunneling amplitude through the barrier, which connects to an outgoing wave in the unbounded space. Therefore, the eigenstates are forming a continuum. However, only those states corresponding to the quasi-bound solutions have a high amplitude in the well of the potential. The energy width Γ of these states is given by $\hbar/\tau$, where τ is the lifetime for the escape from the potential well.

In order to determine the wave function we have to solve the Schrödinger equation for the regions I to III in Fig. 3.25 and then match the solutions at the boundaries (wave matching method). However, since we are not interested in the detailed quantitative result, we disregard algebraic prefactors in the following and concentrate on the exponential factor, which dominates the transmission probability through the barrier. Within the WKB approximation method, in a one-dimensional situation the absolute square $|\Psi(x)|^2$ of the wave function of a particle with mass M and energy E decays in the barrier region as

$$|\Psi(x)|^2 \;\propto\; \exp\left\{-\frac{2}{\hbar}\int\limits_{\mathrm{II}}\sqrt{2M[V(x)-E]}\;dx\right\}\;. \tag{3.5.33}$$

Here the integral extends over the region under the barrier (region II in Fig. 3.25). For a rough estimate we can use a constant average barrier height V_B of width Δx so that (3.5.33) becomes

$$|\Psi(x)|^2 \;\propto\; \exp\left\{-\frac{2}{\hbar}\sqrt{2MV_B}\,\Delta x\right\}\;. \tag{3.5.34}$$

If $U(\varphi) \gg E_0 = \hbar\omega_A/2$ is satisfied, that is, if the ground state energy of the harmonic oscillator is much smaller than the barrier height, we can apply the quasi-classical WKB method to our problem. With respect to the Josephson junction problem we have to replace Δx by $\Delta\varphi$ and have to use $M = (\hbar/2e)^2 C$ (see (3.2.6)). Then we obtain

$$|\Psi(\varphi)|^2 \;\propto\; \exp\left\{-\frac{2}{\hbar}\int\limits_{\mathrm{II}}\sqrt{2\left(\frac{\hbar}{2e}\right)^2 C\left[U(\varphi)-\frac{\hbar\omega_A}{2}\right]}\;d\varphi\right\}\;. \tag{3.5.35}$$

With $U(\varphi) \gg \hbar\omega_A/2$ we can use the approximation $U(\varphi) - \frac{\hbar\omega_A}{2} \simeq U(\varphi)$. Again, for a rough estimate we can use a constant average barrier height U_0 of width $\Delta\varphi$ so that (3.5.35) becomes

$$|\Psi(\varphi)|^2 \;\propto\; \exp\left\{-\sqrt{\frac{U_0}{E_C}}\,\Delta\varphi\right\} \tag{3.5.36}$$

with $E_C = e^2/2C$. This results in the decay rate

$$\Gamma \;=\; \frac{\omega_A}{2\pi}\,\exp\left\{-\sqrt{\frac{U_0}{E_C}}\,\Delta\varphi\right\}\;. \tag{3.5.37}$$

For small tilt angles of the washboard potential we usually (except for very small junctions) have $U_0 \simeq 2E_{J0} \gg E_C$ and $\Delta\varphi \simeq 2\pi$. Therefore, the transmission probability is very small. However, with increasing bias current both U_0 and $\Delta\varphi$ become smaller as

$$U_0 \;\simeq\; 2E_{J0}(1-i^2)^{3/2} \qquad \text{and} \qquad \Delta\varphi \;\simeq\; \pi\sqrt{1-i^2} \tag{3.5.38}$$

and the transmission probability can become significant and can be measured.[61,62,63]

In the following, we briefly give an estimate for the temperature $T^\star$, at which the rate for macroscopic quantum tunneling becomes equal to that for thermal activation. Note that the rate for thermal activation is proportional to $\exp(-U_0/k_BT)$ and therefore also becomes exponentially large when increasing the bias current to the critical current. This already indicates that the temperature $T^\star$ should depend only weakly on the applied current. We start our discussion with $I \simeq 0$. In this limit, $U_0 \simeq 2E_{J0}$, $\hbar\omega_p = \sqrt{8E_{J0}E_C} \simeq 2\sqrt{U_0E_C}$. If we set $\Delta\varphi \simeq \pi$, with these approximations we can rewrite (3.5.37) as

$$\Gamma \;=\; \frac{\omega_p}{2\pi}\,\exp\left\{-2\pi\frac{U_0}{\hbar\omega_p}\right\} \tag{3.5.39}$$

and the rates for macroscopic quantum tunneling and thermal activation become equal at the temperature

$$k_BT^\star \;\simeq\; \frac{\hbar\omega_p}{2\pi}\;. \tag{3.5.40}$$

For $I > 0$, we have to take into account the current dependent factors. We see that with $\sqrt{U_0} \propto (1-i^2)^{3/4}$ and $\Delta\varphi \propto (1-i^2)^{1/2}$ the exponent in (3.5.36) scales with $(1-i^2)^{5/4}$, whereas the exponent in the Boltzmann factor $\exp(-U_0/k_BT)$ scales as $(1-i^2)^{3/2}$. That is, they differ by $(1-i^2)^{1/4}$, which exactly corresponds to the current dependence of the frequency ω_A for small oscillations around the minimum. Thus, for arbitrary currents below I_c we obtain the general result for the cross-over temperature[64]

$$k_BT^\star \;\simeq\; \frac{\hbar\omega_A}{2\pi} \;=\; \frac{\hbar\omega_p}{2\pi}\,(1-i^2)^{1/4}\;. \tag{3.5.41}$$

For a typical plasma frequency of the order of $10^{11}\mathrm{s}^{-1}$ we obtain $T^\star \sim 100\,\mathrm{mK}$. This temperature is easily accessible with dilution refrigerators.[65]

Additional Topic:
Effect of Damping

In our previous discussion we have neglected the effect of damping. To account for damping in quantum tunneling we have to take into account the coupling of the system with the environment (heat bath). This

[61] R.F. Voss, R.A. Webb, Phys. Rev. Lett. **47**, 265 (1981).
[62] J.M. Martinis, M.H. Devoret, J. Clarke, Phys. Rev. **B 35**, 4682 (1987).
[63] J. Clarke, A.N. Cleland, M.H. Devoret, D. Esteve, J.M. Martinis, Science **239**, 992 (1988).
[64] For the decay rate we obtain the result

$$\Gamma \;=\; \frac{\omega_A}{2\pi}\left(\frac{864\pi U_0}{\hbar\omega_A}\right)^{1/2}\exp\left\{-\frac{36U_0}{5\hbar\omega_A}\right\}\;.$$

See K. K. Likharev, *Dynamics of Josephson Junctions and Circuits*, Gordon and Breach Science Publishers, New York (1986).

[65] We note that in a real experiments the rate for macroscopic quantum tunneling should also be large enough that a single event can be measured at least within the lifetime of the person doing the experiment. If a convenient rate required for an experiment is τ^{-1}, we also have to satisfy the criterion

$$\omega_A\,\exp\left\{-\sqrt{\frac{U_0}{E_C}}\,\Delta\varphi\right\} \;\geq\; \tau^{-1}\;.$$

With $\sqrt{U_B} \propto (1-i^2)^{3/4}$ this can of course always be done by using $i \simeq 1$. However, since due to technical reasons one usually has to use $i \leq 0.99$, this sets an upper limit for E_{J0}/E_C. Therefore, in most experiments junctions with small critical currents (typically smaller than $10\,\mu\mathrm{A}$) and, hence, small E_{J0} are used.

results in a much more complicated problem that has been solved by **Caldeira** and **Leggett** within the RCSJ model.[66,67,68,69] According to this work the damping results in a multiplication of the decay rate by the factor $\exp(-2\pi C U_0 \tau/\hbar) < 1$, where $C \simeq 1$ for $\omega_A \tau_{RC} \gg 1$ and $C = 3/2$ for $\omega_A \tau_{RC} \ll 1$. That is, damping strongly suppresses macroscopic quantum tunneling. Due to the strong suppression of quantum tunneling the damped system follows the classical thermal activation behavior to lower temperatures. The crossover temperature $T^\star$ in the presence of damping is no longer given by (3.5.41) but by a similar expression, where ω_A has been replaced by a damping dependent frequency $\omega_R = 1/\tau$:

$$k_B T^\star \simeq \frac{\hbar \omega_R}{2\pi} \tag{3.5.42}$$

with

$$\omega_R = \omega_A \left\{ \sqrt{1+\alpha^2} - \alpha \right\} . \tag{3.5.43}$$

Here, $\alpha = 1/2R_N C\omega_A$ is a dimensionless damping parameter. Obviously, for $\alpha = 0$ we recover the result (3.5.40). For $\alpha \gg 1$, we obtain $\omega_R \simeq \omega_A/2\alpha = \omega_A^2 R_N C \ll \omega_A$.[70] Hence, we obtain a much lower cross-over temperature $T^\star$ and the observation of macroscopic quantum tunneling is more difficult. The strong damping result can be understood by the fact that in the limit of strong damping one has to replace the undamped oscillation frequency ω_A around the minimum of the potential well by the characteristic frequency of an overdamped oscillator, namely by $\omega_A/2\alpha = \omega_A^2 R_N C = \omega_R$.

An experimental example is shown in Fig. 3.26, where the temperature dependence of the escape rate described by an effective temperature T_{esc} is plotted versus the sample temperature for a "quantum junction" and a "classical junction". In the experiment the capacitance was chosen to put the sample into the lightly (quantum junction) and moderate damping regime (classical junction) in the presence of transmission line damping. Excellent agreement with theoretical predictions of the cross-over temperature was found. It is also seen that the escape temperature follows the sample temperature in the classical regime where thermal activation dominates. In the low temperature regime T_{esc} is a fictitious temperature, at which the classical thermal activation would yield the same escape rate as the actual quantum tunneling.

Phase Diffusion by Macroscopic Quantum Tunneling

An interesting situation occurs in the study of small junctions with small coupling energy and high resistance. In such junctions a finite resistance R_p is observed at low current, which is interpreted classically as resulting from phase diffusion. The temperature dependence of R_p is described at least qualitatively in terms of the classical thermally activated phase slippage (compare (3.4.17)). However, at very low temperature the data appear to bottom out at a finite, temperature independent phase slippage rate. Qualitatively this is what one would expect, if macroscopic quantum tunneling takes over below a certain cross-over temperature. Then a temperature independent value is expected for R_p determined by the rate of macroscopic quantum tunneling given by (3.5.36) with $U_0 = 2E_{J0}$ and $\Delta\varphi = \pi$. However, until now the validity of this interpretation is unclear.[71]

[66] A.O. Caldeira, A. Leggett, Phys. Rev. Lett. **46**, 211 (1981).

[67] A.O. Caldeira, A. Leggett, Ann. Phys. **149**, 374 (1983).

[68] A.I. Larkin, Yu.N. Ovchinnikov, JETP Lett. **37**, 322 (1983).

[69] H. Grabert, *Macroscopic Quantum Tunneling and Quantum Coherence in Josephson Systems*, in "Superconducting Quantum Interference Devices and their Applications", H.-D. Hahlbohm and H. Lübbig eds., de Gruyter, Berlin (1985), p. 289.

[70] We use the approximation $\sqrt{1+\alpha^2} = \alpha\sqrt{1+1/\alpha} \simeq \alpha(1+1/2\alpha)$.

[71] For further discussion see M. Tinkham, *Introduction to Superconductivity*, McGraw-Hill Book Company, New York (1996).

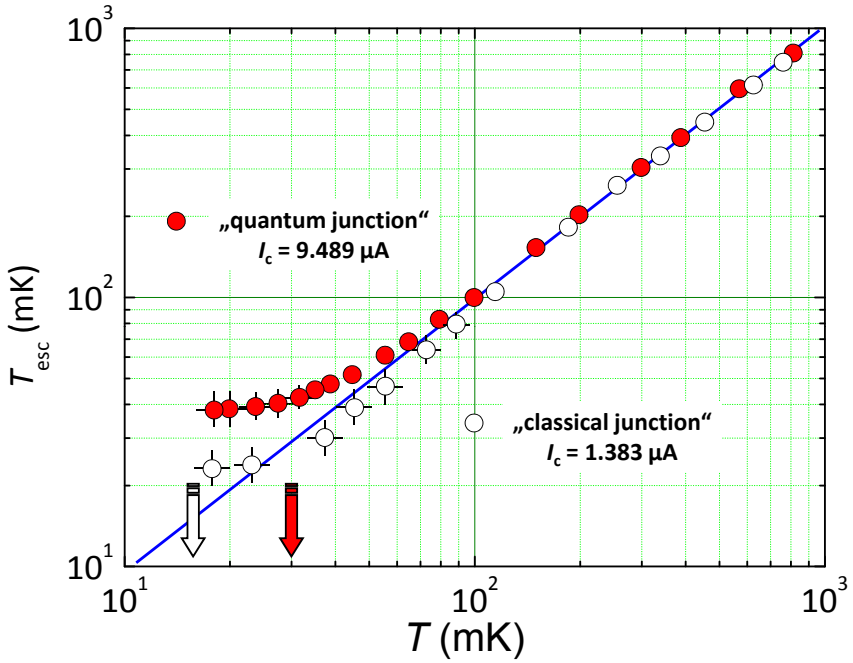

Figure 3.26: Temperature dependence of the escape rate described by an effective temperature for a "quantum junction" and a "classical junction". The arrows mark the theoretically expected cross-over temperatures from thermal activation to macroscopic quantum tunneling (data after Martinis *et al.*, Phys. Rev. **B 35**, 4682 (1987)).

3.6 Voltage State of Extended Josephson Junctions

In the previous sections we have assumed that the Josephson junction can be modeled as a lumped element. That is, we have described the junction by integral quantities such as its maximum Josephson current. Such a description is only possible for small Josephson junctions ($W, L < \lambda_J$) in the absence of an applied magnetic field. In this section we extend the discussion of extended Josephson junctions in the zero voltage state (see section 2.2 and 2.3) to the finite voltage state.

3.6.1 Negligible Screening Effects

As we have done for the zero voltage state (cf. section 2.2.6), for simplicity we first consider the case, where we can completely neglect the effect of the currents flowing in the junction electrodes. In this case the magnetic flux density in the junction is determined solely by the applied magnetic field: $\mathbf{B} = \mathbf{B}^{ex}$. Furthermore, the junction voltage V is given by the applied voltage V_0 throughout the junction. Then, the time dependence of the gauge-invariant phase difference is the same everywhere and given by the voltage-phase relation

$$\frac{\partial \varphi}{\partial t} \;=\; \frac{2e}{\hbar} V_0 \;=\; \omega_0 \;, \tag{3.6.1}$$

whereas the spatial variation (for the junction geometry of Fig. 2.4) is given by

$$\frac{\partial \varphi(z,t)}{\partial z} \;=\; \frac{2\pi}{\Phi_0} t_B B_y(z,t) \;. \tag{3.6.2}$$

Eqs. (3.6.1) and (3.6.2) are satisfied by a gauge-invariant phase difference given by

$$\varphi(z,t) \;=\; \varphi_0 + \omega_0 t + \frac{2\pi}{\Phi_0} B_y t_B \cdot z \;=\; \varphi_0 + \omega_0 t + k \cdot z \;. \tag{3.6.3}$$

This solution gives a periodic Josephson current distribution (compare discussion given in section 2.2.6)

$$J_s(z,t) \;=\; J_c \sin\left(\omega_0 t + k \cdot z + \varphi_0\right) \tag{3.6.4}$$

of exactly the same form as shown in Fig. 2.6. That is, the current distribution has the same form as the Josephson vortices in the zero voltage case except that in the case of a finite voltage these vortices are moving along the z-direction with a velocity (compare section 2.2.6 and Fig. 2.13)

$$v_z \;=\; \frac{\omega_0}{k} \;=\; \frac{V_0}{B_y t_B} \;. \tag{3.6.5}$$

This motion of Josephson vortices is completely analogous to the motion of Abrikosov vortices in a type II superconductor.

3.6.2 The Time Dependent Sine-Gordon Equation

We now take into account the effect of the Josephson currents on the time-dependent electromagnetic fields. We consider a Josephson junction as shown in Fig. 2.4. The barrier is in the yz-plane, the magnetic field is applied in y-direction resulting in phase variations along the z-direction. The applied current is flowing in the negative x-direction. The magnetic flux density in the junction results both from the externally applied field ***and*** the Josephson current density and must satisfy Ampère's law. With $\mathbf{B} = \mu_0\mathbf{H}$ (we assume $\mu = 1$) and $\mathbf{D} = \varepsilon\varepsilon_0\mathbf{E}$ we obtain

$$\nabla \times \mathbf{B} \quad = \quad \mu_0\mathbf{J} + \varepsilon\varepsilon_0\mu_0\frac{\partial \mathbf{E}}{\partial t} \ . \tag{3.6.6}$$

Here, μ_0 and ε_0 are the permeability and permittivity in vacuum, respectively, and ε is the dielectric constant of the barrier material.

In contrast to section 2.2 and 2.3 we now have to take into account the term $\partial\mathbf{E}/\partial t$, which was zero in the zero voltage state of the junction. Then, for the geometry of Fig. 2.4 we obtain

$$\frac{\partial B_y(z,t)}{\partial z} \quad = \quad -\mu_0 J_x(z,t) - \varepsilon\varepsilon_0\mu_0\frac{\partial E_x(z,t)}{\partial t} \ . \tag{3.6.7}$$

Using (3.6.2) we obtain

$$\frac{\partial^2\varphi(z,t)}{\partial z^2} \quad = \quad -\frac{2\pi}{\Phi_0}t_B\left\{\mu_0 J_x(z,t) + \varepsilon\varepsilon_0\mu_0\frac{\partial E_x(z,t)}{\partial t}\right\} \ . \tag{3.6.8}$$

Then, with $E_x = -V/d$, $J_x = -J_c\sin\varphi$ and $\partial\varphi/\partial t = 2\pi V/\Phi_0$ we can rewrite (3.6.8) as

$$\frac{\partial^2\varphi(z,t)}{\partial z^2} \quad = \quad -\frac{2\pi}{\Phi_0}t_B\left\{\mu_0 J_c\sin\varphi(z,t) + \varepsilon\varepsilon_0\mu_0\frac{\Phi_0}{2\pi d}\frac{\partial^2\varphi(z,t)}{\partial t^2}\right\} \ . \tag{3.6.9}$$

With the definition (2.3.6) of the Josephson penetration depth, $\lambda_J \equiv \sqrt{\frac{\Phi_0}{2\pi\mu_0 t_B J_c}}$, we can rearrange this equation and obtain a wave equation for the junction known as the ***time dependent Sine-Gordon equation***:

$$\frac{\partial^2\varphi(z,t)}{\partial z^2} - \frac{1}{\bar{c}^2}\frac{\partial^2\varphi(z,t)}{\partial t^2} - \frac{1}{\lambda_J^2}\sin\varphi(z,t) \quad = \quad 0 \ . \tag{3.6.10}$$

Here,

$$\bar{c} \quad = \quad \sqrt{\frac{d}{\varepsilon\varepsilon_0\mu_0 t_B}} = \frac{1}{\sqrt{\varepsilon_0\mu_0}}\sqrt{\frac{d}{\varepsilon(2\lambda_L + d)}} = c\sqrt{\frac{1}{\varepsilon(1 + 2\lambda_L/d)}} \tag{3.6.11}$$

is the velocity of the TEM mode in the transmission line formed by the two junction electrodes and the dielectric barrier named the ***Swihart velocity***.[72] Since $\varepsilon \sim 5 - 10$ and $2\lambda_L/d \sim 50 - 100$, the Swihart

[72] J.C. Swihart, J. Appl. Phys. **32**, 461 (1961).

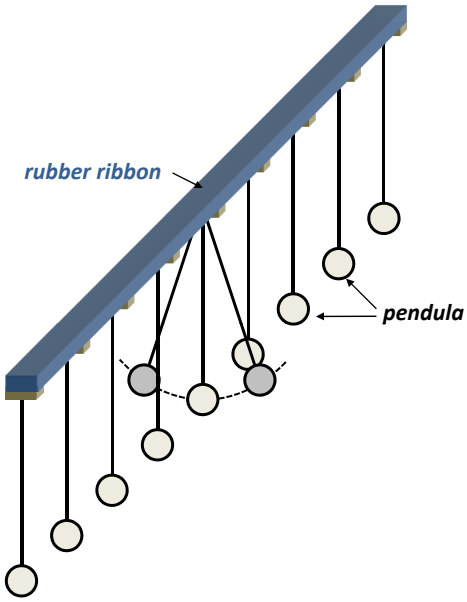

Figure 3.27: Chain of pendula attached to a twistable rubber ribbon as a mechanical analogue for the phase dynamics of a long Josephson junction. If one pendulum is deflected from its equilibrium position, the rubber ribbon is locally twisted and exerts a torque on the neighboring pendula, which in turn are also deflected (not shown).

velocity is usually by more than an order of magnitude smaller than the velocity of light in vacuum. Furthermore, the wavelength is significantly reduced compared to free space. For example, microwaves at $f = 10\,\mathrm{GHz}$, which have a free-space wavelength of about 3 cm, would have a wavelength in the junction of only about 1 mm. This disparity of the wave velocities makes it difficult to couple electromagnetic energy in and out of the junction.

Using the expressions for $\overline{c}$ and λ_J we obtain

$$\frac{\overline{c}}{\lambda_J} = \frac{\omega_p}{2\pi} = \nu_p \tag{3.6.12}$$

and we can rewrite the sine-Gordon equation as

$$\lambda_J^2 \frac{\partial^2 \varphi(z,t)}{\partial z^2} - \frac{4\pi^2}{\omega_p^2} \frac{\partial^2 \varphi(z,t)}{\partial t^2} - \sin\varphi(z,t) = 0\ . \tag{3.6.13}$$

The mechanical analogue to the phase dynamics described by (3.6.10) or (3.6.13) is a chain of mechanical pendula, which are attached to a twistable rubber ribbon (see Fig. 3.27). If we would have a spatially homogeneous current density $J_x(z) = const$, the term $\frac{\partial^2 \varphi}{\partial z^2}$ would vanish and we obtain the result of the RCSJ model. For the pendulum analogue this would mean that we would establish a rigid connection between all pendula so that all pendula have to rotate synchronously. The term $\lambda_J^2 \frac{\partial^2 \varphi}{\partial z^2}$ can be interpreted within the pendulum model as the restoring torque, which is acting on a pendulum at position z by the neighboring pendula. Since the pendula are fixed at a twistable rubber ribbon, a finite restoring force is generated if the neighboring pendula are twisted against each other.

3.6.3 Solutions of the Time Dependent Sine-Gordon Equation

The time dependent Sine-Gordon equation is nonlinear and has many interesting types of behavior. We only address a few simple cases. We restrict ourselves to quasi-one-dimensional junctions having a

width $W \ll \lambda_J$. We call these junctions ***short*** and ***long***, if their length L is small and large compared to the Josephson penetration depth λ_J, respectively.

Short Junctions ($L \ll \lambda_J$), Low and Intermediate Damping

In the short junction limit ($L \ll \lambda_J$) we can neglect the z variation of φ so that the Sine-Gordon equation reduces to

$$\frac{\partial^2 \varphi(z,t)}{\partial t^2} + \frac{\omega_p^2}{4\pi^2} \sin\varphi(z,t) \quad = \quad 0 \ . \tag{3.6.14}$$

This equation is equivalent to the differential equation (compare section 3.2) found from the RCSJ model approximation for zero damping ($G_N = 0$) and zero bias current ($I = 0$). This is expected, since for $L \ll \lambda_J$ the behavior of the lumped junction modeled by the RCSJ model should be recovered. Note that the definition $\omega_p^2 = 2eI_c/\hbar C$ is equivalent to the ω_p^2 value in (3.6.14) with $C/A_i = \varepsilon\varepsilon_0/d$, $I_c/A_i = J_c$ and $c^2 = 1/\varepsilon_0\mu_0$. Of course, the Sine-Gordon equation in the same way as the RCSJ model can be generalized by the inclusion of a damping term which is proportional to $\partial\varphi/\partial t$.[73] However, we will not discuss the case of finite damping here. As already discussed in section 3.2, in the case of small amplitudes we can use the approximation $\sin\varphi \simeq \varphi$, that is, we can linearize the differential equation. In this case the solutions of (3.6.14) are plasma oscillations (compare (3.2.12)).

Long Junction Limit ($L \gg \lambda_J$), Solitons

The time dependent Sine-Gordon equation is invariant under the Lorentz transformation, in which $\bar{c}$ plays the role of the velocity of light. This can be seen by its structure. An interesting type of solution for the (infinitely) long Josephson junction is the ***soliton*** or ***fluxon*** solution, which we already have discussed in section 2.3.2 for the stationary case. The solution has the form

$$\varphi(z,t) \quad = \quad 4\arctan\left\{\exp\left(\pm\frac{\frac{z-z_0}{\lambda_J} - \frac{v_z}{\bar{c}}t}{\sqrt{1-\left(\frac{v_z}{\bar{c}}\right)^2}}\right)\right\} \ . \tag{3.6.15}$$

This solution maintains the value $\varphi = \pi$ at the moving point $z = z_0 + v_z t$ and goes from 0 to 2π as $[z-(z_0+v_z t)]$ goes from $-\infty$ to $+\infty$ for the upper sign ("fluxon") and vice versa for the lower sign ("anti-fluxon"). The solution represents a fluxon or anti-fluxon as shown in Fig. 2.14 moving with velocity v_z along the junction. In the pendulum analogue the fluxon corresponds to a local 360° twist of the rubber ribbon with the twist axis parallel to the ribbon.

Under the action of the Lorentz force due to the applied current the fluxon is moved along the junction. The fluxon behaves as a particle and suffers Lorentz contraction on approaching the Swihart velocity $\bar{c}$, which plays the role of the velocity of light. For example, if a fluxon moves along the z-direction, it becomes narrower proportional to $1/\sqrt{1-v_z^2/\bar{c}^2}$. Furthermore, the moving fluxon causes a temporal change of the local phase difference which according to the 2. Josephson equation corresponds to a voltage. Hence, the moving fluxon corresponds to a voltage pulse, which is becoming sharper with increasing velocity due to Lorentz contraction in order to satisfy the condition $\int V dt = \Phi_0$.

[73] D.W. McLaughlin, A.C. Scott, Phys. Rev. **A 18**, 1652 (1978).

We also note that other solutions exist for the infinitely long lossless junction representing fluxon-fluxon collisions, fluxon-anti-fluxon collisions, bound states, plasma waves etc.. Most of these solutions, which will not be discussed here, have been observed experimentally.[74,75,76]

The linearized Sine-Gordon Equation: Josephson Plasma

Another class of solutions can be studied by linearizing the Sine-Gordon equation. Let

$$\varphi(z,t) \quad = \quad \varphi_0(z)+\varphi_1(z,t) \ , \tag{3.6.16}$$

where $\varphi_0(z)$ is a time independent solution and $\varphi_1(z,t)$ is a small deviation from this solution, i.e. $\varphi_1 \ll \varphi_0$. Then, a good approximation is

$$\sin\varphi \quad \simeq \quad \sin\varphi_0+\varphi_1\cos\varphi_0 \ . \tag{3.6.17}$$

Substitution into the Sine-Gordon equation and keeping only linear terms in φ_1 yields

$$\frac{\partial^2\varphi_0}{\partial z^2}+\frac{\partial^2\varphi_1(z,t)}{\partial z^2}-\frac{1}{\bar{c}^2}\,\frac{\partial^2\varphi_1(z,t)}{\partial t^2}-\frac{1}{\lambda_J^2}\,\sin\varphi_0-\frac{1}{\lambda_J^2}\,\cos\varphi_0\,\varphi_1(z,t) \quad = \quad 0 \ . \tag{3.6.18}$$

With $\frac{\partial^2\varphi_0}{\partial z^2}=\frac{1}{\lambda_J^2}\,\sin\varphi_0$ (φ_0 has to satisfy the time independent Sine-Gordon equation) we obtain

$$\frac{\partial^2\varphi_1(z,t)}{\partial z^2}-\frac{1}{\bar{c}^2}\,\frac{\partial^2\varphi_1(z,t)}{\partial t^2}-\frac{1}{\lambda_J^2}\,\cos\varphi_0\,\varphi_1(z,t) \quad = \quad 0 \ . \tag{3.6.19}$$

If we further assume that φ_0 varies slowly over the scale that φ_1 changes, we can assume $\varphi_0 \simeq const$. In this case the solution is

$$\varphi_1(z,t) \quad = \quad \exp\left(-\imath[kz-\omega t]\right) \tag{3.6.20}$$

and ω has to satisfy the dispersion relation

$$\omega^2 \quad = \quad \bar{c}^2k^2+\omega_{p,J}^2 \ . \tag{3.6.21}$$

Here, $\omega_{p,J}$ is the Josephson plasma frequency and is given by

$$\frac{\omega_{p,J}^2}{4\pi^2} \quad = \quad \frac{\bar{c}^2}{\lambda_J^2}\,\cos\varphi_0 \ . \tag{3.6.22}$$

Note that for frequencies below $\omega_{p,J}$ the wave vector k is imaginary so that no propagating solutions exist. However, for $\omega > \omega_{p,J}$ modes will propagate and at $\omega = \omega_{p,J}$ the wavelength will be infinitely long just as it is for the plasma frequency in a metal. With the typical values $\bar{c} \sim 0.05c$ and $\lambda_J \sim 100\,\mu$m for Nb Josephson junctions we obtain a Josephson plasma frequency of about 10 GHz.

In the pendulum analogue the Josephson plasma waves are obtained, if we deflect a single pendulum within a coupled chain of pendula and then let it relax. This results in a wavelike excitation that propagates along the chain. We note that the above discussion can be extended to the case of larger applied currents. In this case the plasma frequency $\omega_{p,J}$ has to be replaced by the current dependent frequency $\omega_{p,J}(1-i^2)^{1/4}$.

[74] R.A. Fulton, R.C. Dynes, Solid State Commun. **12**, 57 (1973).

[75] B. Duenholm, O.A. Levring, J. Mygind, N.F. Pedersen, O.H. Soerensen, M. Cirillo, Phys, Rev. Lett. **46**, 1299 (1981).

[76] K. Nakajima, H. Mizusawa, Y. Sawada, H. Akoh, S. Takada, Phys. Rev. Lett. **65**, 1667 (1990).

Plane waves: If λ_J is very large or the driving current is very small, we can completely neglect the term $\sin\varphi/\lambda_J^2$ and the Sine-Gordon equation reduces to the familiar linear wave equation

$$\frac{\partial^2\varphi(z,t)}{\partial z^2} - \frac{1}{\bar{c}^2}\frac{\partial^2\varphi(z,t)}{\partial t^2} = 0 \ . \tag{3.6.23}$$

The solutions of this equation are simply plane waves with velocity $\bar{c}$.

3.6.4 Additional Topic: Resonance Phenomena

So far we have discussed Josephson plasma waves and fluxons as possible solutions of the time-dependent sine-Gordon equation. The interaction of these excitations with the oscillating Josephson current results in interesting resonance phenomena appearing as structures in the current-voltage characteristics. In the following we will briefly address a few of them. We will do so, since some of these dynamic phenomena are not only interesting with respect to nonlinear dynamics but also are used in high-frequency applications of Josephson junctions.[77] We will come back to them in chapters 6 and 7.

Flux-Flow Steps and the Eck peak

For $B_{\rm ext} > 0$, the Josephson current density is spatially modulated with a wave vector $k = \frac{2e}{\hbar}B_y t_B$. In the voltage state, this spatially modulated current density is moving along the junction at velocity $v_z = V/B_y t_B$. The oscillating Josephson current density can excite Josephson plasma waves. As for every driven oscillator we expect a resonant behavior, if both the wave vector and the frequency of the two excitations match.[78] That is, the electromagnetic waves are expected to strongly couple to the Josephson currents, if the wave velocity $\bar{c}$ matches the velocity v_z of the moving vortex pattern. This occurs, when the junction voltage is

$$V_{\rm Eck} = \bar{c}B_y t_B = \sqrt{\frac{d}{\varepsilon\varepsilon_0\mu_0 t_B}}\,B_y t_B = \frac{\omega_p}{2\pi}\frac{\lambda_J}{L}B_y t_B L = \frac{\omega_p}{2\pi}\frac{\lambda_J}{L}\Phi_0\frac{\Phi}{\Phi_0} \ , \tag{3.6.24}$$

where we have used $\bar{c} = \frac{\omega_p}{2\pi}\lambda_J$, and $\Phi = B_y t_B L$. The IVCs of Josephson junctions indeed show a current peak at the matching condition. This peak was first found by **R. E. Eck** *et al.*[79] and therefore is called the the ***Eck peak***. The so-called ***Eck voltage*** corresponds to the frequency

$$\omega_{\rm Eck} = \frac{2e}{\hbar}V_{\rm Eck} = \omega_p\frac{\lambda_J}{L}\frac{\Phi}{\Phi_0} \ . \tag{3.6.25}$$

The Eck peak can be interpreted as the result of the nonlinear interaction of the current wave given by (3.6.4) with the traveling electromagnetic wave of the same velocity. In fact the traveling wave of current (3.6.4) excites only the traveling wave of the same direction. When damping is low, the electromagnetic wave reflected at the open end of the junction transmission line can travel back almost without any loss of amplitude. Hence, a standing wave is formed. The Eck peak is therefore observed only at ***medium damping*** and large junction length $kL \gg 1$ (with $k = \frac{2e}{\hbar}B_y t_B$ this is equivalent to $B_y t_B L \gg \Phi_0/2\pi$), where the backward wave is significantly damped after reflection.

[77] For a detailed discussion of the dynamic behavior of long Josephson junctions see:
J. Bindslev-Hansen, P.E. Lindeloff, Rev. Mod. Phys. **56**, 431 (1981).
M. Darula, T. Doderer, S. Beuven, Supercond. Sci. Techn. **12**, R1 (1999).
K. K. Likharev, *Dynamics of Josephson Junctions and Circuits*, Gordon and Breach Science Publishers, New York (1986).

[78] Note that we have to deal with a nonlinear oscillator, which may have a much more complicated behavior in particular for large driving amplitudes.

[79] R.E. Eck, D. J. Scalapino, B.N. Taylor, Phys. Rev. Lett. **13**, 15 (1964).

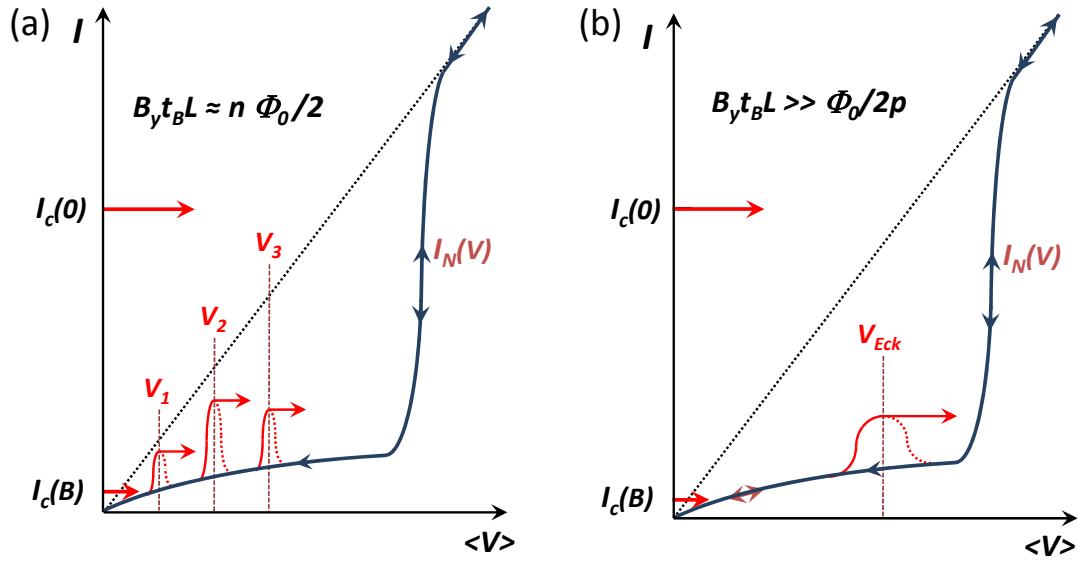

Figure 3.28: Schematic IVCs of a long Josephson tunnel junction at small damping and/or small magnetic field (a) showing the Fiske steps at voltages V_n and at medium damping and/or medium magnetic field (b) showing the Eck peak. Note that if the external source is a current source, there will be horizontal jumps in the IVCs as indicated by the arrows, since the current is fixed by the external source.

The appearance of the Eck peak can be interpreted also as the result of a maximum velocity for moving Josephson vortices. We already have discussed in section 3.6.1 that the Josephson vortices move under the action of the Lorentz force of an applied current at a velocity $v_z = V_{\rm ff}/B_y t_B$ (compare (3.6.5)). Of course, the velocity v_z depends on the damping and a steady state motion is obtained, if the Lorentz force equals the friction force. We denote the resulting voltage as flux-flow voltage $V_{\rm ff}$. If we increase the driving force, i.e. the applied current, we expect that v_z and hence $V_{\rm ff}$ is increasing. However, we have to take into account that the maximum velocity is bound to $\overline{c}$. That is, upon approaching $\overline{c}$ a further increase of the current will no longer result in an increase of the velocity and the corresponding flux-flow voltage. Therefore, in the IVCs we obtain a so-called ***flux-flow step*** at the limiting voltage

$$V_{\rm ffs} \;=\; \overline{c}\, B_y t_B \;=\; \overline{c}\,\frac{\Phi}{L} \;=\; \frac{\omega_p}{2\pi}\,\frac{\lambda_J}{L}\,\Phi_0\,\frac{\Phi}{\Phi_0}\;. \tag{3.6.26}$$

The current step in the IVC is therefore also called ***flow-flow step***. We see that $V_{\rm ffs}$ just corresponds to the Eck voltage.

Fiske steps

A related effect is the observation of steps in the IVCs as first found by **M. D. Fiske**.[80,81] The ***Fiske steps*** occur at junction voltages V_n, where the frequency of the oscillating Josephson currents matches the frequencies

$$\omega_n \;=\; 2\pi f_n \;=\; 2\pi\frac{\overline{c}}{2L}\,n \;=\; \frac{\pi\overline{c}}{L}\,n \tag{3.6.27}$$

[80] M.D. Fiske, Rev. Mod. Phys. **36**, 221 (1964).
[81] D.D. Coon, M.D. Fiske, Phys. Rev. **A 138**, 744 (1965).

of the electromagnetic cavity modes, which can be regarded as standing wave modes. Note that the two junction electrodes separated by the insulating barrier can be regarded as a cavity with the eigenfrequencies given by (3.6.27). The Fiske steps occur at the voltages

$$V_n \;=\; \frac{\hbar}{2e}\omega_n \;=\; \Phi_0\frac{\bar{c}}{2L}\,n \;=\; \frac{\omega_p}{2\pi}\,\frac{\lambda_J}{L}\,\Phi_0\,\frac{n}{2}\;. \tag{3.6.28}$$

For a typical long junction with $L \sim 100\,\mu$m the first Fiske step appears at a frequency of the order of 10 GHz. The corresponding voltage is of the order of several tens of μV, which is much less than the gap voltage (e.g. $V_g \sim 3$ mV for Nb).

The wave length $2\pi/k$ of the Josephson current density modulated along the z-direction is proportional to the applied magnetic field. The resonance condition $L = \frac{\bar{c}}{2f_n}n = \frac{\lambda}{2}n$ results in the condition $kL = n\pi$ or, equivalently, that the applied magnetic flux $\Phi = B_y t_B L$ should be equal to $n\frac{\Phi_0}{2}$. These are exactly the flux values for which the maximum Josephson current density of a short junction vanishes. At these flux values the spatial distribution of the Josephson current density (compare Fig. 2.6) matches the standing wave pattern in the junction allowing an effective nonlinear interaction between the oscillating current modes and the electromagnetic waves. If the oscillating Josephson current has excited a standing wave, it stays locked onto this standing wave for a certain current interval. In analogy to the Shapiro steps one obtains current steps in the IVC called Fiske steps.

We briefly discuss the shape of the IVCs of underdamped extended junctions shown in Fig. 3.28. For voltages that are not equal to $V_{\rm Eck}$ and V_n, the simple solution $J_s(z,t) = J_c\sin(\omega_0 t + k\cdot z + \varphi_0)$ is a good approximation. This means that the time-average of the Josephson current vanishes, $\langle I_s\rangle = 0$, and that the IVCs are given by $I_N(V) = V/R_N(V)$. In the case of a tunnel junction the nonlinear quasiparticle IVC is obtained. However, at all dc voltages close to V_n the nonlinear interaction of the current waves (3.6.4) and the standing waves leads to narrow peaks (the Fiske steps) in the IVCs, whose height depends on the applied magnetic field and can be of the order of I_c (see Fig. 3.28). The Fiske modes appear at low damping. If the damping and/or the applied magnetic field is increasing, the width of the resonance peaks at V_n is increasing so that they are merging into a single Eck peak at $V_{\rm Eck}$.

Zero field steps

Fluxons can be trapped in long Josephson junctions also in the absence of an applied magnetic field.[82] The motion of these fluxons under the Lorentz force of an applied current results in so-called ***zero field steps*** in the IVCs of long Josephson junctions at zero external field. When a propagating fluxon reaches the end of the junction transmission line, it is reflected back as an anti-fluxon. In a junction of length L, a full period for moving back and forth takes the time $T = 2L/v_z$. The associated phase change is 4π, since the passage of a fluxon and the return of an anti-fluxon both change φ by 2π. Thus, in the relativistic limit ($v_z \to \bar{c}$) reached at large bias current (large driving force), the dc voltage across the junction will be

$$V_{\rm zfs} \;=\; \dot{\varphi}\,\frac{\hbar}{2e} \;=\; \frac{4\pi}{T}\,\frac{\hbar}{2e} \;=\; \frac{4\pi}{2L/\bar{c}}\,\frac{\hbar}{2e} \;=\; \frac{h}{2e}\,\frac{\bar{c}}{L} \;=\; \frac{\omega_p}{2\pi}\,\frac{\lambda_J}{L}\,\Phi_0\;. \tag{3.6.29}$$

If n fluxons are present in the junction, the voltage will be n times larger:

$$V_{\rm n,zfs} \;=\; \Phi_0\,\frac{\bar{c}}{L}\,n \;=\; \frac{\omega_p}{2\pi}\,\frac{\lambda_J}{L}\,\Phi_0\,n\;. \tag{3.6.30}$$

[82] A.V. Ustinov *et al.*, Phys. Rev. Lett. **69**, 1815 (1992).

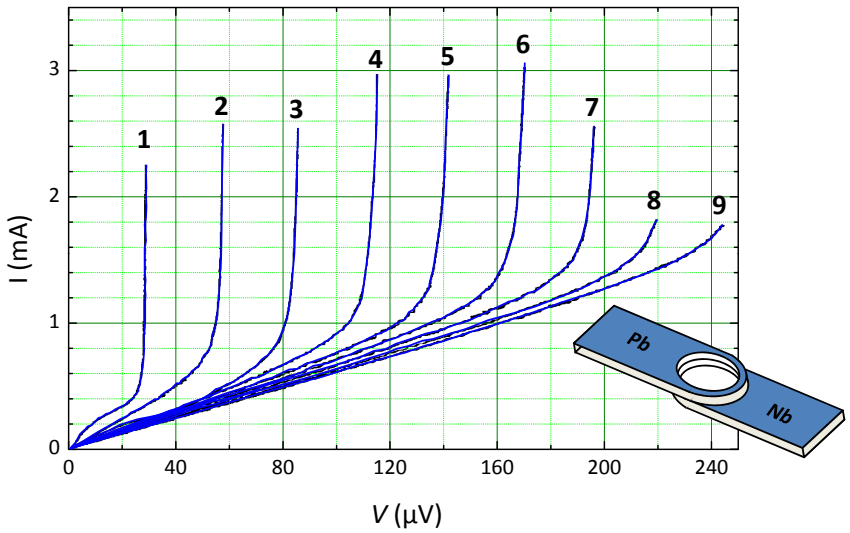

Figure 3.29: IVCs of an annular Nb/insulator/Pb Josephson junction containing a different number of trapped fluxons as indicated by the numbers. The geometry of the junction is shown in the inset. The ring diameter was about 100 μm, the ring width about 10 μm (after A.V. Ustinov *et al.*, Phys. Rev. Lett. **69**, 1815 (1992)).

These constant voltage values are referred to as ***zero field steps***, because they are based on fluxons trapped in the junction in the absence of an external field. An experimental example is shown in Fig. 3.29. We see that $V_{\mathrm{n,zfs}}$ is just twice the Fiske step voltage V_n. Comparing (3.6.28) and (3.6.30) we see that this is caused by the fact that for the Fiske steps the characteristic period for a 2π phase change is $\bar{c}/2L$, whereas it is $\bar{c}/L$ for the zero field step. The reason for this is the fact that in the zero-field step case the fluxon has to move back and forth. We also see that $V_{\mathrm{ffs}} = V_{\mathrm{n,zfs}}$ for $\Phi/\Phi_0 = n$. This is obvious, since the introduction of n fluxons into the junction at zero field is equivalent to generating a flux $\Phi = n\Phi_0$ by applying a corresponding external field.

Interesting phenomena due to the motion and collision of fluxons can be observed in ring-shaped Josephson junctions. For example, if one introduces a fluxon and an anti-fluxon in such a junction, they circulate in opposite direction under the action of a finite driving current and collide during each round-trip. This collision has been observed by Low Temperature Scanning Electron Microscopy.[83] It was found that the collision zone shrinks with increasing speed of the fluxon and anti-fluxon due to Lorentz contraction.[84,85,86]

Vortex-Cherenkov Radiation

Under certain conditions Josephson fluxons can move faster than $\bar{c}$, that is, faster than light.[87,88,89] This is analogous to the motion of charged particles, which are moving in a medium at a velocity very close to the velocity of light. If their velocity is larger than the velocity of light in the medium, they emit electromagnetic radiation, which is called ***Cherenkov radiation***. Such radiation can for example be seen

[83] R. Gross, D. Koelle, *Low Temperature Scanning Electron Microscopy of Superconducting Thin Films and Josephson Junctions* , Reports on Progress in Physiscs **57**, 651-741 (1994).

[84] S. Keil, I. V. Vernik, T. Doderer, A. Laub, H. Preßler, R. P. Huebener, N. Thyssen, A. V. Ustinov, and H. Kohlstedt , Phys. Rev. **B 54**, 14948 (1996).

[85] S. G. Lachenmann, T. Doderer, R. P. Huebener, D. Quenter, J. Niemeyer, and R. Pöpel , Phys. Rev. **B 48**, 3295 (1993).

[86] A. Laub, T. Doderer, S. G. Lachenmann, R. P. Huebener, and V. A. Oboznov , Phys. Rev. Lett. **75**, 1372 (1995).

[87] R.G. Mints, I.B. Snapiro, Phys. Rev. **B 52**, 9691 (1995).

[88] V.V. Kurin, A.V. Yulin, I.A. Shereshevskii, N.K. Vdovicheva, Phys. Rev. Lett. **80**, 3372 (1998).

[89] E. Goldobin, A. Wallraff, N. Thyssen, A.V. Ustinov, Phys. Rev. **B 57**, 130 (1998); see also Phys. Rev. Lett. **79**, 1365 (1997); Phys. Rev. **B 66**, 064527 (2001).

as a blue lightning in water surrounding a nuclear reactor. In the same way fast fluxons are emitting Josephson plasma waves called ***Vortex-Cherenkov radiation***.

Summary

Voltage State of Short Josephson Junctions:

- In the voltage state, the total current across a Josephson junction is given by the sum of the Josephson current I_s, the normal current I_N, the displacement current I_D and a fluctuation current I_F.

- In the RCSJ model the normal current channel is modeled by a voltage independent resistance R. The equation of motion of the phase difference φ is given by

$$\beta_C \frac{d^2\varphi}{d\tau^2} + \frac{d\varphi}{d\tau} + \sin\varphi - i - i_F(\tau) = 0$$

with $\tau = t/\tau_c = t/(2eI_cR/\hbar)$. The motion of φ is equivalent to the motion of a particle with mass $M = (\hbar/2e)^2 C$ in the tilted washboard potential $U = E_{J0}[1 - \cos\varphi - (I/I_c)\varphi]$ at damping $\eta = (\hbar/2e)^2/R$.

The equivalent circuit is a parallel LCR oscillatory circuit with the nonlinear Josephson inductance $L_s = \hbar/2eI_c\cos\varphi = L_c/\cos\varphi$, the junction capacitance C and the junction normal resistance R. The oscillatory circuit is characterized by the characteristic frequencies

$$\omega_p = \sqrt{\frac{1}{L_cC}} = \sqrt{\frac{2eI_c}{\hbar C}} \qquad \omega_c = \frac{R}{L_c} = \frac{2eI_cR}{\hbar} \qquad \omega_{RC} = \frac{1}{RC}$$

and the quality factor

$$Q^2 = \beta_C \equiv \frac{2e}{\hbar} I_c R^2 C \ .$$

- Overdamped Josephson junctions ($\beta_C > 1$) have non-hysteretic IVCs, whereas underdamped junctions ($\beta_C < 1$) show hysteretic IVCs.

- The IVC of an overdamped Josephson junction driven by a dc current source is given by

$$\langle V(t)\rangle = I_cR\sqrt{\left(\frac{I}{I_c}\right)^2 - 1} \qquad \text{for} \quad \frac{I}{I_c} > 1 \ .$$

- Driving a Josephson junction with a voltage $V(t) = V_{\rm dc} + V_1\cos\omega_1 t$ results in current steps (Shapiro steps) at voltages

$$V_n = n\frac{\Phi_0}{2\pi}\omega_1$$

with amplitudes

$$|\langle I_s\rangle_n| = I_c\left|\mathscr{J}_n\left(\frac{2\pi V_1}{\Phi_0\omega_1}\right)\right| \ .$$

Secondary Quantum Macroscopic Effects:

- A classical description of the motion of φ is possible only in the phase regime ($\hbar\omega_p \ll E_{J0}$ or, equivalently, $E_C = e^2/2C \ll E_{J0}$). The phase regime is present for junctions with large area (typically $0.01 - 0.1\,\mu\mathrm{m}^2$) and hence small $E_C \propto A^{-1}$ and large Josephson coupling energy $E_{J0} \propto A$.

- For $\hbar\omega_p \sim E_{J0}$ or, equivalently, $E_C = e^2/2C \sim E_{J0}$, the motion of φ has to be described fully quantum mechanically. For Josephson junctions with negligible damping the adequate Hamiltonian is

$$\mathscr{H} \;=\; -4E_C\,\frac{\partial^2}{\partial\varphi^2} + E_{J0}(1-\cos\varphi)\ .$$

The variables φ and $(\hbar/2e)Q = (\hbar/2e)^2 C\dot{\varphi}$ are canonically conjugate variables just like position and momentum and obey the commutation rule

$$[\varphi, \frac{\hbar}{2e}Q] \;=\; \imath\hbar\ ,$$

resulting in the uncertainty relation

$$\Delta N \cdot \Delta\varphi \;\geq\; 1$$

for the number of Cooper pairs $N = Q/2e$ and the phase difference φ.

- In the phase regime ($\hbar\omega_p \ll E_{J0}$ or, equivalently, $E_C = e^2/2C \ll E_{J0}$) we have $\Delta\varphi \to 0$ and $\Delta N \to \infty$, whereas in the charge regime ($\hbar\omega_p \gg E_{J0}$ or, equivalently, $E_C = e^2/2C \gg E_{J0}$) we have $\Delta N \to 0$ and $\Delta\varphi \to \infty$.

- In the charge regime, at $T = 0$ charge tunneling between the junction electrodes is possible only for $V_{\mathrm{CB}} \geq e/C$ due to the Coulomb blockade effect. In the phase regime, fluxon motion along the junction is possible only for $I_{\mathrm{FB}} \geq \Phi_0/L_c$ due to the flux blockade effect.

- At $I < I_c$ and $T > 0$, the phase difference can escape from a local minimum of the tilted washboard potential by thermal activation, resulting in a finite junction voltage by thermally activated phase slippage.

- The phase difference φ also can escape from a local minimum of the tilted washboard potential by tunneling through the potential barrier. This process is called macroscopic quantum tunneling, since the phase difference describing the collective state of a large number of electrons is tunneling.

- The cross-over temperature between thermal and tunnel escape from a local potential well is

$$k_B T^{\star} \;\simeq\; \frac{\hbar\omega_A}{2\pi} \;=\; \frac{\hbar\omega_p}{2\pi}\left[1 - \left(\frac{I}{I_c}\right)^2\right]^{1/4}\ .$$

Voltage State of Long Josephson Junctions:

- The equation of motion of the phase difference in long Josephson junctions is described by the time-dependent Sine-Gordon equation

$$\frac{\partial^2 \varphi(z,t)}{\partial z^2} - \frac{1}{\bar{c}^2} \frac{\partial^2 \varphi(z,t)}{\partial t^2} - \frac{1}{\lambda_J^2} \sin \varphi(z,t) \quad = \quad 0 \ ,$$

  where the Swihart velocity $\bar{c}$ is the propagation velocity of electromagnetic waves in the junction.

- Prominent solutions of the Sine-Gordon equation are plasma oscillations and solitons. The nonlinear interaction of these excitations with the oscillating Josephson current results in various resonant phenomena such as flux-flow steps, Fiske steps, or zero-field steps.